Diplomarbeit von
Moritz Schütte

Bose-Einstein Condensates with Long-Range Interactions

vorgelegt dem
Fachbereich Physik der
Freien Universität Berlin

Hauptgutachter: Prof. Dr. Hagen Kleinert

Februar 2007

Contents

1. Introduction

1.1. Brief Review of BEC

The big increase in research in the field of Bose-Einstein condensation (BEC) began in 1995 with its first experimental realization in dilute gases, honored with the Nobel prize in 2001. Groups at JILA [1] and MIT [2] succeeded to produce condensates of ^{87}Rb and ^{23}Na, respectively. This was 70 years after that A. Einstein [3], motivated by a letter from S.N. Bose [4], had predicted a phase transition of a gas of non-interacting particles with integer spin, called bosons and obeying the bose statistics, to a phase where the quantum mechanical ground state is macroscopically occupied, forming a so-called Bose-Einstein condensate.

Such a condensate contains a large number of coherent atoms. These represent a controllable many-particle system which allows to investigate quantum phenomena on a macroscopic level. An important example of that control is the adjustability of the interaction strength, which may be varied from attractive to repulsive, as shown in Fig. 1.1(a). It could be achieved by means of *Feshbach resonances* [5–7]. Feshbach resonances were originally found in the scattering cross section of neutrons on nuclei. The kinetic energy of the incoming neutron is equal to the binding energy of a compound nucleus. A corresponding effect in BEC is the formation of a long-living bound state during a collision. The important point for the accessibility of the interaction lies in the fact that the incoming atoms and the bound state have different spin arrangements or hyperfine states. Therefore, it is possible to address them separately by an applied magnetic field. For instance, two fermionic atoms can form a bosonic pair that condenses later on. Such a "molecule" of two fermions has a similar structure as a Cooper pair in the BCS (Bardeen-Cooper-Schrieffer)-theory of superconductivity where two electrons with opposite spins and wave vectors combine. It has been observed that two ^{6}Li atoms can be combined and that the resulting molecules cool to a BEC [8]. Via the applied magnetic field the interaction can be tuned to change from attractive to repulsive, where the molecule splits into two fermions. The existence of two separate states, a fermionic and a bound bosonic one, can be seen from the emergence of characteristic superfluid vortices. Superfluidity can be produced experimentally as the atom fluid is stirred with a laser. The transition between the bosonic and fermionic state is called the *BEC-BCS crossover*. As BCS is a solid-state phenomenon, there is a bridge between BEC from atomic physics and solid state physics. Another solid-state phenomenon in BEC arises from the fact that ultracold

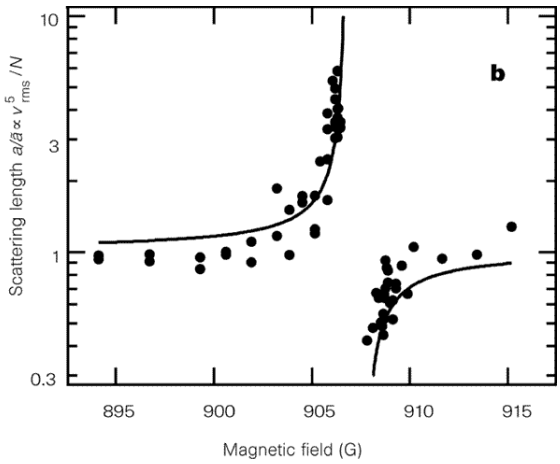

(a) Feshbach tuning.

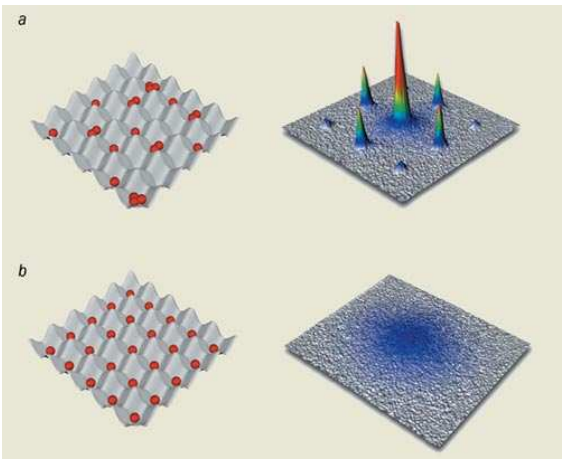

(b) BEC in optical lattice.

Fig. 1.1: (a): Experimental data showing the interaction strength tuned by an applied magnetic field in the vicinity of a Feshbach resonance (from Ref. [7]). (b): Mott insulator and superfluid phase (from Ref. [9]). After release from the trap the coherent superfluid atoms show a characteristic interference pattern. In the Mott state the phase of the matter-wave remains uncertain and no interferences are observed.

bosonic atoms can be arranged in a lattice structure using an *optical lattice*, which is simply a standing laser wave where the minima work as potential valleys [9,10]. Here, two phases exist that are controlled by the height of the potential walls between the minima. If the walls are low enough to allow tunneling, the atoms will form one coherent superfluid macroscopic matter wave over the entire lattice. If the walls are raised too high, a state with single atoms isolated on every lattice site is obtained. Because in such a state the atoms of different valleys can not tunnel anymore, it is called a Mott insulator. Both phases yield different interference patterns, once the optical lattice is switched off and the atomic cloud expands, as depicted in Fig. 1.1(b).

A possible application of BEC could be a massive atom beam [11]. A photon laser requires coherent photons of the same energy, just as we have coherent atoms of the same quantum state and ground-state energy in a BEC. But this is a big way ahead as todays BEC's are still rather unstable structures.

So far, we have not yet mentioned the essential criterion for condensation to happen. BEC *occurs* once the wave functions of the single atoms start to overlap. The criterion is stated with help of the thermal wavelength

$$\lambda_{\mathrm{T}} = \sqrt{2\pi\hbar^2/(Mk_{\mathrm{B}}T)}\,. \tag{1.1}$$

The overlap happens if λ_{T} becomes comparable to the interatomic distances in the atom

cloud. Therefore, either the density should become high or the temperature low. However, in a dense system the particles could form molecules and, further on, even liquids or solids, i.e., states much more stable than a BEC. For the formation of a molecule two atoms approach each other and combine, but this process is only possible if a third particle takes some momentum away. To avoid such a scenario, the gas must be sufficiently dilute so that only two particle interactions appear in the vast majority. So, the requirements for BEC are low temperature and low density, i.e., the gas must be ultracold and dilute. If n is the density and a the s-wave scattering length, measuring the strength of the interaction, the latter condition of density and interaction reads $na^3 \ll 1$.

1.2. Experimental Challenges

The reason why it took so long from the prediction of BEC to its realization lies in the *experimental difficulties* to cool down the atoms to temperatures in the nK regime and catch them in a trap. Previous cooling methods were not applicable to reach such low temperatures. New *cooling techniques* had to be found: laser cooling and evaporative cooling. To cool atoms to about $100\,\mu$K *laser cooling* is the appropriate method, which was awarded a Nobel prize in 1997 [12]. Here, the atom is radiated by laser beams from six different directions, $\pm\hat{\mathbf{x}}$, $\pm\hat{\mathbf{y}}$, $\pm\hat{\mathbf{z}}$, with wavelengths tuned slightly below an electric transition, i.e., detuned to red. So the atoms can only catch a photon due to the Doppler shift, if they move in the direction towards a laser. Once they absorb the photon, they experience a boost away from it due to momentum conservation. When they spontaneously emit the photon again, they experience another boost in an arbitrary direction so that the average momentum transfer of the emitted photon is zero. Only the first deceleration by the laser beam has a net effect on the atom. One might think that from a certain point on the Doppler shift is not any longer large enough to fill the energy gap between laser and atom. If the velocity of the atom becomes too small, it would not react to the laser. This however, does not happen since the atoms take some energy from the magnetic field of the trap as will be discussed later on. However, the temperatures in a BEC experiment are about some hundred nK, i.e., after laser cooling the temperature is still about a factor 1000 away.

A second cooling step is necessary, the so-called *evaporative cooling* that exists only in a trap that catches the atoms. It works by tuning the trap in a way that the energetically higher atoms in the vapor can escape from the trap and only the less energetic ones remain. To understand this process we need to know about the *operating mode of the trap*. Usually magneto-optical traps are favoured. Strong harmonic magnetic fields couple to the spin of the atom and thus fix it in a certain Zeeman state. Atoms with bigger kinetic energy can reach regions with a stronger magnetic field and the energy difference of its Zeeman state, which is proportional to the strength of the magnetic field, grows as well. The optical part of the trap is a radio frequency, which is tuned in such a way that it

flips the spin of those atoms with higher energy. Because the trap couples to the spin, the latter atoms escape from the trap and leave an ensemble of colder atoms behind.

A third method not that widely-used in BEC is sympathetic cooling. Usually, it is used to cool strongly interacting ions, but it has been applied to BEC too. For instance, a BEC mixture of ^{87}Rb of two different spin states was brought to overlap [13]. As one of them was cooled evaporatively, the thermal contact brought nearly lossless sympathetic cooling of the other.

But how can one *gain information* from such a trapped gas? Actually, it is impossible to measure properties of a condensate directly. Instead, the method is to switch off the trap, let the condensate fly apart and observe the expansion of the released gas. With laser absorption measurements after a certain time of flight, one can recover an image of the velocity distribution in the condensate. This is possible because atoms with higher momenta will escape faster and thus are located more on the edge of the expanding cloud. The expansion is a dynamic procedure just like the measurements of collective excitations of the condensate. Such dynamical measurements can be done with high precision. Furthermore, they can be compared to theoretical models and are sensitive to the interactions. For instance, they allow to determine the strength of the interaction as we shall see in the subsequent section.

1.3. Interactions in BEC

In the beginning of BEC experiments the condensing atoms were alkali metals. In such dilute alkali gases the interaction is described quite well by the Lennard-Jones potential, see Fig. 1.2(a). It consists of an attractive part proportional to r^{-6} coming from the van der Waals interaction, a second-order perturbation correction to the ideal gas, and a repulsive term of the form r^{-12}. The zero of the potential lies at the van der Waals radius r_0 that corresponds to the size of an atom supposed to be a hard sphere.

In the theory of pseudopotentials, boundary conditions are replaced by an additional inhomogeneous term in the wave equation, which is called the pseudopotential [14]. Therefore, it is sufficient to model two-particle interactions in dilute alkali gases theoretically using the short-range pseudopotential, see Fig. 1.2(b):

$$V_\delta^{(\mathrm{int})}(\mathbf{r}-\mathbf{r}') = \frac{4\pi\hbar^2 a}{M}\,\delta(\mathbf{r}-\mathbf{r}')\,. \tag{1.2}$$

The parameter a is the s-wave scattering length known from classical scattering theory. Higher orbital waves like p-, d- or f-waves are suppressed at low energy due to the centrifugal barrier in such extremely cooled systems. This makes the pseudopotential (1.2) a good approximation for describing collisions, scattering, and van der Waals forces. The pseudopotential is called contact- or delta-potential.

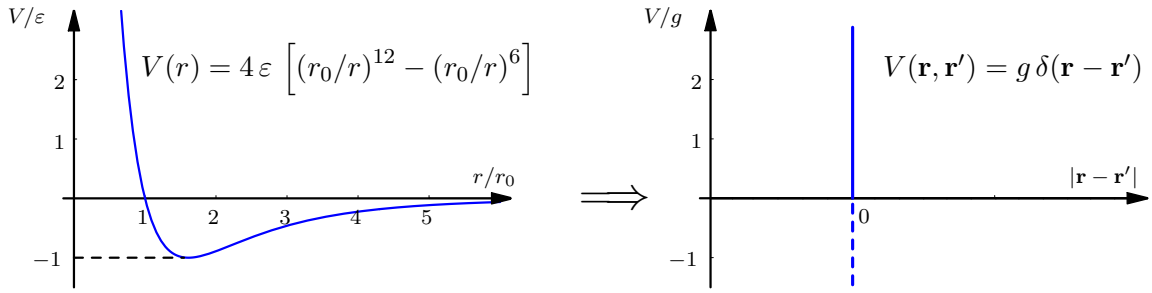

(a) Lennard-Jones potential.

(b) Pseudopotential.

Fig. 1.2: Illustration of the approximation of the pseudopotenial (b) from a physical point of view. The repulsive part of the Lennard-Jones potential (a) is approximated by a δ-functional. The dashed part in (b) betokens the possibility of tuning the strength into a negative, attractive regime by using Feshbach resonances where the bound state of (a) is taken into account.

In 2005, the first dipolar BEC was realized in a gas of ^{52}Cr [15]. Chromium was recommendable because of its electronic structure $[\mathrm{Ar}]3d^5\,4s^1$, which according to Hund's rule leads to a large magnetic dipole moment of six Bohr magnetons. So, apart from (1.2), the atoms interact additionally via a magnetic *dipole-dipole* potential

$$V_{\mathrm{dd}}^{(\mathrm{int})}(\mathbf{r}) = -\frac{\mu_0}{4\pi}\frac{3(\mathbf{m}_1\cdot\hat{\mathbf{r}})(\mathbf{m}_2\cdot\hat{\mathbf{r}}) - \mathbf{m}_1\cdot\mathbf{m}_2}{r^3} \tag{1.3}$$

which, in contrast to (1.2), is not isotropic but depends on the specific angle between the dipoles and their distance vector. For a gas of identical atoms, $\mathbf{m}_1 = \mathbf{m}_2$, there are two possibilities to align the dipoles. Either they are oriented parallel ($\rightarrow\rightarrow$) or perpendicular ($\uparrow\uparrow$) with respect to their relative positions. Whereas in the first case the potential becomes attractive, it is repulsive in the latter. This can also be seen from Fig. 1.3(b). An attractive interaction shifts the critical temperature upwards and a repulsive one downwards. A further significant difference between contact and dipole interaction is their particular range. While the pseudopotential acts only on contact of two atoms, the dipole-dipole interaction falls off with $1/r^3$ and thus acts over long distances. The relative strength of dipole interaction and pseudopotential is measured with help of the dimensionless quantity

$$\epsilon_{\mathrm{dd}} = \frac{\mu_0 m^2 M}{12\pi\hbar^2 a}. \tag{1.4}$$

First, it was not experimentally proven that the chromium atoms really interact via their magnetic dipoles. The evidence was supplied by a measurement of the expansion of the chromium condensate [16]. The dipole forces led to an anisotropic deformation of the

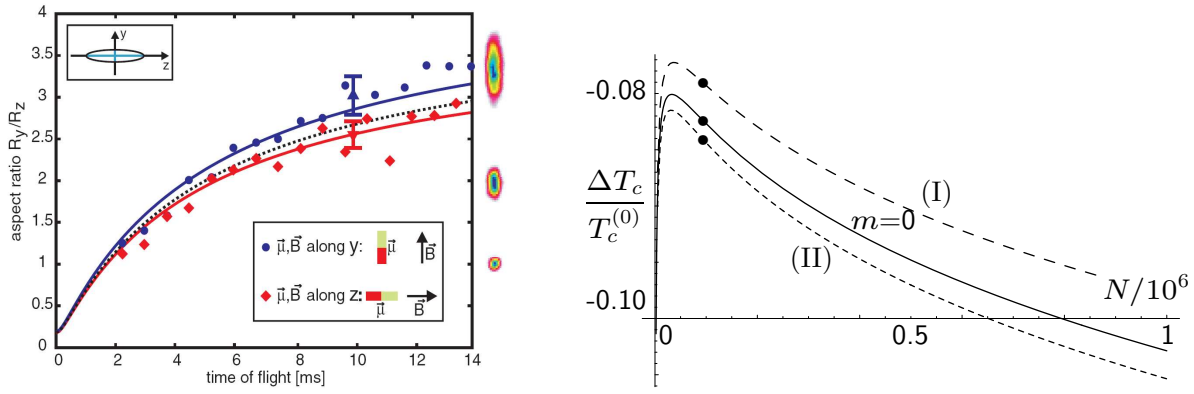

(a) Expansion.

(b) Critical temperature shift.

Fig. 1.3: Data proving the effect of magnetic dipole-dipole interaction in chromium BEC. (a): using the expansion of the condensate (taken from Ref. [16]). The dotted black line shows the theoretical curve of a delta-interaction only. But the data agree perfectly with both predictions of the two possibilities to align the dipoles in the magnetic field. (b): theoretical calculation of the critical temperature shift (from Ref. [17]); the two shifts (I) and (II) belong to a situation where the magnetic dipole moments are parallel and perpendicular to the symmetry axis of the trap.

expanding condensate which was caused by the particular orientation of the atomic dipoles and the data agreed well with the theoretical description, see Fig. 1.3(a). A second way to see the effect of the magnetic dipole-dipole interaction would be a measurement of the shift of the critical temperature caused by the dipole interaction and a comparison with the theoretical result [17,18], see Fig. 1.3(b). We have mentioned above that the long-range behaviour of the dipole-dipole interaction is a contrast to the contact interaction. A more dramatic *long-range interaction* is supplied by an $1/r$ *potential* in the focus of this thesis:

$$V_{1/r}^{(\mathrm{int})}(\mathbf{r}-\mathbf{r}') = \frac{C}{|\mathbf{r}-\mathbf{r}'|}\,. \tag{1.5}$$

This could be a repulsive Coulomb interaction of charged atoms ($C > 0$). Theoretical estimates have been made on a charged Bose gas at absolute zero [19,20]. Both papers deal with the ground-state energy and the excitation spectrum. The first version is based on the use of response and Green's functions, while in the second version a Bogoliubov theory is worked out. A Coulomb interaction has a large effect and prevents from condensing in a translationally invariant system, where the atoms prefer to form a Wigner crystal [21]. A second possibility of an $1/r$ interaction is gravitation, which is however too weak to become measurable in dilute atom gases ($C < 0$). Therefore, we basically follow an idea of

Ref. [22] to artificially create an attractive $1/r$ interaction which is similar to gravitation but up to 17 orders of magnitude stronger. Such tremendous gravitational forces are only possible in nature on stellar scales. Thus, ultracold quantum gases can be used to *simulate cosmology in the laboratory*. As the interaction is attractive, one could assume self-binding situations balanced by the attractive $1/r$ interaction and the kinetic energy as well as contact interaction on the other side. So far, all known types of stars are made of fermions. A famous example are neutron stars. These are formed from the collapsed residue of a massive star after a supernova. They are extremely dense with less than 1.4 sun masses within a radius of only 10 km. Their stability is ensured by the interplay between the quantum pressure in the star, i.e., the resistance against squeezing due to obeying Pauli's exclusion principle, and gravity. At a certain size, called Chandrasekhar mass, the Pauli exclusion principle can not hold any more against gravity and the star collapses merging in a black hole.

The equivalent concept of a *Bose star* was discussed theoretically in Refs. [23,24]. The role of the quantum pressure of fermions is replaced by the contact interaction for bosons. Although Bose stars have not yet been observed, this does not mean that they do not exist. There are still big missing links in cosmology, like for instance the origin of dark matter which accounts for about 25% of the universal mass [25].

1.4. Outline of the Thesis

We start in the *2nd chapter* with a detailed analysis on how the attractive long-range interaction is actually obtained. In fact, it is a fourth-order perturbation result of neutral atoms interacting with a radiation field. Therefore, some quantum-electrodynamical calculations are executed. We also discuss the possible *experimental realizations* and suggest an additional one worked out by ourselves. Finally, we give a brief review of an experiment with cold ions.

To describe the system properly, we will use the functional integral formalism. We will explain this method and give a review on some properties of the non-interacting Bose gas in the grand-canonical ensemble in the *3rd chapter*. Afterwards, in *chapter 4*, we develop a *Hartree-Fock mean-field theory* that takes into account the long-range $1/r$ interaction as well as the contact interaction. The theory will be valid for all temperatures, i.e., for both the condensed and gas phase.

An application of this theory will be made for two special cases that can be treated analytically. First, in *chapter 5*, we investigate the zero-temperature limit. We show, how the *Gross-Pitaevskii equation* is solved exactly in Thomas-Fermi approximation and, furthermore, use a variational approach to include the kinetic energy. The obtained Thomas-Fermi solution is equivalent to the physical situation of a Bose star.

Later, in *chapter 6*, we analyze the *dynamical properties*, which describe small excitations from the static behaviour at absolute zero. Here, two methods are used. On the

one hand, we adopt a hydrodynamical approach to treat the condensate as a quantum liquid and later on make a time-dependent Gaussian variational ansatz, both in order to calculate excitation frequencies. These are of big interest, because they are precisely measurable.

The critical region, where the phase transition occurs, will be the main topic of *chapter 7*. An important item is the *critical temperature*. We will calculate the shift regarding the ideal gas in a harmonic trap caused by the interaction, once starting from the Hartree-Fock mean-field theory and in a second way using Feynman graphs of perturbation theory and show that both ways match.

The results, problems, and an outlook on perspectives will be discussed in the concluding *chapter 8*.

2. Experimental Situation

In this chapter we describe the experimental situation of our system. At first, we reproduce the experimental proposal on the artificial creation of a strong attractive $1/r$ interaction [22]. We derive the theoretical background basing on quantum-electrodynamical calculations of Refs. [26–28]. In fact, it is a fourth order perturbation result of the interaction between two neutral atoms and an external radiation field. We will show, how one gets the total correction to the interatomar interaction and how it reduces for a rotational average in the near zone to an attractive $1/r$ interaction. Thereafter, we will show some experimental possibilities to realize it. At the end of the chapter, we will briefly explain an experiment to catch and cool ions. This shall motivate extending some of the calculations to a Coulomb regime.

2.1. Theoretical Basis of Experiment

The theoretical basis of the experiment is the interaction between atoms and a radiation field, which stems, for instance, from a laser. The total Hamiltonian of the system looks as follows

$$H = H_{\mathrm{A}} + H_{\mathrm{B}} + H_{\mathrm{rad}} + H_{\mathrm{int}} \,. \tag{2.1}$$

Here, H_{A}, H_{B}, and H_{rad} are the undisturbed Hamiltonians of the atoms A, B and the radiation field, respectively. Their eigenvalue problems are solved and the eigenvectors orthonormalized:

$$H_{\mathrm{A,B}} \left|E_m^{\mathrm{A,B}}\right\rangle = E_m^{\mathrm{A,B}} \left|E_m^{\mathrm{A,B}}\right\rangle , \qquad H_{\mathrm{rad}} \left|n(\mathbf{q},\lambda)\right\rangle = E^n \left|n(\mathbf{q},\lambda)\right\rangle . \tag{2.2}$$

$E_m^{\mathrm{A,B}}$ label the energy eigenstates of the atoms, while n gives the number of photons in a certain state number state determined by their wave vector $\mathbf{q}$ and corresponding wavelengths λ. The interaction between atoms and radiation field is dominated by the coupling between the electric dipole moments of the atoms and the radiation field. Furthermore, the interaction Hamiltonian H_{int} is supposed to be that small that we can treat it within the framework of perturbation theory. In electric dipole approximation the interaction reads in SI units

$$H_{\mathrm{int}} = -\frac{1}{\varepsilon_0}\boldsymbol{\mu}(A)\cdot\mathbf{d}^{\perp}(\mathbf{r}_A) - \frac{1}{\varepsilon_0}\boldsymbol{\mu}(B)\cdot\mathbf{d}^{\perp}(\mathbf{r}_B) \,, \tag{2.3}$$

Fig. 2.1: Time-ordered graphs of the second-order dynamic Stark-shift with time going from bottom to top. s and r label the particular energy of the atom state. An atom catches a photon, gets excited, and reemits the photon again.

where $\boldsymbol{\mu}(A,B)$ are the dipole moments of the atoms and we use the mode expansion of the radiation field

$$\mathbf{d}^{\perp}(\mathbf{r}) = \imath \sum_{\mathbf{k},\epsilon} \left(\frac{\hbar c k}{2\varepsilon_0 V}\right)^{1/2} \left[\hat{\mathbf{e}}^{(\epsilon)}(\mathbf{k})\, a^{(\epsilon)}(\mathbf{k})\, e^{\imath \mathbf{k}\cdot\mathbf{r}} - \hat{\mathbf{e}}^{(\epsilon)*}(\mathbf{k})\, a^{(\epsilon)\dagger}(\mathbf{k})\, e^{-\imath \mathbf{k}\cdot\mathbf{r}}\right] . \tag{2.4}$$

In (2.4), $\hat{\mathbf{e}}^{(\epsilon)}$ are the polarization vectors of the two transversal polarizations $\epsilon = \pm$, $\mathbf{k}$ the wave vectors of the photons, c the speed of light, V the volume, and $a^{(\epsilon)}(\mathbf{k})$, $a^{(\epsilon)\dagger}(\mathbf{k})$ represent the corresponding photon creation and annihilation operators

$$a^{(\epsilon)}(\mathbf{k})|n(\mathbf{p},\lambda)\rangle = \sqrt{n}\,|(n-1)(\mathbf{k},\epsilon)\rangle\,\delta_{\epsilon\lambda}\,\delta_{\mathbf{pk}}\,, \tag{2.5}$$

$$a^{(\epsilon)\dagger}(\mathbf{k})|n(\mathbf{p},\lambda)\rangle = \sqrt{(n+1)}\,|(n+1)(\mathbf{k},\epsilon)\rangle\,\delta_{\epsilon\lambda}\,\delta_{\mathbf{pk}}\,. \tag{2.6}$$

The expectation value of the electric dipole operator $\boldsymbol{\mu}(\mathbf{r})$ is an electric transition dipole moment abbreviated by

$$\langle E_m^{\mathrm{A}}|\boldsymbol{\mu}(\mathbf{r}_{\mathrm{A}})|E_n^{\mathrm{A}}\rangle = \boldsymbol{\mu}^{mn}(\mathbf{r}_{\mathrm{A}})\,. \tag{2.7}$$

For $m = n$ no transition happens and the expectation in (2.7) vanishes.

It can easily be seen that only even orders of the perturbative calculation can contribute because the odd orders vanish due to the symmetry of the interaction (2.3). Hence, the first non-vanishing contribution stems from the *second-order* perturbation correction

$$\Delta E^{(2)} = \sum_I \frac{\langle f|H_{\mathrm{int}}|I\rangle\langle I|H_{\mathrm{int}}|i\rangle}{E_i - E_I}. \tag{2.8}$$

$|i\rangle$ and $\langle f|$ are arbitrary initial and final states of the system, respectively. This order describes the coupling of the radiation field to the induced electric dipole moments. Here, the summation labelled by I actually contains a summation over all possible intermediate states. The result of the second order is the dynamic Stark-shift calculated from the diagrams in Fig. 2.1. Those are similar to the diagrams of elastic scattering of a photon at an atom, like in Rayleigh scattering.

The result of the second order reads with the common convention that equal indices have to be summed

$$\Delta E^{(2)} = \left(\frac{n\hbar c k}{2\varepsilon_0 V}\right) \hat{e}_i\, \hat{e}_j^{*} \alpha_{ij}(k), \tag{2.9}$$

where the dynamic polarizability is defined, using the abbreviation $E_i^{\mathrm{X}} - E_0^{\mathrm{X}} = E_{i0}^{\mathrm{X}}$, as

$$\alpha_{ij}(k) = \sum_r \left(\frac{\mu_i{}^{sr}\mu_j{}^{rs}}{E_{rs} - \hbar ck} + \frac{\mu_j{}^{sr}\mu_i{}^{rs}}{E_{rs} + \hbar ck} \right) . \tag{2.10}$$

In the case of a freely rotating atom, like in a gas, (2.10) simplifies to:

$$\alpha(k) = \frac{2}{3} \sum_r E_r \frac{E_{rs} \left| \boldsymbol{\mu}^{rs} \right|^2}{E_{rs}^2 - (\hbar ck)^2} . \tag{2.11}$$

Thus, we see from Eq. (2.9), that the second order only displaces the energy levels of the single atoms but does not affect their mutual interaction. A comparison of (2.9) with Eq. (2.4) shows that the energy shift (2.9) depends quadratically on the strength of the applied electric field, $\sqrt{n\hbar ck/2\varepsilon_0 V}$, just as expected for the Stark-shift.

The next even order perturbation theory is the *fourth* one:

$$\Delta E^{(4)} = - \sum_{I,II,III} \frac{\langle 0|H_{\mathrm{int}}|III\rangle\langle III|H_{\mathrm{int}}|II\rangle\langle II|H_{\mathrm{int}}|I\rangle\langle I|H_{\mathrm{int}}|0\rangle}{(E_I - E_0)(E_{II} - E_0)(E_{III} - E_0)} . \tag{2.12}$$

This order represents the energy changing caused by the coupling between the atoms by exchange of virtual photons only, while the atoms remain unexcited. To get the correction to the ground-state energy, we suppose the initial and final states as the ground state. It is the leading contribution to the intermolecular energy, i.e., the interaction potential. It is calculated best using time-ordered graph techniques, with the intermediate states $|I\rangle, |II\rangle, |III\rangle$. The formation of the sets in Fig. 2.2 has been made for the following reasons. The virtual (exchange) and real photons can run either from A to B or vice versa in time. Therefore we have Fig. 2.2(a) with both photons going from A to B, Fig. 2.2(d) with both from B to A, Fig. 2.2(b) with the real from B to A and the virtual from A to B, and last Fig. 2.2(c) the real from A to B and the virtual from B to A.

As an example, we calculate *graph a of 2.2(a)* with the ground state

$$|0\rangle = |E_0^{\mathrm{A}}; E_0^{\mathrm{B}}; n(\mathbf{k}, \lambda)\rangle . \tag{2.13}$$

The intermediate states can be read off from Fig. 2.3. To calculate the expectations of (2.12), we use the Eqs. (2.3) to (2.7). Herewith, we get the following contributions

$$\langle 0|H_{\mathrm{int}}|III\rangle = \imath \left(\frac{\hbar cp}{2\varepsilon_0 V} \right)^{1/2} \mu_i^{0s}(\mathbf{r}_{\mathrm{B}}) \hat{e}_i^{(\epsilon)}(\mathbf{p}) e^{\imath \mathbf{p}\mathbf{r}_{\mathrm{B}}} , \tag{2.14}$$

$$\langle III|H_{\mathrm{int}}|II\rangle = -\imath \left(\frac{\hbar ck}{2\varepsilon_0 V} \right)^{1/2} \mu_j^{s0}(\mathbf{r}_{\mathrm{B}}) \hat{e}_j^{(\lambda)*}(\mathbf{k}) \sqrt{n} e^{-\imath \mathbf{k}\mathbf{r}_{\mathrm{B}}} , \tag{2.15}$$

$$\langle II|H_{\mathrm{int}}|I\rangle = \imath \left(\frac{\hbar ck}{2\varepsilon_0 V} \right)^{1/2} \mu_l^{0r}(\mathbf{r}_{\mathrm{A}}) \hat{e}_l^{(\lambda)}(\mathbf{k}) \sqrt{n} e^{\imath \mathbf{k}\mathbf{r}_{\mathrm{A}}} , \tag{2.16}$$

$$\langle I|H_{\mathrm{int}}|0\rangle = -\imath \left(\frac{\hbar cp}{2\varepsilon_0 V} \right)^{1/2} \mu_m^{r0}(\mathbf{r}_{\mathrm{A}}) \hat{e}_m^{(\epsilon)*}(\mathbf{p}) e^{-\imath \mathbf{p}\mathbf{r}_{\mathrm{A}}} . \tag{2.17}$$

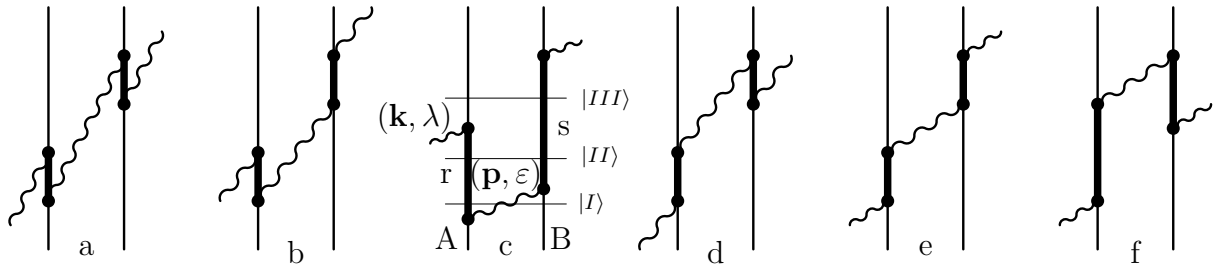

(a) Set I. ↑↑

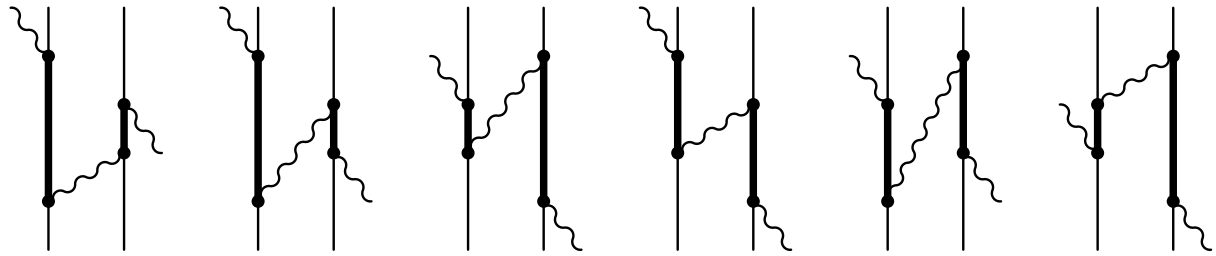

(b) Set II. ↓↑

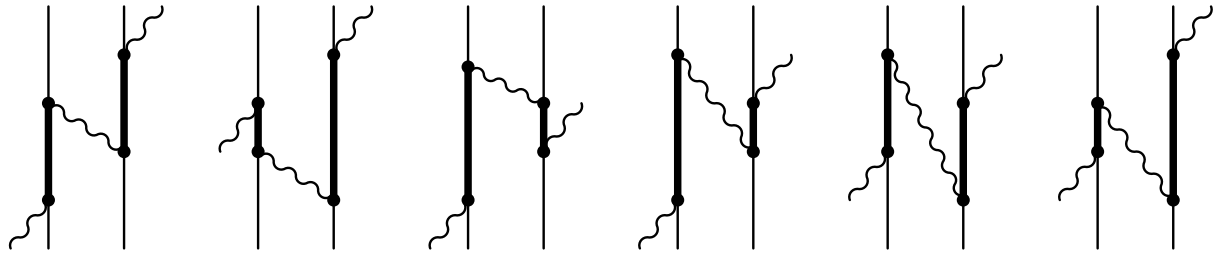

(c) Set III. ↑↓

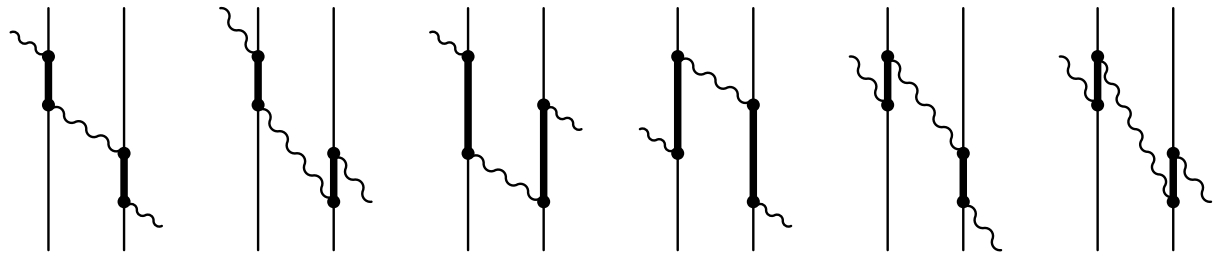

(d) Set IV. ↓↓

Fig. 2.2: Four sets of the fourth order perturbation graphs. Here time runs from bottom to top. The sets are grouped by the fact that the real and virtual photon can either go from A to B or vice versa (arrows in sublabels). Set I c is labelled exemplary. One atom catches a real photon $(\mathbf{k}, \lambda)$ of the radiation field, gets excited, exchanges a virtual photon $(\mathbf{p}, \varepsilon)$ with the other atom which emits a real photon later on. Both atoms remain unexcited in total.

		Set I	Set II	Set III	Set IV
	I	$\|r,\,0;\,n,\,1\rangle$	$\|r,\,0;\,n,\,1\rangle$	$\|r,\,0;\,n-1,\,0\rangle$	$\|0,\,s;\,n-1,\,0\rangle$
a	II	$\|0,\,0;\,n-1,\,1\rangle$	$\|r,\,s;\,n,\,0\rangle$	$\|r,\,s;\,n-1,\,1\rangle$	$\|0,\,0;\,n-1,\,1\rangle$
	III	$\|0,\,s;\,n,\,1\rangle$	$\|r,\,0;\,n-1,\,0\rangle$	$\|0,\,s;\,n-1,\,0\rangle$	$\|r,\,0;\,n-1,\,0\rangle$
	I	$\|r,\,0;\,n,\,1\rangle$	$\|r,\,0;\,n,\,1\rangle$	$\|0,\,s;\,n,\,1\rangle$	$\|0,\,s;\,n,\,1\rangle$
b	II	$\|0,\,0;\,n-1,\,1\rangle$	$\|r,\,s;\,n-1,\,1\rangle$	$\|r,\,s;\,n,\,0\rangle$	$\|0,\,0;\,n-1,\,1\rangle$
	III	$\|0,\,s;\,n-1,\,0\rangle$	$\|r,\,0;\,n-1,\,0\rangle$	$\|0,\,s;\,n-1,\,0\rangle$	$\|r,\,0;\,n-1,\,0\rangle$
	I	$\|r,\,0;\,n,\,1\rangle$	$\|0,\,s;\,n-1,\,0\rangle$	$\|r,\,0;\,n-1,\,0\rangle$	$\|0,\,s;\,n,\,1\rangle$
c	II	$\|r,\,s;\,n,\,0\rangle$	$\|r,\,s;\,n-1,\,1\rangle$	$\|r,\,s;\,n,\,0\rangle$	$\|r,\,s;\,n,\,0\rangle$
	III	$\|0,\,s;\,n-1,\,0\rangle$	$\|0,\,s;\,n,\,1\rangle$	$\|r,\,0;\,n,\,1\rangle$	$\|r,\,0;\,n-1,\,0\rangle$
	I	$\|r,\,0;\,n-1,\,0\rangle$	$\|0,\,s;\,n-1,\,0\rangle$	$\|r,\,0;\,n-1,\,0\rangle$	$\|0,\,s;\,n-1,\,0\rangle$
d	II	$\|0,\,0;\,n-1,\,1\rangle$	$\|r,\,s;\,n-1,\,1\rangle$	$\|r,\,s;\,n-1,\,1\rangle$	$\|r,\,s;\,n,\,0\rangle$
	III	$\|0,\,s;\,n,\,1\rangle$	$\|r,\,0;\,n-1,\,0\rangle$	$\|r,\,0;\,n,\,1\rangle$	$\|r,\,0;\,n,\,1\rangle$
	I	$\|r,\,0;\,n-1,\,0\rangle$	$\|r,\,0;\,n,\,1\rangle$	$\|0,\,s;\,n,\,1\rangle$	$\|0,\,s;\,n-1,\,0\rangle$
e	II	$\|0,\,0;\,n-1,\,1\rangle$	$\|r,\,s;\,n-1,\,1\rangle$	$\|r,\,s;\,n-1,\,1\rangle$	$\|0,\,0;\,n-1,\,1\rangle$
	III	$\|0,\,s;\,n-1,\,0\rangle$	$\|0,\,s;\,n,\,1\rangle$	$\|r,\,0;\,n,\,1\rangle$	$\|r,\,0;\,n,\,1\rangle$
	I	$\|r,\,0;\,n-1,\,0\rangle$	$\|0,\,s;\,n-1,\,0\rangle$	$\|0,\,s;\,n,\,1\rangle$	$\|0,\,s;\,n,\,1\rangle$
f	II	$\|r,\,s;\,n,\,0\rangle$	$\|r,\,s;\,n,\,0\rangle$	$\|r,\,s;\,n-1,\,1\rangle$	$\|0,\,0;\,n-1,\,1\rangle$
	III	$\|0,\,s;\,n,\,1\rangle$	$\|0,\,s;\,n,\,1\rangle$	$\|0,\,s;\,n-1,\,0\rangle$	$\|r,\,0;\,n,\,1\rangle$

Fig. 2.3: Modes corresponding to the graphs in Fig. 2.2. The first two entries give the state of atoms A, B which is either an excited state "r, s" or the ground state "0". The third entry shows the state of real photons from the radiation field while the last gives the state of a virtual photon.

The denominator of (2.12) becomes, with $E_0 = E_0^{\mathrm{A}} + E_0^{\mathrm{B}} + n\hbar ck$,

$$(E_I - E_0)(E_{II} - E_0)(E_{III} - E_0) = (E_{r0}^{\mathrm{A}} + \hbar cp)(\hbar cp - \hbar ck)(E_{s0}^{\mathrm{B}} + \hbar cp)\,. \tag{2.18}$$

The energy Eq. (2.12) contains summations over intermediate states I, II, III which are characterized by $\mathbf{p}$, ϵ, s, r. Hence, we get the composed contribution for Fig. 2.2(a)a, with $\mathbf{r} = \mathbf{r}_{\mathrm{B}} - \mathbf{r}_{\mathrm{A}}$:

$$\sum_{\mathbf{p},\epsilon,s,r} \frac{\left(\frac{\hbar cp}{2\varepsilon_0 V}\right)\left(\frac{n\hbar ck}{2\varepsilon_0 V}\right)\mu_i^{0s}(\mathbf{r}_{\mathrm{B}})\mu_j^{s0}(\mathbf{r}_{\mathrm{B}})\mu_l^{0r}(\mathbf{r}_{\mathrm{A}})\mu_m^{r0}(\mathbf{r}_{\mathrm{A}})\hat{e}_i^{(\epsilon)}(\mathbf{p})\hat{e}_j^{(\lambda)*}(\mathbf{k})\hat{e}_l^{(\lambda)}(\mathbf{k})\hat{e}_m^{(\epsilon)*}(\mathbf{p})e^{\imath\mathbf{pr}}e^{-\imath\mathbf{kr}}}{(E_{r0}^{\mathrm{A}} + \hbar cp)(\hbar cp - \hbar ck)(E_{s0}^{\mathrm{B}} + \hbar cp)} \tag{2.19}$$

The summation over the polarization vectors for right (−) or left (+) circular polarized atoms is done using the identity

$$\sum_{\pm} \hat{e}_i^{*(\pm)}(\mathbf{p})\, \hat{e}_j{}^{(\pm)}(\mathbf{p}) = \frac{1}{2}\left[(\delta_{ij} - \hat{p}_i\hat{p}_j) \pm \imath\epsilon_{ijl}\hat{p}_l\right] . \tag{2.20}$$

This relation is applied to the summation of the ϵ-polarization vectors of the virtual photons. The summation over all quantum numbers $\mathbf{p}$ can be replaced by an integral if the spectrum is very narrow. This is the case if the volume is big enough. Therefore, we use the approximation

$$\frac{1}{V}\sum_{\mathbf{p}} \to \int \frac{d^3p}{(2\pi)^3} . \tag{2.21}$$

Now, we use these two relations and furthermore, replace the dipole transition moments and the summation over the energies r, s with help of the polarizabilities $\alpha(k)$ (2.11). The summation of all 24 graphs of Fig. 2.2 and integration over $\mathbf{p}$ leads to [26]

$$\Delta E^{(4)} = \left(\frac{n\hbar ck}{\varepsilon_0 V}\right) \hat{e}_i^{(\lambda)*}(\mathbf{k})\, \hat{e}_j^{(\lambda)}(\mathbf{k})\, \alpha^{\mathrm{A}}(k)\, \alpha^{\mathrm{B}}(k)\, V_{ij}(\mathbf{r},k) \cos(\mathbf{k}\cdot\mathbf{r}) . \tag{2.22}$$

Here, we introduced the retarded dipole-dipole interaction tensor

$$V_{ij}(\mathbf{r},k) = \frac{1}{4\pi\varepsilon_0 r^3}\left[(\delta_{ij} - 3\,\hat{r}_i\hat{r}_j)\,(\cos kr + kr\sin kr) - (\delta_{ij} - \hat{r}_i\hat{r}_j)\,k^2r^2\cos kr\right] , \tag{2.23}$$

which consists of two parts. The traceless dyadic $(\delta_{ij} - 3\,\hat{r}_i\hat{r}_j)$ bears the full dipolar coupling, while the other part $(\delta_{ij} - \hat{r}_i\hat{r}_j)$ describes the transversal coupling.

For identical atoms A and B the polarizabilities are the same: $\alpha^{\mathrm{A}}(k) = \alpha^{\mathrm{A}}(k) = \alpha(k)$. Further, we can collect some constants to the laser intensity $I = n\hbar c^2k/V$ and rewrite the energy shift (2.22) which depends on the interatomar distance as the potential

$$\boxed{U(\mathbf{r}) = \tfrac{I\alpha^2(k)}{\varepsilon_0 c}\hat{e}_i{}^*(\mathbf{k})\,\hat{e}_j(\mathbf{k})V_{ij}(\mathbf{r},k)\cos(\mathbf{k}\cdot\mathbf{r})\,.} \tag{2.24}$$

It was shown in Ref. [26] that a pair orientation or tumbling average leaves a purely $1/r$ dependence in the near zone limit. Such an average is well fulfilled for gases or liquids where the atoms are randomly oriented. Without loss of generality, we can assume the radiation field to be oriented along the $\hat{z}$-axis. Therefore, using (2.20), the polarization vectors without further specializing them yield $(\delta_{11} + \delta_{22})/2$. The rotational average of all angular orientations reads

$$\begin{aligned}\langle U(\mathbf{r})\rangle \;=\; & \frac{I\alpha^2(k)}{4\pi\varepsilon_0^2 cr^3}\,\frac{1}{4\pi}\int_0^{2\pi} d\varphi \int_{-1}^{1} d\cos\vartheta\;\cos(kr\cos\vartheta)\,\frac{1}{2}\Big[(2-3\sin^2\vartheta)\,(\cos kr + kr\sin kr) \\ & -(2-\sin^2\vartheta)k^2r^2\cos kr\Big] ,\end{aligned} \tag{2.25}$$

from where we easily get the result

$$\langle U(\mathbf{r})\rangle = \frac{I\alpha^2(k)}{8\pi\varepsilon_0^2 c r^3}\left[\frac{6\cos(2kr)}{k^2r^2} - 2\cos(2kr) - kr\sin(2kr) + \frac{5\sin(2kr)}{kr} - \frac{3\sin(2kr)}{k^3r^3}\right]. \tag{2.26}$$

This reduces in the near zone $kr \ll 1$ to

$$\langle U(\mathbf{r})\rangle = -\frac{11Ik^2\alpha^2(k)}{60\pi\varepsilon_0^2 c}\,\frac{1}{r}\,. \tag{2.27}$$

It is interesting to notice that the near zone potential with the characteristic attractive $1/r$ dependence is caused by the transversal part of (2.23). As we have seen that the derived potential has the $1/r$ dependence in the near zone, the question arises how one can realize such a tumbling average experimentally. This shall be the goal of the following sections.

2.2. Experimental Setup with Static Lasers

The experimental proposal of how such an orientation average could be realized for cold gases has been made in Ref. [22]. The simplest model that suppresses the $1/r^3$ parts consists of three orthogonal, circularly polarized laser beams, as shown in Fig. 2.4(a):

$$\mathbf{k}_1 = k\hat{\mathbf{e}}_\mathrm{x}, \quad \mathbf{k}_2 = k\hat{\mathbf{e}}_\mathrm{y}, \quad \mathbf{k}_3 = k\hat{\mathbf{e}}_\mathrm{z}\,. \tag{2.28}$$

For the near zone we can use identity (2.20) and simply superpose the three terms to get the resulting near zone potential

$$U_3(\mathbf{r}) = -\frac{3Ik^2\alpha^2}{16\pi c\varepsilon_0^2}\,\frac{1}{r}\left[\frac{7}{3} + (\sin\vartheta\,\cos\varphi)^4 + (\sin\vartheta\,\sin\varphi)^4 + (\cos\vartheta)^4\right]. \tag{2.29}$$

The angles φ and ϑ describe the orientation of the atoms with respect to the incident beam. The result is attractive for all angles ϑ and φ as long as the polarizability α is real. The derivation of (2.29) from a sphere is shown in Fig. 2.4(a). For a purely isotropic $1/r$ potential a second scheme was suggested in Ref. [22] which consists of six times three lasers, called a triad of lasers, described above. But now each triad of three lasers is turned by the following Euler angles

Triad	1	2	3	4	5	6
$\hat{\mathbf{z}}$ axis	0	0	0	0	0	0
new $\hat{\mathbf{y}}$ axis	$\pi/4$	$\pi/4$	$\pi/4$	$\pi/4$	0	0
final $\hat{\mathbf{z}}$ axis	$\pi/8$	$-\pi/8$	$3\pi/8$	$-3\pi/8$	$\pi/8$	$-\pi/8$

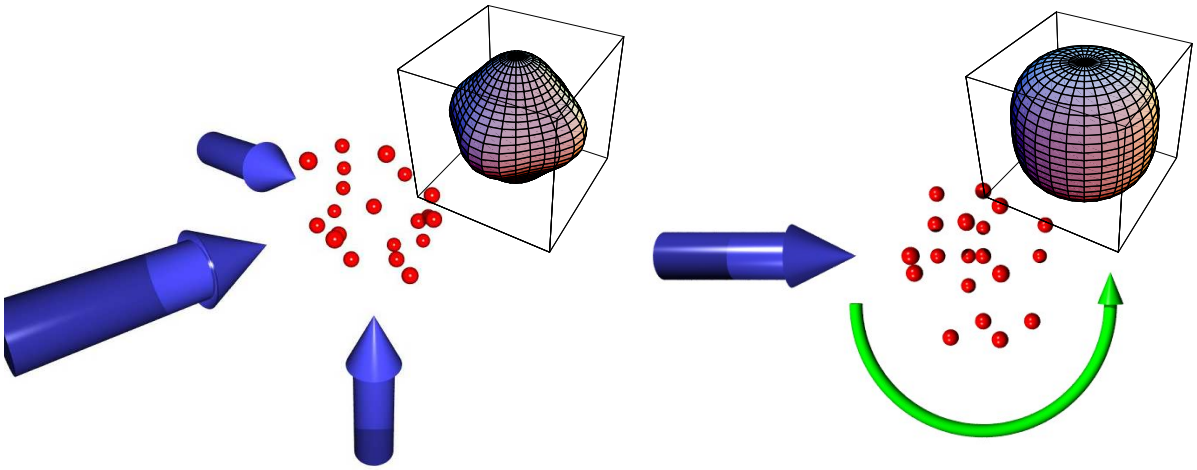

(a) Static Setup $U_3(\mathbf{r})$.

(b) Rotating Setup $U_{1\times\mathrm{rot}}(\mathbf{r})$.

Fig. 2.4: Illustration of the two proposed setups (laser = blue, atoms = red). Small upper right pictures: Spherical behaviour of the particular potentials, Eqs. (2.29) and (2.40).

The superposition of the 6 triads gives the purely $1/r$ potential

$$U_{18}(r) = -\frac{u}{r}\,, \qquad u = \frac{11}{4\pi}\frac{Ik^2\alpha^2}{c{\varepsilon_0}^2}\,. \tag{2.30}$$

Experimentally, however, a problem not brought up yet is the interference between the laser beams. Since the lasers are arranged such that they interfere inevitably, this must be avoided somehow. In Ref. [22] the authors suggest to detune the lasers against each other. The difference between the resulting oscillations of two lasers should be much larger than the relevant frequencies of the condensate like the excitation frequencies of collective motions for example. If these are not disturbed, the total influence of the interference to the interaction potential averages out.

2.3. Interaction Strength

The strength of the interaction in (2.30) is determined by the setting of the laser arrangement. But it can be reexpressed by using a classical picture. If a particle is attracted by a central force, it depends on its angular momentum, whether it takes a stable position or not. The effective potential consists of the angular momentum barrier and the attractive $1/r$-potential:

$$V_{\mathrm{eff}}(r) = -\frac{u}{r} + \frac{\mathbf{L}^2}{2Mr^2}. \tag{2.31}$$

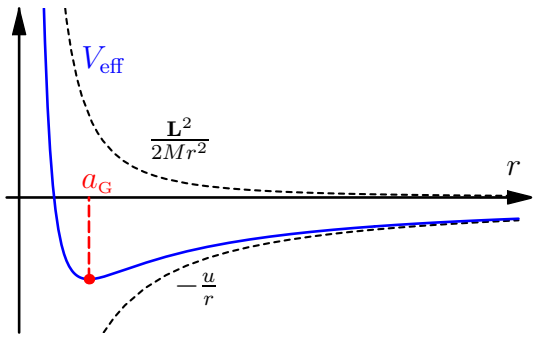

static polarizability α	^{23}Na: $24.1 \cdot 10^{-24}\,\text{cm}^3$ ^{87}Rb: $46.3 \cdot 10^{-24}\,\text{cm}^3$
wavelength of a CO_2-laser	$\lambda = 10.6\,\mu\text{m}$
laser intensity	$I = 10^8\,\text{W/cm}^2$
s-wave scattering length a	3 nm
gravitation-like length a_{G}	^{23}Na: 0.1 m ^{87}Rb: 0.027 m

Fig. 2.5: Left: Clarification of the definition of the characteristic length of the interaction. Right: Typical values of the appearing parameters. The characteristic length a_{G} will be used to determine the strength of the interaction in the further discussion.

The potential is stable around its minimum, see Fig. 2.5, which follows from

$$\frac{dV_{\text{eff}}(r)}{dr} = \frac{u}{r^2} - \frac{\mathbf{L}^2}{Mr^3} = 0. \tag{2.32}$$

If we assume that the angular momentum is of the size $|\mathbf{L}| = 2\pi\hbar$ as in the Bohr model, the equilibrium position depends on

$$a_{\text{G}} = \frac{4\pi^2\hbar^2}{M\,u}\,. \tag{2.33}$$

Thus, Eq. (2.33) defines in analogy to the Bohr model a new characteristic length scale. So, from now on we will use the interaction (2.30) with

$$u = \frac{4\pi^2\hbar^2}{M a_{\text{G}}}\,, \tag{2.34}$$

where the information about the specific laser setup is contained in a_{G}. Typical values following from (2.30) and (2.33) are given in the table in Fig. 2.5.

2.4. Alternative Setup with Rotating Lasers

Although the perturbative derivation of the interaction is only valid for static perturbations we will present here a setup of rotating lasers. For a dynamic setup valid for every rotation speed, the calculations of Section 2.1 must be repeated within time-dependent perturbation theory of QED. But in a quasi-static frame, where the rotation frequency

ω is much smaller than the frequency of the laser ω_{L}, the theoretical derivation should remain valid. On the other hand, the excitation frequencies of the BEC ω_{exc} must "see" the desired potential. Therefore, we arrive at the following condition:

$$\omega_{\mathrm{exc}} \ll \omega \ll \omega_{\mathrm{L}} \,. \tag{2.35}$$

Instead of a static wave vector $\mathbf{k}$ we use the time-dependent one

$$\mathbf{k}(t) = k\,(\sin\gamma\,\cos\omega t, \sin\gamma\,\sin\omega t, \cos\gamma) \tag{2.36}$$

with a free parameter γ that we will adjust shortly. As the approach is time-dependent one has to average the potential (2.24) over one period:

$$U(\mathbf{r}) = \frac{\omega}{2\pi} \int_0^{2\pi/\omega} U(\mathbf{r}, t)\, dt \,. \tag{2.37}$$

The resulting potential contains one part proportional to $1/r^3$ and one proportional to $1/r$. The free angle γ will be chosen in such a way that only the latter term survives. After the integration over one period, the potential has the following form:

$$U_{1\times\mathrm{rot}}(\mathbf{r}) = \frac{I\alpha^2k^2}{4\pi c\varepsilon_0^2 r^3}\left\{\frac{(\cos^2\gamma - 1/3)\,(96 + 288\cos 2\vartheta)}{31} + \frac{q^2r^2}{256}\Big[4\cos 2\vartheta - 9\cos 4\vartheta - 187 - 3\cos^4\gamma\,(20\cos 2\vartheta + 35\cos 4\vartheta + 9) + \cos^2\gamma\,(24\cos 2\vartheta + 90\cos 4\vartheta + 14)\Big]\right\}. \tag{2.38}$$

Obviously, the first term vanishes for the angle

$$\cos^2\gamma = \frac{1}{3} \qquad \Longrightarrow \qquad \gamma \approx 54.74^\circ \,, \tag{2.39}$$

which appears in another context as well. It is called "magic angle" in NMR-spectroscopy of solids. Here, the dipole-dipole interaction of the spins becomes important but with the magic angle between applied magnetic field and spins it can be tuned to zero [29]. That idea has been used in the dipolar BEC as well. Like in Feshbach resonance, the dipole-dipole interaction could be changed from an attractive to a repulsive regime, tuning the applied magnetic field, and even vanishes at the magic angle [30].

With that magic angle (2.39) the further terms of (2.38) reduce to the near-zone potential

$$U_{1\times\mathrm{rot}}(\mathbf{r}) = -\frac{I\alpha^2k^2}{96\pi c\varepsilon_0^2}\,\frac{1}{r}\,(17 + 6\cos^2\vartheta - 7\cos^4\vartheta). \tag{2.40}$$

This potential $U_{1\times\mathrm{rot}}$ is always attractive and its angular dependence is shown in Fig. 2.4(b). Obviously, it does not depend on the azimuthal angle and has a more spherical shape than (2.29). The angular dependent part is an aberration from spherical symmetry of the order smaller than 6 %.

A totally spherical symmetric potential can be achieved by combining three rotating lasers with the following orientations

$$\mathbf{k}_1 = \begin{pmatrix} \cos\omega t \sin\gamma \\ \sin\omega t \sin\gamma \\ \cos\gamma \end{pmatrix}, \qquad \mathbf{k}_2 = \begin{pmatrix} \cos\gamma \\ \cos\omega t \sin\gamma \\ \sin\omega t \sin\gamma \end{pmatrix}, \qquad \mathbf{k}_3 = \begin{pmatrix} \cos\omega t \sin\gamma \\ \cos\gamma \\ \sin\omega t \sin\gamma \end{pmatrix}. \tag{2.41}$$

If we proceed in a similar manner like for one rotating laser, namely we superpose the three terms, take the average of one period, and choose the free angle γ to get rid of the $1/r^3$ terms, so we get for the variable angle

$$\cos^2\gamma = \frac{1}{2} + \frac{1}{70}\left(-5 + 4\sqrt{30}\right) \qquad \Longrightarrow \qquad \gamma \approx 30.56^\circ\,. \tag{2.42}$$

The resulting potential is now spherically symmetric

$$U_{3\times\mathrm{rot}}(r) = -\frac{11 I \alpha^2 k^2}{20\pi c \varepsilon_0^2}\,\frac{1}{r}\,. \tag{2.43}$$

In comparison with the static setup, in our rotating proposal less lasers are required and therefrom the experimental realization is easier and cheaper. On the other side, interference effects become crucial in the rotating framework but can still be overcome by frequency shifts as in a static frame.

2.5. Experiment with Ions

In the last section of the chapter we briefly present a recent experiment on the trapping and cooling of ions [31]. This shall motivate enlarging some results to a Coulomb interaction.

To store the ions, a linear quadrupole trap is used. The trap is built of four equivalent cylindrical electrodes, each of them split into three parts. The electrodes are driven by a radio frequency voltage V_{rf} and a DC voltage V_{DC} plus an additional DC voltage V_{EC} at each of the end caps that provides confinement in the axial direction of Fig. 2.6. While the rf voltage is fixed, the latter can be tuned to transform the shape of the trapped ion cloud.

Theoretically, the motion of a particle in the quadrupole potential

$$\Phi(x, y, z, t) = \Phi(t)(x^2 + y^2 + z^2) \tag{2.44}$$

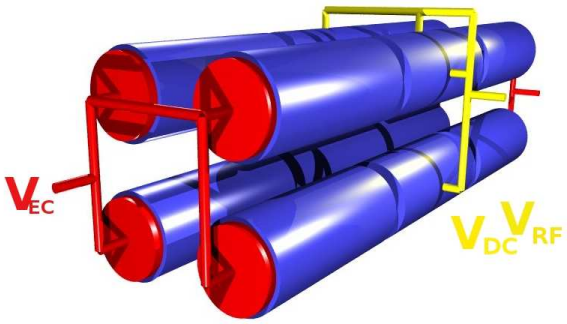

Fig. 2.6: Schematic picture of the quadrupole trap of Ref. [31] and the connection of the voltages.

leads with proper boundary conditions to the set of equations [32]

$$M\ddot{x} = Q\left(\frac{V_{\rm DC}+V_{\rm rf}\cos\Omega t}{r_0^2}-\kappa V_{\rm EC}\right)x\,, \tag{2.45}$$

$$M\ddot{y} = Q\left(-\frac{V_{\rm DC}+V_{\rm rf}\cos\Omega t}{r_0^2}-\kappa V_{\rm EC}\right)y\,, \tag{2.46}$$

$$M\ddot{z} = 2Q\kappa V_{\rm EC}z\,. \tag{2.47}$$

Here, r_0 is the distance from the center to the electrodes and κ is a parameter describing the trap geometry. The Eqs. (2.45)–(2.47) are special cases of the general Mathieu differential equation

$$\frac{d^2u(s)}{ds^2}+(a-2q\cos 2s)u(s)=0\,. \tag{2.48}$$

where a and q are the stability parameters. The equations (2.45)–(2.47) describe the motion in a fast oscillating field. This can be approximated by the motion of particles in an effective cylinder-symmetric potential [33] :

$$U_{\rm eff}(r,z)=\frac{M}{2}\left(\omega_{\rm r}^2r^2+\omega_{\rm z}^2z^2\right)\,. \tag{2.49}$$

The frequencies are connected by the trap parameters via

$$\omega_{\rm r}^2=\frac{Q^2V_{\rm rf}^2}{2M^2r_0^4\Omega^2}+\frac{QV_{\rm DC}}{Mr_0^2}-\frac{Q\kappa V_{\rm EC}}{M}\,,\qquad \omega_{\rm z}^2=\frac{2\kappa QV_{\rm EC}}{M}\,. \tag{2.50}$$

Numerical values of Ref. [31] are $V_{\rm rf}=380\,{\rm V}$, $\Omega=2\pi\cdot 14.2\,{\rm MHz}$, $r_0=4.3\,{\rm mm}$, $\kappa=3\cdot10^{-3}\,{\rm mm}^{-2}$, and $V_{\rm DC}=0-4\,{\rm V}$.

In the experiment, once the atoms are caught in the quadrupole trap experiment, they get ionized by an electron beam, and cooled down by the mutual interaction of $^4{\rm He}^+$ with

$^9Be^+$ which have previously been cooled by laser cooling. The possibility of cooling by the mutual interaction is limited by the mass ratio $M_{\mathrm{sc}}/M_{\mathrm{lc}} > 0.3$. Here, M_{sc} is the mass of the sympathetically cooled atoms and M_{lc} the one of the laser cooled ones. In Ref. [31] the ratio is $M_{\mathrm{sc}}/M_{\mathrm{lc}} = 0.44$. At a critical temperature, the atoms perform a phase transition from a plasma to a Wigner crystal [21]. Finally, the number of ions trapped, cooled, and crystallized that way are estimated to be about $6.2 \cdot 10^3$ of Beryllium and about 150 of Helium. The temperature of the crystallized ions is estimated less than 20 mK.

Although in this experiment the ions are fermions, there is no restriction to extend it to bosons as well. The only limit is given by the mass ratio.

3. Quantum Statistics of Non-Interacting Bose Gas

To give an introduction to many-body quantum statistics and to the functional integral method we use, we will first discuss the properties of the non-interacting Bose gas. As we already mentioned in the introduction, even without any interaction, a Bose gas undergoes a phase transition between the gas and the condensed state.

At first, we recall some properties of the grand-canonical ensemble and present its major thermodynamic quantities. Afterwards, we introduce the functional integral method which is a many-body generalization of the path integral formalism. To become familiar with this method, we calculate the critical temperature of the phase transition from a Bose gas to BEC within the semiclassical approximation in the last section of this chapter.

3.1. Grand-Canonical Ensemble

The quantum statistical properties of a dilute ideal Bose gas in equilibrium are conveniently described using the grand-canonical ensemble [34]. It is valid for a set of identical particles connected to a heat bath at equilibrium temperature and a particle basin. The most important quantity is the grand-canonical partition function

$$\mathcal{Z}(\beta,\mu) = \operatorname{Tr} e^{-\beta(H-\mu N)} \tag{3.1}$$

with the Hamiltonian H and the particle number operator N. μ is the chemical potential that governs the particle exchange and $\beta = 1/k_{\mathrm{B}}T$ the reciprocal temperature. The trace can be carried out with respect to any suitable set of eigenfunctions. The expectation values for some operator O is calculated via

$$\langle O\rangle = \frac{\operatorname{Tr}\left[O\, e^{-\beta(H-\mu N)}\right]}{\mathcal{Z}}\,. \tag{3.2}$$

The grand-canonical free energy is obtained by

$$\mathcal{F} = -\frac{1}{\beta}\ln\mathcal{Z}\,. \tag{3.3}$$

As a function of other thermodynamic quantities it is a double Legendre-transform of the internal energy U

$$\mathcal{F} = U - TS - \mu N\,. \tag{3.4}$$

Therefore, it allows to calculate entropy and particle number according to

$$S = -\left.\frac{\partial \mathcal{F}}{\partial T}\right|_{V,\mu}, \tag{3.5}$$

$$N = -\left.\frac{\partial \mathcal{F}}{\partial \mu}\right|_{V,T}. \tag{3.6}$$

This was just a short repetition of thermodynamics but now we will say how we execute calculations in detail.

3.2. Path Integral Formalism

Feynman's *path-integral formalism* [35] is an alternative way to the Schrödinger theory to describe one-particle quantum mechanics with an infinite number of ordinary integrals instead of operators. Here, we give only a brief review on the main aspects, as it is discussed in text books rather well [36]. Its idea was motivated by the double-slit experiment where a particle simultaneously passes both slits. So, if the entire space is thought of as a lattice with numerous slits, a particle could pass all slits at the same time and the effective path is a superposition of all possible paths. Therefore, the probability of propagation from space-time point $(x_\mathrm{a}, t_\mathrm{a})$ to $(x_\mathrm{b}, t_\mathrm{b})$ is given by a sum over all possible paths which reads in a shorthand notation

$$(x_\mathrm{b}\, t_\mathrm{b}|x_\mathrm{a}\, t_\mathrm{a}) = \int\limits_{x(t_\mathrm{a})=x_\mathrm{a}}^{x(t_\mathrm{b})=x_\mathrm{b}} \mathcal{D}'x \int \frac{\mathcal{D}p}{2\pi\hbar}\, e^{\imath\mathcal{A}[p,x]/\hbar} \tag{3.7}$$

with the action $\mathcal{A}$ that is a time integral of the Lagrange function:

$$\mathcal{A}[p,x] = \int\limits_{t_\mathrm{a}}^{t_\mathrm{b}} dt\, [p(t)\dot{q}(t) - H\,(p(t), x(t))]\,. \tag{3.8}$$

As the path integral is the probability of propagation, it is also possible to derive a quantum-mechanical partition function for one particle in this formalism by

$$Z = \int\limits_{-\infty}^{\infty} dx\,(x\, t_\mathrm{b}|x\, t_\mathrm{a}) = \oint \mathcal{D}x \int \frac{\mathcal{D}p}{2\pi\hbar} e^{\imath\mathcal{A}[p,x]/\hbar}\,, \tag{3.9}$$

where $\oint$ implies an averaging over all configurations with $x(t_\mathrm{a}) = x(t_\mathrm{b})$. To connect it to statistical mechanics, the "Wick-rotation" is introduced with a summation over all paths $x(t)$ which are periodic in imaginary time and the time distance

$$\tau = \imath t\,, \qquad t_\mathrm{b} - t_\mathrm{a} = -\imath\hbar\beta\,. \tag{3.10}$$

Herewith, the partition function becomes

$$Z = \oint \mathcal{D}x \int \frac{\mathcal{D}p}{2\pi\hbar}\, e^{-\mathcal{A}_\mathrm{e}[p,x]/\hbar}\,, \tag{3.11}$$

where the paths run along the imaginary time axis and the euclidean action $\mathcal{A}_\mathrm{e}$ reads

$$\mathcal{A}_\mathrm{e}[p,x] = \int_0^{\hbar\beta} d\tau\, [-\imath p(\tau)\dot{x}(\tau) + H(p(\tau),x(\tau))]\ . \tag{3.12}$$

3.3. Functional Integral Formalism

The introduced path integral can be generalized to a *functional integral* [37,38] that describes many-body systems. It amounts to replacing the space variables by corresponding fields. This is equivalent to second quantization where the former operators like $\hat{x}$, $\hat{p}, \ldots$ are replaced by field operators creating and annihilating particles. So, here we have the replacement $x \to \psi(x)$ and $p \to \psi^*(x)$. In the Wick rotated frame, we get the grand-canonical partition function

$$\mathcal{Z}^{(0)} = \oint \mathcal{D}\psi^*\, \mathcal{D}\psi\ e^{-\mathcal{A}^{(0)}[\psi^*,\psi]/\hbar}\,, \tag{3.13}$$

where the functional integral sums over all possible bosonical field configurations $\psi(\mathbf{x},\tau)$, $\psi^*(\mathbf{x},\tau)$ which are periodic in imaginary time, i.e., $\psi(\mathbf{x},0) = \psi(\mathbf{x},\hbar\beta)$, $\psi^*(\mathbf{x},0) = \psi^*(\mathbf{x},\hbar\beta)$. Therefore, we can treat the time-behaviour using a Matsubara decomposition of the fields

$$\psi(\mathbf{x},\tau) = \sum_{\mathbf{k}} \sum_{m=-\infty}^{\infty} c_{\mathbf{k}m}\psi_{\mathbf{k}}(\mathbf{x})\, e^{-\imath\omega_m\tau}\,, \qquad \psi^*(\mathbf{x},\tau) = \sum_{\mathbf{k}} \sum_{m=-\infty}^{\infty} c^*_{\mathbf{k}m}\psi^*_{\mathbf{k}}(\mathbf{x})\, e^{\imath\omega_m\tau}\,. \tag{3.14}$$

with the Matsubara frequencies

$$\omega_m = 2\pi m/\hbar\beta \tag{3.15}$$

and coefficients $c_{\mathbf{k}m}$, $c^*_{\mathbf{k}m}$. However, the spatial fields $\psi_{\mathbf{k}}(\mathbf{x})$ and $\psi^*_{\mathbf{k}}(\mathbf{x})$ are the eigenfunctions of the particular one-particle Schrödinger equations

$$\left[-\frac{\hbar^2}{2M}\Delta + V^{(\mathrm{ext})}(\mathbf{x})\right]\psi_{\mathbf{k}}(\mathbf{x}) = E_{\mathbf{k}}\psi_{\mathbf{k}}(\mathbf{x})\,, \tag{3.16}$$

$$\left[-\frac{\hbar^2}{2M}\Delta + V^{(\mathrm{ext})}(\mathbf{x})\right]\psi^*_{\mathbf{k}}(\mathbf{x}) = E_{\mathbf{k}}\psi^*_{\mathbf{k}}(\mathbf{x})\,, \tag{3.17}$$

where $\mathbf{k}$ labels the different quantum states. For common potentials, like a harmonic oscillator one, the eigenfunctions and energies are well-known.

Furthermore, the undisturbed *euclidean action* in (3.13) is defined by

$$\mathcal{A}^{(0)}[\psi^*,\psi] = \hbar \int_0^{\hbar\beta} d\tau \int_0^{\hbar\beta} d\tau' \int d^3x \int d^3x'\, \psi^*(\mathbf{x},\tau)\, G^{(0)\,-1}(\mathbf{x},\tau;\mathbf{x}',\tau')\, \psi(\mathbf{x}',\tau')\,, \quad (3.18)$$

with an integral kernel whose relevancy will become clear within this section

$$G^{(0)\,-1}(\mathbf{x},\tau;\mathbf{x}',\tau') = \frac{1}{\hbar}\,\delta(\mathbf{x}-\mathbf{x}')\delta(\tau-\tau')\,\left\{\hbar\frac{\partial}{\partial\tau} - \frac{\hbar^2}{2M}\,\mathbf{\Delta} + V^{(\mathrm{ext})}(\mathbf{x}) - \mu\right\}. \quad (3.19)$$

Here, M denotes the particle mass, $V^{(\mathrm{ext})}(\mathbf{x})$ the external trap potential, and μ the chemical potential.

To calculate the non-interacting partition function (3.13) we assume to know the energy spectrum of (3.16), (3.17). The functional integration over all possible bosonical fields in Eq. (3.13) corresponds to an integration over all possible coefficients $c_{\mathbf{k}m}$, $c^*_{\mathbf{k}m}$

$$\oint \mathcal{D}\psi^*\,\mathcal{D}\psi = \prod_{\mathbf{k}}\prod_{m=-\infty}^{\infty}\frac{1}{2\pi}\int dc^*_{\mathbf{k}m}dc_{\mathbf{k}m}. \quad (3.20)$$

Thus the new partition function reads

$$\mathcal{Z}^{(0)} = \prod_{\mathbf{k}}\prod_{m=-\infty}^{\infty}\frac{1}{2\pi}\int dc^*_{\mathbf{k}m}dc_{\mathbf{k}m}\exp\left[-\beta\left(-\imath\hbar\omega_m + E_{\mathbf{k}} - \mu\right)|c_{\mathbf{k}m}|^2\right]. \quad (3.21)$$

To carry out the integration we decompose the $c_{\mathbf{k}m}$, $c^*_{\mathbf{k}m}$ into real and imaginary parts:

$$c_{\mathbf{k}m} = a_{\mathbf{k}m} + \imath b_{\mathbf{k}m}\,, \quad (3.22)$$

$$c^*_{\mathbf{k}m} = a_{\mathbf{k}m} - \imath b_{\mathbf{k}m}. \quad (3.23)$$

With a factor 2 from the Jacobian of the transformation (3.22), (3.23), we get

$$\mathcal{Z}^{(0)} = \prod_{\mathbf{k}}\prod_{m=-\infty}^{\infty}\frac{1}{\pi}\int da_{\mathbf{k}m}db_{\mathbf{k}m}\exp\left[-\beta\left(-\imath\hbar\omega_m + E_{\mathbf{k}} - \mu\right)\left(a^2_{\mathbf{k}m} + b^2_{\mathbf{k}m}\right)\right] \quad (3.24)$$

which is the product of two Gaussian integrals and leads to the final result of the partition function

$$\mathcal{Z}^{(0)} = \prod_{\mathbf{k}}\prod_{m=-\infty}^{\infty}\left[\beta\left(-\imath\hbar\omega_m + E_{\mathbf{k}} - \mu\right)\right]^{-1}. \quad (3.25)$$

The expectation (3.2) in the functional integral formalism for non-interacting particles reads

$$\langle\, \text{☆} \,\rangle = \frac{1}{\mathcal{Z}^{(0)}}\oint \mathcal{D}\psi^*\,\mathcal{D}\psi\ \text{☆}\, e^{-\mathcal{A}^{(0)}[\psi^*,\psi]/\hbar}. \quad (3.26)$$

An important expectation value is the correlation of two fields, denoted by the *correlation function or propagator* $G^{(0)}(\mathbf{x},\tau;\mathbf{x}',\tau')$:

$$G^{(0)}(\mathbf{x},\tau;\mathbf{x}',\tau') = \frac{1}{\mathcal{Z}^{(0)}} \oint \mathcal{D}\psi^* \, \mathcal{D}\psi \; \psi(\mathbf{x},\tau)\psi^*(\mathbf{x}',\tau') \, e^{-\mathcal{A}^{(0)}[\psi^*,\psi]/\hbar} \,. \tag{3.27}$$

It obeys the integral equation

$$\int_0^{\hbar\beta} d\tau'' \int d^D x'' G^{(0)-1}(\mathbf{x},\tau;\mathbf{x}'',\tau'') G^{(0)}(\mathbf{x}'',\tau'';\mathbf{x}',\tau') = \delta(\tau-\tau')\delta(\mathbf{x}-\mathbf{x}') \,, \tag{3.28}$$

while the inverse of the correlation function turns out to be just the integral kernel (3.19). Because the calculation of the propagator is rather technical, it is relegated to Appendix A.2.

The grand-canonical free energy follows from (3.25) according to (3.3) and is calculated in Appendix A.1, but we basically use the semiclassical expressions of these quantities explained in the next section.

3.4. Semiclassical Approximation

The semiclassical approximation is based on the (classical) assumption that $\hbar$ is small so that all states are that narrowly distributed that they can be described as a continuum [36]. So, instead of a sum of all discrete quantum states that is somehow difficult to work with in the particular case, we simply extract the quantum-mechanical ground state and describe all excited states by a classical Hamilton function. Now, instead of the sum we obtain a classical phase space integration. For simplicity the ground-state energy is grasped by the chemical potential:

$$E_{\mathbf{n}} \to H(\mathbf{p},\mathbf{x}), \qquad \sum_{\mathbf{n}} \to \int \frac{d^D p}{(2\pi\hbar)^D}, \qquad \mu \to \mu - E_0 \,. \tag{3.29}$$

The semiclassical approximation is physically related to the thermodynamical limit. As we will see at the end of this chapter, the critical temperature is related to the particle number via $T \propto N^{1/3}$. The approximation is valid as long as the quantum energy $\hbar\omega$ is much smaller than the thermal energy $1/\beta$: $\hbar\omega\beta \ll 1$.

3.4.1. Non-Interacting Propagator

The result of the quantum-mechanical propagator (A.22) can be approximated within the semiclassical regime. To this end, we treat the one-particle wave functions $\psi_{\mathbf{k}}(\mathbf{x})$ and $\psi^*_{\mathbf{k}}(\mathbf{x})$ as plane waves with wave vector $\mathbf{k} = \mathbf{p}/\hbar$ and replace the trap potential $V^{(\mathrm{ext})}(\mathbf{x})$

in the Hamilton function by its value at the mean distance between start and end points [36,37]:

$$G^{(0)}(\mathbf{x},\tau;\mathbf{x}',\tau') = \int \frac{d^3p}{(2\pi\hbar)^3}\, e^{\imath\,\mathbf{p}(\mathbf{x}-\mathbf{x}')/\hbar} \left\{ \Theta(\tau-\tau') \sum_{n=0}^{\infty} e^{-\frac{1}{\hbar}\left[\frac{\mathbf{p}^2}{2M}+V^{(\mathrm{ext})}\left(\frac{\mathbf{x}+\mathbf{x}'}{2}\right)-\mu\right](\tau-\tau'+n\hbar\beta)} \right.$$
$$\left. + \Theta(\tau'-\tau) \sum_{n=1}^{\infty} e^{-\frac{1}{\hbar}\left[\frac{\mathbf{p}^2}{2M}+V^{(\mathrm{ext})}\left(\frac{\mathbf{x}+\mathbf{x}'}{2}\right)-\mu\right](\tau-\tau'+n\hbar\beta)} \right\}. \tag{3.30}$$

For equal imaginary times, the propagator is defined as the limit of $\tau' \downarrow \tau$ according to (A.22):

$$G^{(0)}(\mathbf{x},\tau;\mathbf{x}',\tau) = \int \frac{d^3p}{(2\pi\hbar)^3}\, e^{\imath\,\mathbf{p}(\mathbf{x}-\mathbf{x}')/\hbar} \sum_{n=1}^{\infty} e^{-\frac{1}{\hbar}\left[\frac{\mathbf{p}^2}{2M}+V^{(\mathrm{ext})}\left(\frac{\mathbf{x}+\mathbf{x}'}{2}\right)-\mu\right](\tau-\tau'+n\hbar\beta)}. \tag{3.31}$$

3.4.2. Grand-Canonical Free Energy

Starting from Eq. (A.10), we can derive a semiclassical expression for the free energy as well. As the free energy is related to the trace of the propagator according to (A.12), we also have to integrate over the real space in addition to the semiclassical rules. With the expansion of the logarithm, we get from (A.10)

$$\mathcal{F}^{(0)} = -\frac{1}{\beta}\sum_{n=1}^{\infty}\frac{1}{n}\int d^3x \int \frac{d^3p}{(2\pi\hbar)^3}\, \exp\left\{-n\beta\left[\frac{\mathbf{p}^2}{2m}+V^{(\mathrm{ext})}(\mathbf{x})-\mu\right]\right\}. \tag{3.32}$$

At this place, we specialize to a gas confined in a harmonic trapping potential

$$V^{(\mathrm{ext})}(\mathbf{x}) = \frac{M}{2}\sum_i \omega_i^2 x_i^2\,. \tag{3.33}$$

Because all integrals become Gaussian, we can state the result

$$\mathcal{F}^{(0)} = -\frac{1}{\beta\left(\hbar\beta\tilde{\omega}\right)^3}\zeta_4\left(e^{\beta\mu}\right). \tag{3.34}$$

Here, we used the geometric mean of the trap frequencies

$$\tilde{\omega} = \left(\omega_1\omega_2\omega_3\right)^{1/3} \tag{3.35}$$

and the summation was abbreviated by

$$\zeta_a(z) = \sum_{n=1}^{\infty}\frac{z^n}{n^a} \tag{3.36}$$

which is called polylogarithmic function.

3.5. T_c-Shift in Non-Interacting Gas

Because of two reasons we calculate the shift of the critical temperature of the non-interacting gas in a harmonic trap. First of all, it is a good application of the derived theory and the semiclassical approximation. And secondly, because we will need the result in the later discussion.

Since we would like to calculate a quantity in the critical region, we first need to know what is the criterion for the critical phenomenon. A phase transition comes along with enormous fluctuations. Thus, the correlation (3.27) between particles diverges. This divergence in $G^{(0)}$ coincides with the vanishing of $G^{(0)-1}$. For this purpose, we use the semiclassical result for the propagator (3.30) and calculate its Fourier-Matsubara transform which is easier to handle:

$$G^{(0)}(\mathbf{p},\omega_m;\mathbf{x}) = \int_0^{\hbar\beta} d\tau\, e^{\imath\omega_m\tau} \int d^D x'\, e^{-\imath\mathbf{p}\mathbf{x}'/\hbar}\, G^{(0)}\left(\mathbf{x}+\frac{\mathbf{x}'}{2},\tau;\mathbf{x}-\frac{\mathbf{x}'}{2},0\right). \tag{3.37}$$

The τ-integration permits only the first Heavyside-function to be non-zero. The integrations are performed in a standard way to give

$$G^{(0)}(\mathbf{p},\omega_m;\mathbf{x}) = -\hbar\sum_{n=0}^{\infty} e^{-n\beta\left[V^{(\mathrm{ext})}(\mathbf{x})-\mu+\frac{\mathbf{p}^2}{2M}\right]} \frac{e^{-\beta\left[-\imath\hbar\omega_m+V^{(\mathrm{ext})}(\mathbf{x})-\mu+\frac{\mathbf{p}^2}{2M}\right]}-1}{-\imath\hbar\omega_m+V^{(\mathrm{ext})}(\mathbf{x})-\mu+\frac{\mathbf{p}^2}{2M}}. \tag{3.38}$$

The summation over n is simply a geometric series, that cancels the last factor except for the term $e^{\imath\beta\hbar\omega_m}$, which is exactly 1 by definition of the Matsubara frequencies (3.15). So, we get the simple result

$$G^{(0)}(\mathbf{p},\omega_m;\mathbf{x}) = \frac{\hbar}{-\imath\hbar\omega_m+\frac{\mathbf{p}^2}{2M}+V^{(\mathrm{ext})}(\mathbf{x})-\mu}\,. \tag{3.39}$$

Obviously, (3.39) represents the functional inverse of the semiclassical analogon of the integral kernel (3.19). Of course this integral kernel vanishes at the critical point, where the correlation function (3.39) diverges due to the integral relation (3.28). That means in the semiclassical approximation for the Fourier-Matsubara transform of (3.19)

$$\hbar G^{(0)-1}(\mathbf{p},\omega_m;\mathbf{x}) = -\imath\hbar\omega_m+\frac{\mathbf{p}^2}{2M}+V^{(\mathrm{ext})}(\mathbf{x})-\mu = 0\,. \tag{3.40}$$

But this equation can only be fulfilled for vanishing momentum $\mathbf{p}=\mathbf{0}$ as well as Matsubara frequency $\omega_m = 0$ at the critical chemical potential

$$\mu_c^{(0)} = \min_{\mathbf{x}} V^{(\mathrm{ext})}(\mathbf{x})\,. \tag{3.41}$$

In the case of a harmonic trap (3.33), Eq. (3.41) reduces to

$$\mu_c^{(0)} = 0\,. \tag{3.42}$$

In order to get an equation for the critical temperature, we keep the particle number fixed, use relation (3.6) and apply it on the semiclassical result of the free energy (3.34):

$$N = \frac{1}{(\hbar\beta\tilde{\omega})^3}\,\zeta_3\left(e^{\beta\mu}\right)\,. \tag{3.43}$$

But N is the total number of particles and on the right-hand side of (3.43) we have only the semiclassical result of the free energy. Therefore, this theory is only valid if it approaches the critical point from above. The transition temperature is obtained by plugging the critical chemical potential (3.42) into (3.43):

$$T_c^{(0)} = \frac{\hbar\tilde{\omega}}{k_B}\left[\frac{N}{\zeta(3)}\right]^{1/3}\,. \tag{3.44}$$

The value of the appearing Riemann zeta-function

$$\zeta(a) = \sum_{n=1}^{\infty}\frac{1}{n^a} \tag{3.45}$$

is $\zeta(3) = 1.20206$. We see that we get the proportionality between temperature T and the cubic root of the particle number $N^{1/3}$ which was mentioned in Section 3.4.

To give an impression of the size of the transition temperature we use numerical values from a recent experiment [39] where the critical temperature of a weakly interacting gas is measured. About 10^6 ^{87}Rb atoms are caught in a cylindrically-symmetric harmonic trap driven by $\omega_\mathrm{r} = 2\pi\cdot 413\,\mathrm{Hz}$ and $\omega_\mathrm{z} = 2\pi\cdot 8.69\,\mathrm{Hz}$. The resulting temperature is $T_c^{(0)} = 514\,\mathrm{nK}$. The derivation of the critical temperature was done using the semiclassical approximation. To improve the result, quantum corrections have to be taken into account. The first contribution is the finite-size correction from Refs. [40–43]:

$$\left(\frac{\Delta T_\mathrm{c}}{T_\mathrm{c}^{(0)}}\right)_\mathrm{FS} = -\frac{\zeta(2)\bar{\omega}}{2\zeta(3)^{2/3}\tilde{\omega}N^{1/3}}\,. \tag{3.46}$$

Here, $\bar{\omega} = (\omega_1+\omega_2+\omega_3)/3$ is the arithmetic mean of the trap frequencies. The name "finite-size" bases on the fact that it is proportional to $N^{-1/3}$. We also point out that it is independent of the trapping frequencies in the case of an isotropic trap. For our example the temperature is shifted 9 nK downwards, i.e., about 1.8%. Further corrections appear due to the interactions which will be the topic of Chapter 7.

4. Hartree-Fock Mean-Field Theory

After the presentation of the main properties of the non-interacting Bose gas we will now include interactions. As we said before in the introduction, Bose gases are that dilute that only two-particle interactions have to be taken into account. We will treat the interaction using the background method to derive a self-consistent Hartree-Fock mean field theory, [44–46].

In the previous chapter we showed how to treat the interaction-free gas exactly within the functional integral formalism. The problem with the interaction is a term quartic in the fields of the action. Actually, we are only able to solve Gaussian-like integrals. Therefore, we have to approximate the quartic part in a way to reduce it to a quadratic form. One way could be a Hubbard-Stratonovich transformation [47,48], where the bilocality of the interaction is switched to a local form with help of an auxiliary field. We attempted to treat the system this way but the method has some ambiguity that does not reproduce the three different interaction channels of Hartree, Fock, and Bogoliubov properly. In fact, e.g., instead of the Hartree and Fock channel one gets only one single channel. In the case of a contact interaction this is expressed by a missing factor "2" [49] but it has even more crucial impacts for other interactions.

Therefore, we use the background method that will be explained in the subsequent section to differ terms describing either the condensate or the thermal fluctuations. To simplify the quartic interaction term, we apply a Gaussian approximation that reduces the quartic interaction term to a quadratic form which can be treated within the functional integral formalism. Therefrom, we derive a system of two coupled equations determining the background fields and the fluctuations. In the posterior part of this chapter, we solve the system in first-order perturbation theory.

4.1. Background Method and Order Parameter

An excellent way to distinguish theoretically between different phases and to describe transitions between them is the introduction of an order parameter. A rather simple example is to differ the gas, liquid, and solid phase of water. Here, it is obvious that the phases are characterized by their particular density which is therefore a convenient order parameter. Another more sophisticated example is the transition from a ferromagnet to a paramagnet in the famous Ising-model. So called "spins" on every lattice site can adopt the values $+1$ (up) or -1 (down). Now, the order parameter is the average alignment of

all spins $\langle \mathbf{m} \rangle$. A value of the order of 1 describes the ferromagnetic phase, that means a majority is aligned into the same direction, whereas $\langle \mathbf{m} \rangle = 0$ characterizes the paramagnet. The order parameter is usually temperature-dependent and the temperature at the point of the transition is called critical temperature. A further feature of phase transitions is the breaking of symmetry. In the present example, the spins are symmetrically distributed in up and down in the paramagnetic state but at the transition this symmetry is broken and the distribution becomes inequitable.

So what is the order parameter in BEC? The transition occurs between the gas phase and the condensate phase and the characteristic of the BEC state is a macroscopic occupation of the ground state. The order parameter is properly introduced using the background method [36,50,51]. In detail, the periodic fields (3.14) are decomposed into the background field Ψ and a fluctuating contribution $\delta\psi$

$$\psi(\mathbf{x},\tau) = \Psi(\mathbf{x},\tau) + \delta\psi(\mathbf{x},\tau)\,, \qquad \psi^*(\mathbf{x},\tau) = \Psi^*(\mathbf{x},\tau) + \delta\psi^*(\mathbf{x},\tau)\,. \tag{4.1}$$

The background fields are constant with respect to the functional integration but can depend on space and time arguments. The fluctuating fields carry the thermal behaviour and the integral measure transforms

$$\oint \mathcal{D}\psi \to \oint \mathcal{D}\delta\psi\,, \qquad \oint \mathcal{D}\psi^* \to \oint \mathcal{D}\delta\psi^*\,. \tag{4.2}$$

In the former treatment, the expectation of $\langle\psi\rangle$ would have simply vanished due to symmetry reasons. But now, the $U(1)$ symmetry of the phase is broken and the expectation yields according to (3.26)

$$\langle\psi\rangle = \frac{1}{\mathcal{Z}^{(0)}} \oint \mathcal{D}\delta\psi^*\,\mathcal{D}\delta\psi\;\; (\Psi + \delta\psi)\, e^{-\mathcal{A}^{(0)}[\delta\psi^*,\delta\psi,\Psi^*,\Psi]/\hbar} = \Psi\,. \tag{4.3}$$

Although we used the non-interacting expectation in (4.3), we will see in the subsequent section that this expectation (4.3) remains valid in the interacting case. Hence, the background fields of (4.1) will become the *order parameter* of BEC defined by

$$\langle\psi(\mathbf{x},\tau)\rangle = \begin{cases} 0 & \text{gas phase} \\ \Psi(\mathbf{x},\tau) & \text{condensed phase}\,. \end{cases} \tag{4.4}$$

Here, the order parameter is normalized to the number of condensed particles

$$\int d^D x\, |\Psi(\mathbf{x},\tau)|^2 = N_0\,. \tag{4.5}$$

This also implies that N_0 becomes of the order of the total number of particles N in the BEC state and hence, it signals a macroscopic occupation. The formulation using the background method is equivalent to the Bogoliubov approximation in second quantization.

4.2. Derivation of Mean-Field Theory

In this chapter, we derive a Hartree-Fock mean-field theory using the background method. We start with the grand-canonical partition function for interacting bosons

$$\mathcal{Z} = \oint \mathcal{D}\psi^* \oint \mathcal{D}\psi \exp\left\{-\frac{1}{\hbar}\mathcal{A}[\psi,\psi^*]\right\}, \tag{4.6}$$

where the action consists of the free action (3.18), (3.19) and a new contribution due to the interaction

$$\mathcal{A}[\psi,\psi^*] = \mathcal{A}^{(0)}[\psi,\psi^*] + \mathcal{A}^{(\mathrm{int})}[\psi,\psi^*]\ . \tag{4.7}$$

The interaction contribution reads

$$\mathcal{A}^{(\mathrm{int})}[\psi,\psi^*] = \frac{1}{2}\int_0^{\hbar\beta} d\tau \int d^Dx \int d^Dx'\, V^{(\mathrm{int})}(\mathbf{x},\mathbf{x}')\,\psi^*(\mathbf{x},\tau)\psi^*(\mathbf{x}',\tau)\psi(\mathbf{x},\tau)\psi(\mathbf{x}',\tau)\,. \tag{4.8}$$

The latter one is quartic in the fields and therefore, the functional integral is not a Gaussian integral any more. Now, we apply the background method (4.1) to separate the action into background fields that describe the condensate and the fluctuating fields. For the non-interacting action, we get

$$\begin{aligned}
\mathcal{A}^{(0)} \;=\; & \int_0^{\hbar\beta} d\tau \int d^Dx \left\{\Psi^*(\mathbf{x},\tau)\left[\hbar\frac{\partial}{\partial\tau} - \frac{\hbar^2}{2M}\Delta + V^{(\mathrm{ext})}(\mathbf{x}) - \mu\right]\Psi(\mathbf{x},\tau)\right. \\
& + \int_0^{\hbar\beta} d\tau \int d^Dx \left\{\Psi^*(\mathbf{x},\tau)\left[\hbar\frac{\partial}{\partial\tau} - \frac{\hbar^2}{2M}\Delta + V^{(\mathrm{ext})}(\mathbf{x}) - \mu\right]\delta\psi(\mathbf{x},\tau)\right. \\
& + \int_0^{\hbar\beta} d\tau \int d^Dx \left\{\delta\psi^*(\mathbf{x},\tau)\left[\hbar\frac{\partial}{\partial\tau} - \frac{\hbar^2}{2M}\Delta + V^{(\mathrm{ext})}(\mathbf{x}) - \mu\right]\Psi(\mathbf{x},\tau)\right. \\
& + \int_0^{\hbar\beta} d\tau \int d^Dx \left\{\delta\psi^*(\mathbf{x},\tau)\left[\hbar\frac{\partial}{\partial\tau} - \frac{\hbar^2}{2M}\Delta + V^{(\mathrm{ext})}(\mathbf{x}) - \mu\right]\delta\psi(\mathbf{x},\tau)\,.
\end{aligned} \tag{4.9}$$

For the interacting action, we collect all terms of the same power in the fluctuating fields. Herewith, we get the result

$$\begin{aligned}
\mathcal{A}^{(\mathrm{int})} &= \frac{1}{2}\int_0^{\hbar\beta} d\tau \int d^D x \int d^D x'\, V^{(\mathrm{int})}(\mathbf{x},\mathbf{x}') \qquad (4.10)\\
&\times \Big[\Psi(\mathbf{x},\tau)\Psi\left(\mathbf{x}',\tau\right)\delta\psi^*\left(\mathbf{x}',\tau\right)\Psi^*(\mathbf{x},\tau) + \Psi(\mathbf{x},\tau)\Psi\left(\mathbf{x}',\tau\right)\delta\psi^*(\mathbf{x},\tau)\Psi^*\left(\mathbf{x}',\tau\right)\\
&+ \delta\psi\left(\mathbf{x}',\tau\right)\Psi(\mathbf{x},\tau)\Psi^*\left(\mathbf{x}',\tau\right)\Psi^*(\mathbf{x},\tau) + \delta\psi(\mathbf{x},\tau)\Psi\left(\mathbf{x}',\tau\right)\Psi^*\left(\mathbf{x}',\tau\right)\Psi^*(\mathbf{x},\tau)\\
&+ \Psi(\mathbf{x},\tau)\Psi\left(\mathbf{x}',\tau\right)\delta\psi^*(\mathbf{x},\tau)\delta\psi^*\left(\mathbf{x}',\tau\right) + \delta\psi\left(\mathbf{x}',\tau\right)\Psi(\mathbf{x},\tau)\Psi^*(\mathbf{x},\tau)\delta\psi^*\left(\mathbf{x}',\tau\right)\\
&+ \delta\psi(\mathbf{x},\tau)\Psi\left(\mathbf{x}',\tau\right)\Psi^*(\mathbf{x},\tau)\delta\psi^*\left(\mathbf{x}',\tau\right) + \delta\psi\left(\mathbf{x}',\tau\right)\Psi(\mathbf{x},\tau)\delta\psi^*(\mathbf{x},\tau)\Psi^*\left(\mathbf{x}',\tau\right)\\
&+ \delta\psi(\mathbf{x},\tau)\Psi\left(\mathbf{x}',\tau\right)\delta\psi^*(\mathbf{x},\tau)\Psi^*\left(\mathbf{x}',\tau\right) + \delta\psi(\mathbf{x},\tau)\delta\psi\left(\mathbf{x}',\tau\right)\Psi^*(\mathbf{x},\tau)\Psi^*\left(\mathbf{x}',\tau\right)\\
&+ \delta\psi\left(\mathbf{x}',\tau\right)\Psi(\mathbf{x},\tau)\delta\psi^*(\mathbf{x},\tau)\delta\psi^*\left(\mathbf{x}',\tau\right) + \delta\psi(\mathbf{x},\tau)\Psi\left(\mathbf{x}',\tau\right)\delta\psi^*(\mathbf{x},\tau)\delta\psi^*\left(\mathbf{x}',\tau\right)\\
&+ \delta\psi(\mathbf{x},\tau)\delta\psi\left(\mathbf{x}',\tau\right)\Psi^*(\mathbf{x},\tau)\delta\psi^*\left(\mathbf{x}',\tau\right) + \delta\psi(\mathbf{x},\tau)\delta\psi\left(\mathbf{x}',\tau\right)\delta\psi^*(\mathbf{x},\tau)\Psi^*\left(\mathbf{x}',\tau\right)\\
&+ \delta\psi(\mathbf{x},\tau)\delta\psi\left(\mathbf{x}',\tau\right)\delta\psi^*(\mathbf{x},\tau)\delta\psi^*\left(\mathbf{x}',\tau\right) + \Psi(\mathbf{x},\tau)\Psi\left(\mathbf{x}',\tau\right)\Psi^*(\mathbf{x},\tau)\Psi^*\left(\mathbf{x}',\tau\right)\Big].
\end{aligned}$$

If we combine the two actions (4.9) and (4.10), we get terms from zeroth to fourth order in the fluctuating fields. The main aim is to reduce the cubic and quartic terms to a quadratic form in the fields. Therefore, we use as an approximation a Gaussian factorization [44] that can also be understood from a variational approach [52]. In contrast to the usual Wick rule for the expectation value of creation and annihilation operators, here, terms have to be subtracted from the Lagrangian, too. The reason is to keep the left- and right-hand side expectations equal. The expectation is defined analogous to (3.26) as

$$\langle\, \bigstar \,\rangle = \mathcal{Z}^{-1}\oint \mathcal{D}\delta\psi^* \oint \mathcal{D}\delta\psi \;\; \bigstar\, e^{-\mathcal{A}[\delta\psi^*,\delta\psi,\Psi,\Psi^*]/\hbar}\,. \qquad (4.11)$$

Applying the Gaussian factorization, the product of three fluctuating fields becomes

$$\begin{aligned}
\delta\psi^*(\mathbf{x},\tau)\delta\psi(\mathbf{x},\tau)\delta\psi(\mathbf{x}',\tau) \;\approx\; & \langle\delta\psi^*(\mathbf{x},\tau)\delta\psi(\mathbf{x},\tau)\rangle\delta\psi(\mathbf{x}',\tau) + \langle\delta\psi^*(\mathbf{x},\tau)\delta\psi(\mathbf{x}',\tau)\rangle\delta\psi(\mathbf{x},\tau)\\
& + \langle\delta\psi(\mathbf{x},\tau)\delta\psi(\mathbf{x}',\tau)\rangle\delta\psi^*(\mathbf{x},\tau) \qquad (4.12)
\end{aligned}$$

and the quartic part reads

$$\begin{aligned}
&\delta\psi^*(\mathbf{x},\tau)\delta\psi^*(\mathbf{x}',\tau)\delta\psi(\mathbf{x},\tau)\delta\psi(\mathbf{x}',\tau)\\
&\quad\approx \langle\delta\psi^*(\mathbf{x},\tau)\delta\psi(\mathbf{x},\tau)\rangle\delta\psi^*(\mathbf{x}',\tau)\delta\psi(\mathbf{x}',\tau) + \langle\delta\psi^*(\mathbf{x},\tau)\delta\psi(\mathbf{x}',\tau)\rangle\delta\psi^*(\mathbf{x}',\tau)\delta\psi(\mathbf{x},\tau)\\
&\quad+ \langle\delta\psi^*(\mathbf{x}',\tau)\delta\psi(\mathbf{x},\tau)\rangle\delta\psi^*(\mathbf{x},\tau)\delta\psi(\mathbf{x}',\tau) + \langle\delta\psi^*(\mathbf{x}',\tau)\delta\psi(\mathbf{x}',\tau)\rangle\delta\psi^*(\mathbf{x},\tau)\delta\psi(\mathbf{x},\tau)\\
&\quad+ \langle\delta\psi^*(\mathbf{x},\tau)\delta\psi^*(\mathbf{x},\tau)\rangle\delta\psi(\mathbf{x}',\tau)\delta\psi(\mathbf{x}',\tau) + \langle\delta\psi(\mathbf{x},\tau)\delta\psi(\mathbf{x}',\tau)\rangle\delta\psi^*(\mathbf{x},\tau)\delta\psi^*(\mathbf{x}',\tau)\\
&\quad- \langle\delta\psi^*(\mathbf{x}',\tau)\delta\psi(\mathbf{x},\tau)\rangle\langle\delta\psi^*(\mathbf{x},\tau)\delta\psi(\mathbf{x}',\tau)\rangle - \langle\delta\psi^*(\mathbf{x}',\tau)\delta\psi(\mathbf{x}',\tau)\rangle\langle\delta\psi^*(\mathbf{x},\tau)\delta\psi(\mathbf{x},\tau)\rangle\\
&\quad- \langle\delta\psi(\mathbf{x},\tau)\delta\psi(\mathbf{x}',\tau)\rangle\langle\delta\psi^*(\mathbf{x},\tau)\delta\psi^*(\mathbf{x}',\tau)\rangle\,.
\end{aligned} \qquad (4.13)$$

As the expectation of two fields in the action is not affected by the functional integration in the partition function, we see that the Gaussian approximation decomposes the action into one part independent of the fluctuating fields and parts depending on one or the product of two fluctuating fields. So, the action (4.7) becomes

$$\mathcal{A}[\delta\psi,\delta\psi^*,\Psi,\Psi^*]=\mathcal{A}_{\mathrm{BG}}\left[\Psi,\Psi^*\right]+\mathcal{A}^{(1)}\left[\delta\psi,\delta\psi^*,\Psi,\Psi^*\right]+\mathcal{A}^{(2)}\left[\delta\psi,\delta\psi^*,\Psi,\Psi^*\right]. \quad (4.14)$$

We do not write down the different contributions of (4.14) but first simplify it. The background method is related to the saddle-point approximation with the background field Ψ located at the saddle point. Therefore, terms carrying only one fluctuating field $\delta\psi$ vanish, so we can neglect the term $\mathcal{A}^{(1)}\left[\delta\psi,\delta\psi^*\right]$. Furthermore, we restrict ourselves to a Hartree-Fock theory. This takes into account Hartree or direct terms that consist of two fields with equal spatio-temporal arguments $\delta\psi^*(\mathbf{x},\tau)\delta\psi(\mathbf{x},\tau)$. And further, we include Fock or exchange terms with different arguments $\delta\psi^*(\mathbf{x}',\tau)\delta\psi(\mathbf{x},\tau)$. But we neglect anomalous fluctuations, which are of the form $\delta\psi\delta\psi$, $\delta\psi^*\delta\psi^*$. Those would be only essential, if we would work out a Hartree-Fock-Bogoliubov theory. Combining the contributions to the action (4.14), we obtain

$$\mathcal{A}[\delta\psi,\delta\psi^*,\Psi,\Psi^*]=\mathcal{A}_{\mathrm{BG}}\left[\Psi,\Psi^*\right]+\mathcal{A}^{(2)}\left[\delta\psi,\delta\psi^*,\Psi,\Psi^*\right]. \quad (4.15)$$

Now, we introduce for the expectation of two fields the correlation function or propagator

$$g\left(\mathbf{x},\tau;\mathbf{x}',\tau'\right)=\left\langle\delta\psi(\mathbf{x},\tau)\delta\psi^*(\mathbf{x}',\tau')\right\rangle. \quad (4.16)$$

Herewith, the first term of (4.15) is the background action independent of the fluctuating fields

$$\begin{aligned}\mathcal{A}_{\mathrm{BG}} &= \int_0^{\hbar\beta}d\tau\int d^Dx\,\Psi^*(\mathbf{x},\tau)\left[\hbar\frac{\partial}{\partial\tau}-\frac{\hbar^2}{2M}\Delta+V^{(\mathrm{ext})}(\mathbf{x})-\mu\right]\Psi(\mathbf{x},\tau)\\ &\quad+\frac{1}{2}\int_0^{\hbar\beta}d\tau\int d^Dx\int d^Dx'\,V^{(\mathrm{int})}(\mathbf{x},\mathbf{x}')\Big[\Psi^*(\mathbf{x},\tau)\Psi^*(\mathbf{x}',\tau)\Psi(\mathbf{x},\tau)\Psi(\mathbf{x}',\tau)\\ &\quad-g\left(\mathbf{x}',\tau;\mathbf{x}',\tau\right)g\left(\mathbf{x},\tau;\mathbf{x},\tau\right)-g\left(\mathbf{x}',\tau;\mathbf{x},\tau\right)g\left(\mathbf{x},\tau;\mathbf{x}',\tau\right)\Big], \quad (4.17)\end{aligned}$$

and the second one describes the thermal fluctuations and is quadratic in the respective fields

$$\begin{aligned}\mathcal{A}^{(2)} &= \int_0^{\hbar\beta}d\tau\int d^Dx\,\delta\psi^*(\mathbf{x},\tau)\left[\hbar\frac{\partial}{\partial\tau}-\frac{\hbar^2}{2M}\Delta+V^{(\mathrm{ext})}(\mathbf{x})-\mu\right]\delta\psi(\mathbf{x},\tau) \quad (4.18)\\ &\quad+\int_0^{\hbar\beta}d\tau\int d^Dx\int d^Dx'\,V^{(\mathrm{int})}(\mathbf{x},\mathbf{x}')\Big\{\delta\psi^*(\mathbf{x}',\tau)\delta\psi(\mathbf{x}',\tau)\big[\Psi^*(\mathbf{x},\tau)\Psi(\mathbf{x},\tau)\\ &\quad+g\left(\mathbf{x},\tau;\mathbf{x},\tau\right)\big]+\delta\psi^*(\mathbf{x}',\tau)\delta\psi(\mathbf{x},\tau)\big[\Psi^*(\mathbf{x},\tau)\Psi(\mathbf{x}',\tau)+g\left(\mathbf{x},\tau;\mathbf{x}',\tau\right)\big]\Big\}.\end{aligned}$$

For the calculation of expectation values (4.11), we can use the fact that $\mathcal{A}_{\mathrm{BG}}$ does not depend on the fluctuating fields and simply drops out. Therefore, instead using the full action, we can write the expectation with respect to the action $\mathcal{A}^{(2)}$ as

$$\langle \, \bigstar \, \rangle = \tilde{\mathcal{Z}}^{-1} \oint \mathcal{D}\delta\psi^* \oint \mathcal{D}\delta\psi \;\; \bigstar \, e^{-\mathcal{A}^{(2)}[\delta\psi^*,\delta\psi,\Psi,\Psi^*]/\hbar} \,, \tag{4.19}$$

where the partition function is defined as

$$\tilde{\mathcal{Z}} = \oint \mathcal{D}\delta\psi^* \oint \mathcal{D}\delta\psi \, e^{-\mathcal{A}^{(2)}[\delta\psi^*,\delta\psi,\Psi,\Psi^*]/\hbar} \,. \tag{4.20}$$

The full partition function and (4.20) are connected by

$$\mathcal{Z} = e^{-\mathcal{A}_{\mathrm{BG}}[\Psi,\Psi^*]/\hbar} \;\; \tilde{\mathcal{Z}} \,. \tag{4.21}$$

Comparing the correlation functions of the non-interacting system (3.27) and the one of the interacting system (4.16), we notice that the latter one is self-consistent as the expectation (4.16) depends on itself via the action (4.18). This is typical for a Hartree-Fock theory.

4.3. Effective Action

For the further treatment, we introduce the effective action which is a functional of the background fields and the correlation function defined in analogy to the free energy as

$$\Gamma \left[\Psi^* \, , \Psi \, , g\right] = -\frac{1}{\beta} \ln \mathcal{Z} \,. \tag{4.22}$$

The grand-canonical free energy is obtained as the effective action evaluated at the minimum

$$\mathcal{F} = \Gamma \left[\Psi^*_{\mathrm{min}} \, , \Psi_{\mathrm{min}} \, , g_{\mathrm{min}}\right] \,. \tag{4.23}$$

According to its definition (4.22), the effective action reads

$$\Gamma \left[\Psi^* \, , \Psi \, , g\right] = \frac{1}{\hbar\beta} \mathcal{A}_{\mathrm{BG}} \left[\Psi, \Psi^*, g\right] - \frac{1}{\beta} \ln \left\{ \oint \mathcal{D}\delta\psi^* \oint \mathcal{D}\delta\psi \, e^{-\mathcal{A}^{(2)}[\delta\psi,\delta\psi^*,\Psi,\Psi^*,g]/\hbar} \right\} \,. \tag{4.24}$$

To obtain the free energy, we calculate the minima of (4.24):

$$\frac{\delta\Gamma \left[\Psi^* \, , \Psi \, , g\right]}{\delta\Psi(\mathbf{x},\tau)} = 0 \,, \tag{4.25}$$

$$\frac{\delta\Gamma \left[\Psi^* \, , \Psi \, , g\right]}{\delta\Psi^*(\mathbf{x},\tau)} = 0 \,, \tag{4.26}$$

$$\frac{\delta\Gamma \left[\Psi^* \, , \Psi \, , g\right]}{\delta g(\mathbf{x},\tau;\mathbf{x}',\tau')} = 0 \,. \tag{4.27}$$

As we have to calculate the functional derivatives of the effective action with respect to $\Psi(\mathbf{x},\tau)$, $\Psi^*(\mathbf{x},\tau)$, and $g(\mathbf{x},\tau;\mathbf{x}',\tau')$, we first need to define the functional derivative and its bilocal generalization [53,54]:

$$\frac{\delta\Psi(\mathbf{x}',\tau')}{\delta\Psi(\mathbf{x},\tau)} = \delta(\mathbf{x}'-\mathbf{x})\delta(\tau'-\tau)\,, \tag{4.28}$$

$$\frac{\delta g(\mathbf{x}'',\tau'';\mathbf{x}''',\tau''')}{\delta g(\mathbf{x},\tau;\mathbf{x}',\tau')} = \delta(\mathbf{x}''-\mathbf{x})\delta(\tau''-\tau)\delta(\mathbf{x}'-\mathbf{x}''')\delta(\tau'-\tau''')\,. \tag{4.29}$$

For the case of the derivative of (4.24) with respect to the conjugate field $\Psi^*(\mathbf{x},\tau)$, we get

$$\begin{aligned} 0 &= \left\{\hbar\frac{\partial}{\partial\tau} - \frac{\hbar^2}{2M}\Delta + V^{(\mathrm{ext})}(\mathbf{x}) - \mu + \int d^Dx'\ |\Psi(\mathbf{x}',\tau)|^2\, V^{(\mathrm{int})}(\mathbf{x},\mathbf{x}')\right\}\Psi(\mathbf{x},\tau) \\ &\quad + \int d^Dx'\, V^{(\mathrm{int})}(\mathbf{x},\mathbf{x}')\Big[\Psi(\mathbf{x},\tau)\, g\,(\mathbf{x}',\tau;\mathbf{x}',\tau) + \Psi(\mathbf{x}',\tau)\, g\,(\mathbf{x},\tau;\mathbf{x}',\tau)\Big] \end{aligned} \tag{4.30}$$

and an analogous equation for the other field $\Psi(\mathbf{x},\tau)$. The functional differentiation with respect to the correlation function yields the following result:

$$\begin{aligned} 0 = &-\int d^Dx'' V^{(\mathrm{int})}(\mathbf{x},\mathbf{x}'') g\,(\mathbf{x}'',\tau;\mathbf{x}'',\tau)\,\delta(\mathbf{x}-\mathbf{x}') - V^{(\mathrm{int})}(\mathbf{x},\mathbf{x}') g\,(\mathbf{x},\tau;\mathbf{x}',\tau) \\ &+ \int d^Dx'' V^{(\mathrm{int})}(\mathbf{x},\mathbf{x}'')\langle\delta\psi^*(\mathbf{x}'',\tau)\delta\psi(\mathbf{x}'',\tau)\rangle\delta(\mathbf{x}-\mathbf{x}') + V^{(\mathrm{int})}(\mathbf{x},\mathbf{x}')\langle\delta\psi^*(\mathbf{x}',\tau)\delta\psi(\mathbf{x},\tau)\rangle \end{aligned} \tag{4.31}$$

which is fulfilled by relation (4.16). Such theories are called "conserving" [55]. Thus, we have a system of two coupled equations, namely the integro-differential equation (4.30) for the background field describing the ground state and the relation (4.16) for the correlation function carrying the thermal features.

4.4. T → 0 Limit

In the limit of zero temperature we neglect all terms carrying thermal properties. As we already said, these are the fluctuating fields $\delta\psi, \delta\psi^*$ and their correlations $g(\mathbf{x},\tau;\mathbf{x}',\tau')$. In that limit, the effective action becomes

$$\begin{aligned} \hbar\beta\Gamma^{(0)}\left[\Psi^*\,,\Psi\right] &= \int_0^{\hbar\beta} d\tau \int d^Dx\,\Psi^*(\mathbf{x},\tau)\left[\hbar\frac{\partial}{\partial\tau} - \frac{\hbar^2}{2M}\Delta + V^{(\mathrm{ext})}(\mathbf{x}) - \mu\right]\Psi(\mathbf{x},\tau) \\ &\quad + \frac{1}{2}\int_0^{\hbar\beta} d\tau \int d^Dx \int d^Dx'\, V^{(\mathrm{int})}(\mathbf{x},\mathbf{x}')\,\Psi^*(\mathbf{x},\tau)\Psi^*(\mathbf{x}',\tau)\Psi(\mathbf{x},\tau)\Psi(\mathbf{x}',\tau)\,. \end{aligned} \tag{4.32}$$

If we apply the variation with respect to the background field we obtain the Gross-Pitaevskii equation. It was derived by Gross and Pitaevskii [56–58] first and is described in detail in recent textbooks as well [49,59]. It is convenient for a discussion of the equation to use the Wick rotation (3.10) to switch back to real time. Performing the variation with respect to the conjugate field Ψ^* leads to the time-dependent Gross-Pitaevskii equation

$$\left[-\imath\hbar\frac{\partial}{\partial t} - \mu - \frac{\hbar^2}{2M}\nabla^2 + V^{(\mathrm{ext})}(\mathbf{x}) + \frac{1}{2}\int d^D x'\; V^{(\mathrm{int})}(\mathbf{x},\mathbf{x}')\Psi^*(\mathbf{x}',t)\Psi(\mathbf{x}',t)\right]\Psi(\mathbf{x},t) = 0\,. \tag{4.33}$$

For the second variational case we get the complex conjugate of (4.33)

$$\left[\imath\hbar\frac{\partial}{\partial t} - \mu - \frac{\hbar^2}{2M}\nabla^2 + V^{(\mathrm{ext})}(\mathbf{x}) + \frac{1}{2}\int d^D x'\; V^{(\mathrm{int})}(\mathbf{x},\mathbf{x}')\Psi^*(\mathbf{x}',t)\Psi^*(\mathbf{x}',t)\right]\Psi^*(\mathbf{x},t) = 0\,. \tag{4.34}$$

As long as the potential and interaction do not explicitly depend on time, one can factorize the solution according to

$$\Psi(\mathbf{x},t) = \Psi(\mathbf{x})\, e^{-\imath(\mu-E_0)t/\hbar}\,, \tag{4.35}$$

where E_0 appears as separation constant and is identified with the ground-state energy. With the substitution $\bar{\mu} \to \mu - E_0$, we obtain

$$\left[-\bar{\mu} - \frac{\hbar^2}{2M}\nabla^2 + V^{(\mathrm{ext})}(\mathbf{x}) + \frac{1}{2}\int d^D x'\; V^{(\mathrm{int})}(\mathbf{x},\mathbf{x}')\Psi^*(\mathbf{x}')\Psi(\mathbf{x}')\right]\Psi(\mathbf{x}) = 0\,. \tag{4.36}$$

After the derivation we will now discuss the form of the time-independent equation and its area of validity. As one can read off from (4.36), it is a nonlinear, second order integro-differential equation. Except for the quadratic self-consistent interaction term, the equation corresponds to the Schrödinger equation with the energy replaced by the chemical potential.

Originally, in the works of Gross and Pitaevskii [56–58] the interaction has been a contact interaction but (4.36) is also valid for any two-body interaction. One can also see from Eq. (4.36), that the interaction term is an effective mean-field one, that requests a self-consistent solution for the order parameter Ψ. The physical conditions are a sufficiently low temperature and high particle number as well as the diluteness of the sample. The low temperature is necessary so that the thermal depletion is negligible and the total number of particles remains in the ground state. The ground state-wave function is normalized to the number of condensed particles which is for $T = 0$ identical to the total number of particles, a condition that fixes the chemical potential. This can be seen using the relation $N = -\partial\mathcal{F}/\partial\mu$ with $\mathcal{F}$ from (4.23) that leads to

$$\int d^D x\; \Psi^*(\mathbf{x})\Psi(\mathbf{x}) = N\,. \tag{4.37}$$

The Gross-Pitaevskii equation (4.36) and its solution will be discussed in detail in Chapter 5.

4.5. Chemical Potential

After this excursus to zero temperature, we will now continue with the treatment of the system of the two coupled equations derived in Section 4.3. In particular, we calculate in first-order perturbation theory how the chemical potential is affected by the two-particle interaction. In order to keep track of the perturbation corrections we introduce an artificial smallness parameter λ which will be set to 1 in the end. Therefore, we decompose the order parameter field and the chemical potential according to

$$\Psi(\mathbf{x}) = \psi_0(\mathbf{x}) + \lambda\psi_1(\mathbf{x}) + \dots\,, \qquad \mu = \mu_0 + \lambda\mu_1 + \dots\,. \tag{4.38}$$

The field $\psi_0(\mathbf{x})$ is supposed to solve the unperturbed system following from (4.30) as

$$\left[-\frac{\hbar^2}{2M}\Delta + V^{(\mathrm{ext})}(\mathbf{x}) - \mu_0\right]\psi_0(\mathbf{x}) = 0\,. \tag{4.39}$$

We said in the previous section that in the Gross-Pitaevskii theory at $T = 0$ all particles are in the condensed state. It does not matter whether an interaction is added or not. Therefore, we obtain for the background field Ψ and the zero-order field $\psi_0(\mathbf{x})$ the same normalization condition (4.37):

$$\int d^D x \Psi^*(\mathbf{x})\Psi(\mathbf{x}) = N_0\,, \qquad \int d^D x \psi_0^*(\mathbf{x})\psi_0(\mathbf{x}) = N_0\,. \tag{4.40}$$

Because we also include the thermal excitations in this chapter, we have to differ between the number of condensed particles N_0 and the number of total particles N that coincides with N_0 for $T = 0$. Without loss of generality, we assume ψ_0 and ψ_1 to be real, so it follows immediately from (4.40) that ψ_0 and ψ_1 are orthogonal

$$\int d^D x\, \psi_0(\mathbf{x})\, \psi_1(\mathbf{x}) = 0\,. \tag{4.41}$$

Now we substitute the expansions (4.38) into (4.30) and expand up to first order in the smallness parameter λ. We treat the interaction in first order which, therefore, gets also a factor λ. Herewith, we obtain

$$\begin{aligned} 0 \;=\; & \left[-\frac{\hbar^2}{2M}\Delta + V^{(\mathrm{ext})}(\mathbf{x}) - \mu_0 - \lambda\mu_1\right]\psi_0(\mathbf{x}) + \left[-\frac{\hbar^2}{2M}\Delta + V^{(\mathrm{ext})}(\mathbf{x}) - \mu_0\right]\lambda\psi_1(\mathbf{x}) \\ & + \lambda\int d^D x'\; |\psi_0(\mathbf{x}')|^2\, V^{(\mathrm{int})}(\mathbf{x},\mathbf{x}')\psi_0(\mathbf{x}) \\ & + \lambda\int d^D x'\, V^{(\mathrm{int})}(\mathbf{x},\mathbf{x}')\Big[\psi_0(\mathbf{x})\, g\,(\mathbf{x}',\tau;\mathbf{x}',\tau) + \psi_0(\mathbf{x}')\, g\,(\mathbf{x}',\tau;\mathbf{x},\tau)\Big]\,. \end{aligned} \tag{4.42}$$

Here, we multiply with $\psi_0^*(\mathbf{x})$ from the left and integrate over $d^D x$. Let us have a closer look on what happens to the first two terms

$$\int d^D x\, \psi_0^*(\mathbf{x}) \left[-\frac{\hbar^2}{2M}\Delta + V^{(\mathrm{ext})}(\mathbf{x}) - \mu_0 \right] \psi_0(\mathbf{x}) - \lambda \int d^D x \mu_1 \left|\psi_0(\mathbf{x})\right|^2$$
$$+\lambda \int d^D x\, \psi_0^*(\mathbf{x}) \left[-\frac{\hbar^2}{2M}\Delta + V^{(\mathrm{ext})}(\mathbf{x}) - \mu_0 \right] \psi_1(\mathbf{x})\,. \tag{4.43}$$

The first term in (4.43) vanishes because of (4.39), the second term gives $N_0\mu_1$with the normalization condition (4.40), and the third term vanishes because of the hermiticity of the one-particle Hamiltonian in (4.39) and the orthogonality condition (4.41). Thus, we get an equation for the correction to the chemical potential μ_1 that does not dependent on the correction ψ_1 to the wave function:

$$\begin{aligned} N_0\mu_1 \;=\; & \int d^D x\, \psi_0^*(\mathbf{x}) \int d^D x'\; \left|\psi_0(\mathbf{x}')\right|^2 V^{(\mathrm{int})}(\mathbf{x},\mathbf{x}')\psi_0(\mathbf{x}) \\ & + \int d^D x\, \psi_0^*(\mathbf{x}) \int d^D x'\, V^{(\mathrm{int})}(\mathbf{x},\mathbf{x}') \Big[\psi_0(\mathbf{x})\, g^{(0)}\left(\mathbf{x}',\tau;\mathbf{x}',\tau\right) + \psi_0(\mathbf{x}')\, g^{(0)}\left(\mathbf{x}',\tau;\mathbf{x},\tau\right) \Big]\,. \end{aligned} \tag{4.44}$$

The first contribution is from now on called "J", while the other two, that arrived due to the Hartree-Fock-theory, will be labelled by "H" and "F".

For a harmonic potential (3.33), we use the known ground-state wave function of a harmonic oscillator

$$\psi_0(\mathbf{x}) = \sqrt{N_0} \left(\frac{M\tilde{\omega}}{\hbar\pi} \right)^{3/4} \exp\left(-\frac{M}{2\hbar} \sum_{i=1}^{3} \omega_i x_i^2 \right) \tag{4.45}$$

with $\tilde{\omega}$ given in (3.35). The propagator (4.16) in lowest order is equal to the non-interacting propagator $G^{(0)}(\mathbf{x},\tau;\mathbf{x}',\tau')$ from (3.27). Thus, for equal times in semiclassical approximation, it follows from (3.31) for a harmonic trap

$$g^{(0)}(\mathbf{x},\tau;\mathbf{x}',\tau) = \int \frac{d^3p}{(2\pi\hbar)^3} e^{\imath\, \mathbf{p}(\mathbf{x}-\mathbf{x}')/\hbar} \sum_{n=1}^{\infty} \exp\left\{ -n\beta \left[\frac{\mathbf{p}^2}{2M} + \frac{M}{2} \sum_i \omega_i^2 \left(\frac{x_i + x_i'}{2} \right)^2 - \mu \right] \right\}, \tag{4.46}$$

where the $\mathbf{p}$-integration can be done immediately to give

$$g^{(0)}(\mathbf{x},\tau;\mathbf{x}',\tau) = \sum_{n=1}^{\infty} \frac{1}{\lambda_{\mathrm{T}}^3 n^{3/2}} \exp\left[-\frac{n\beta M}{2} \sum_i \omega_i^2 \left(\frac{x_i + x_i'}{2} \right)^2 - \frac{M}{2n\hbar^2\beta} \left(\mathbf{x}-\mathbf{x}'\right)^2 + n\beta\mu \right], \tag{4.47}$$

with the thermal De Broglie wavelength λ_{T} (1.1).

Contact Interaction

In the case of a contact interaction (1.2) the terms H and F in (4.44) coincide. In general, all integrals of (4.44) reduce to Gaussian ones. Hence, we simply get with the definitions of J, H, F from (4.44)

$$\mathrm{J} = N_0^2 g \left(\frac{M\tilde{\omega}}{2\pi\hbar}\right)^{3/2}, \tag{4.48}$$

$$\mathrm{H} = N_0 \frac{g}{\lambda_\mathrm{T}^3} \sum_{n=1}^{\infty} \frac{e^{n\beta\mu_0}}{n^{3/2}} \left[\prod_{i=1}^{3} \left(1 + \frac{n\beta\hbar\omega_i}{2}\right)\right]^{-1/2}, \tag{4.49}$$

$$\mathrm{F} = \mathrm{H}\,. \tag{4.50}$$

Therefore, the contribution of the contact interaction to the chemical potential reads

$$\mu_1^{(\delta)} = N_0 g \left(\frac{M\tilde{\omega}}{2\pi\hbar}\right)^{3/2} + \frac{2g}{\lambda_\mathrm{T}^3} \sum_{n=1}^{\infty} \frac{e^{n\beta\mu_0}}{n^{3/2}} \left[\prod_{i=1}^{3} \left(1 + \frac{n\beta\hbar\omega_i}{2}\right)\right]^{-1/2}. \tag{4.51}$$

Long-Range Interaction

Now, we calculate the contributions in (4.44) for the long-range interaction (1.5). Therefore, we use the Schwinger representation to calculate the appearing integrals [50]. The Schwinger formula is given by

$$\frac{1}{a^z} = \frac{1}{\Gamma(z)} \int_0^\infty dy\, y^{z-1} e^{-ay} \tag{4.52}$$

and is valid for $a > 0$. The gamma function is defined as

$$\Gamma(z) = \int_0^\infty dt\, t^{z-1} e^{-t}\,. \tag{4.53}$$

In our case we need to rewrite the long-range interaction. This is done with the upper rule:

$$\frac{1}{\sqrt{(\mathbf{x}-\mathbf{x}')^2}} = \frac{1}{\Gamma(1/2)} \int_0^\infty dy\, y^{-1/2} e^{-y(\mathbf{x}-\mathbf{x}')^2} \tag{4.54}$$

where we add that $\Gamma(1/2) = \sqrt{\pi}$ which follows from (4.53) with the substitution $t = x^2$.

With that representation, all spatial integrals are of the Gaussian type and can immediately be evaluated. However, the remaining Schwinger integrals with respect to y are

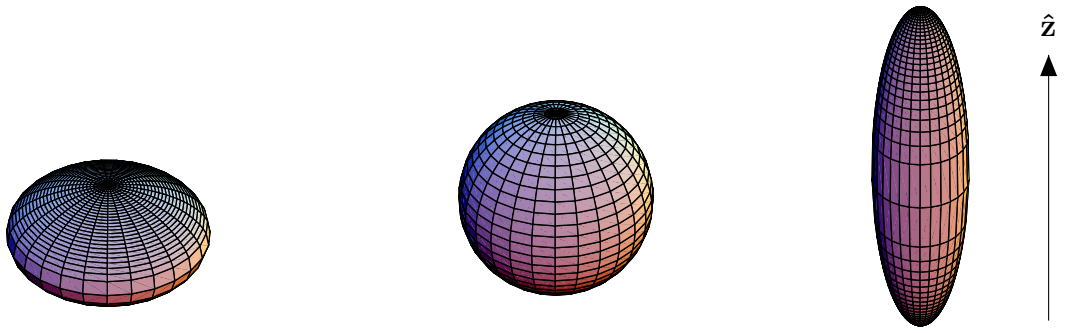

(a) (b) (c)

Fig. 4.1: Qualitative shape of a cylindrically-symmetric trap potential; (a): $\omega_z > \omega_r$, (b): $\omega_z = \omega_r$, (c): $\omega_z < \omega_r$. The sketched $\hat{\mathbf{z}}$ axis lies along the symmetry axis of the trap.

more difficult. They read for all three terms

$$\mathrm{J} = \frac{N_0^2 C}{\sqrt{\pi}} \left(\frac{M\tilde{\omega}}{\hbar}\right)^3 \int_0^\infty \frac{dy}{\sqrt{y}} \left\{ \prod_{i=1}^{3} \left[\frac{2M\omega_i}{\hbar} y + \left(\frac{M\omega_i}{\hbar}\right)^2 \right] \right\}^{-1/2}, \tag{4.55}$$

$$\mathrm{H} = \sum_{n=1}^{\infty} \frac{N_0 C \left(M\tilde{\omega}\right)^{3/2} \pi e^{n\beta\mu_0}}{\lambda_T^3 n^{3/2} \hbar^{3/2}} \int_0^\infty \frac{dy}{\sqrt{y}} \left\{ \prod_{i=1}^{3} \left[\left(\frac{M\omega_i}{\hbar} + \frac{n\beta M\omega_i^2}{2} \right) y + \frac{n\beta M^2 \omega_i^3}{2} \right] \right\}^{-1/2}, \tag{4.56}$$

$$\begin{aligned} \mathrm{F} &= \sum_{n=1}^{\infty} \frac{N_0 C \left(M\tilde{\omega}\right)^{3/2} \pi e^{n\beta\mu_0}}{\lambda_T^3 n^{3/2} \hbar^{3/2}} \\ &\quad \times \int_0^\infty \frac{dy}{\sqrt{y}} \left\{ \prod_{i=1}^{3} \left[\left(\frac{M\omega_i}{2\hbar} + \frac{n\beta M\omega_i^2}{2} \right) y + \frac{M^2\omega_i}{4n\beta\hbar^3} + \frac{M^2\omega_i^2}{2\hbar^2} + \frac{n\beta M^2\omega_i^3}{4\hbar} \right] \right\}^{-1/2}. \end{aligned} \tag{4.57}$$

In the following, motivated by the experiment discussed in Section 2.5, we restrict ourselves to a cylindrically symmetric trap with $\omega_1 = \omega_2 = \omega_r$, $\omega_3 = \omega_z$, illustrated in Fig. 4.1. So, the integrals reduce to the common form

$$I(a_1, a_3; b_1, b_3) = \int_0^\infty dy \left[(a_1 y + b_1) \sqrt{a_3\, y^2 + b_3 y} \right]^{-1}, \tag{4.58}$$

with the solution [60, 2.266]

$$I(a_1,a_3;b_1,b_3)=\frac{2\arccos\left(\sqrt{\frac{a_3b_1}{b_3a_1}}\right)}{\sqrt{a_1b_1b_3}\sqrt{1-\frac{a_3b_1}{b_3a_1}}}\,. \tag{4.59}$$

The combinations of the constants read for the different integrals:

$$\frac{a_3b_1}{b_3a_1}: \qquad\qquad a_1b_1b_3:$$

$$\text{J}: \quad \frac{\omega_\mathrm{r}}{\omega_\mathrm{z}} \qquad\qquad 2\omega_\mathrm{r}^3\omega_\mathrm{z}^2M^5/\hbar^5 \tag{4.60}$$

$$\text{H}: \quad \frac{\omega_\mathrm{r}^2(n\beta\omega_\mathrm{z}\hbar/2+1)}{\omega_\mathrm{z}^2(n\beta\omega_\mathrm{r}\hbar/2+1)} \qquad \frac{M^5n^2\beta^2\omega_\mathrm{r}^4\omega_\mathrm{z}^3(n\beta\omega_\mathrm{r}\hbar/2+1)}{4\hbar^3} \tag{4.61}$$

$$\text{F}: \quad \frac{n\beta\omega_\mathrm{r}\hbar/2+1}{n\beta\omega_\mathrm{z}\hbar/2+1} \qquad \frac{M^5\omega_\mathrm{r}^2\omega_\mathrm{z}(n\beta\omega_\mathrm{r}\hbar/2+1)^3(n\beta\omega_\mathrm{z}\hbar/2+1)^2}{4n^2\beta^2\hbar^7}\,. \tag{4.62}$$

If we combine the results of both interactions and sum the constants properly, we yield, with the definition of the trap anisotropy parameter $\kappa=\omega_\mathrm{r}/\omega_\mathrm{z}$, the total contribution to the chemical potential (4.44)

$$\begin{aligned}\mu_1 \;=\;& N_0g\left(\frac{M\tilde{\omega}}{2\pi\hbar}\right)^{3/2}+2\,\frac{g}{\lambda_\mathrm{T}^3}\sum_{n=1}^{\infty}\frac{e^{n\beta\mu_0}}{n^{3/2}}\left[\prod_{i=1}^{3}\left(1+\frac{n\beta\hbar\omega_i}{2}\right)\right]^{-1/2}+2N_0C\sqrt{\frac{M\tilde{\omega}}{2\pi\hbar}}\,f\left(\sqrt{\kappa}\right)\\ &+\frac{C4\pi\hbar^2\beta}{\lambda_\mathrm{T}^3M\left(\hbar\beta\tilde{\omega}\right)^2}\sum_{n=1}^{\infty}\frac{e^{n\beta\mu_0}}{n^{5/2}}\left(\frac{n\beta\omega_\mathrm{r}\hbar+2}{n\beta\omega_\mathrm{z}\hbar+2}\right)^{1/6}f\left(\kappa\sqrt{\frac{n\beta\omega_\mathrm{z}\hbar+2}{n\beta\omega_\mathrm{r}\hbar+2}}\right)\\ &+\frac{C4\pi\hbar^2\beta}{\lambda_\mathrm{T}^3M}\sum_{n=1}^{\infty}\frac{e^{n\beta\mu_0}}{n^{1/2}}\,\frac{\left(\frac{n\beta\omega_\mathrm{z}\hbar+2}{n\beta\omega_\mathrm{z}\hbar+2}\right)^{1/6}}{(n\beta\omega_\mathrm{r}\hbar/2+1)^{3/2}(n\beta\omega_\mathrm{z}\hbar/2+1)}\,f\left(\sqrt{\frac{n\beta\omega_\mathrm{r}\hbar+2}{n\beta\omega_\mathrm{z}\hbar+2}}\right)\,.\end{aligned} \tag{4.63}$$

Here, we introduced the function $f(\kappa)$ which measures the anisotropy of the trap. In general the function is of the following type

$$f(\kappa)=\kappa^{1/3}\frac{\arccos\kappa}{\sqrt{1-\kappa^2}}\,. \tag{4.64}$$

The function $f(\kappa)$ is well defined for $\kappa<1$. In the limit $\kappa\to1$, we find by using the L'Hospital rule $f(1)=1$. For values of $\kappa>1$ the function is also applicable as its analytic continuation. Both terms $\arccos\kappa$ and $\sqrt{1-\kappa^2}$ become purely imaginary so that the imaginary unit cancels. The asymptotic behaviour of $f(\kappa)$, see Fig. 4.2, shows a slow convergence to zero for κ to infinity and a rather fast one for $\kappa\to0$. The maximum is obtained for an isotropic trap , i.e., at $\kappa=1$.

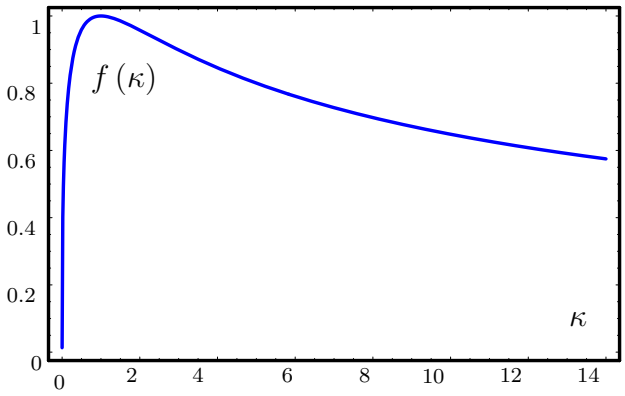

Fig. 4.2: Function $f(\kappa)$ that describes the anisotropy of a cylindrically-symmetric trap. The maximum lies at $\kappa = 1$ that refers to an isotropic trap.

4.6. Free Energy

In the last section of this chapter we calculate the grand-canonical free energy. We need its expression to calculate the particle number according to (3.6). In our case the grand-canonical free energy $\mathcal{F}$ is gained as the minimum of the effective action (4.24) with respect to the order parameter. The constraining equation for the minimum is simply the Gross-Pitaevskii equation (4.30). As we argued before we can not solve it exactly but will instead approximate the wave functions again in first-order perturbation theory, (4.38). To keep track of the different terms we will evaluate them separately. We recall the orthogonality condition (4.41) and remind of the fact that the interaction is already of first order. For the background term of (4.24), we obtain

$$\begin{aligned}\mathcal{A}_{\mathrm{BG}} &= \hbar\beta N_0\mu_1 + \frac{\hbar\beta}{2}\int d^Dx \int d^Dx'\, V^{(\mathrm{int})}(\mathbf{x},\mathbf{x}')\Big[\psi_0(\mathbf{x})^2\psi_0(\mathbf{x}')^2 \\ &\quad - g^{(0)}(\mathbf{x}',\tau;\mathbf{x}',\tau)\, g^{(0)}(\mathbf{x},\tau;\mathbf{x},\tau) - g^{(0)}(\mathbf{x}',\tau;\mathbf{x},\tau)\, g^{(0)}(\mathbf{x},\tau;\mathbf{x}',\tau)\Big]\,. \end{aligned} \tag{4.65}$$

The second term in (4.24) will be expanded in the interaction up to first order:

$$\begin{aligned}&\oint \mathcal{D}\delta\psi^* \oint \mathcal{D}\delta\psi\, e^{-\mathcal{A}^{(2)}[\delta\psi,\delta\psi^*]/\hbar} = \oint \mathcal{D}\delta\psi^* \oint \mathcal{D}\delta\psi\, e^{-\mathcal{A}_0^{(2)}[\delta\psi,\delta\psi^*]/\hbar} \\ &\times\Bigg[1 - \frac{1}{\hbar}\int_0^{\hbar\beta} d\tau \int d^Dx \int d^Dx'\, V^{(\mathrm{int})}(\mathbf{x},\mathbf{x}')\Bigg\{\delta\psi^*(\mathbf{x}',\tau)\delta\psi(\mathbf{x}',\tau)\Big[\psi_0^*(\mathbf{x},\tau)\psi_0(\mathbf{x},\tau) \\ &+ g^{(0)}(\mathbf{x},\tau;\mathbf{x},\tau)\Big] + \delta\psi^*(\mathbf{x}',\tau)\delta\psi(\mathbf{x},\tau)\Big[\psi_0^*(\mathbf{x},\tau)\psi_0(\mathbf{x}',\tau) + g^{(0)}(\mathbf{x},\tau;\mathbf{x}',\tau)\Big]\Bigg\} + \dots\Bigg]\,, \end{aligned} \tag{4.66}$$

where $\mathcal{A}_0^{(2)}$ is just the interaction-less part of (4.18). The functional integration can be easily performed using the expectation value (4.11) and the definition of the correlation

function (4.16). The τ integration can be performed for the following reasons. The wave functions do not depend on τ at all and the propagator does only depend on the time difference, so for equal times this is zero. Hence, we can evaluate the integral and obtain

$$\begin{aligned}\oint \mathcal{D}\delta\psi^* \oint \mathcal{D}\delta\psi\, e^{-\mathcal{A}^{(2)}[\delta\psi,\delta\psi^*]/\hbar} &= \tilde{\mathcal{Z}}_0\Bigg[1-\beta\int d^Dx\int d^Dx'\,V^{(\mathrm{int})}(\mathbf{x},\mathbf{x}') \\ &\quad\times\Bigg\{g^{(0)}\left(\mathbf{x}',0;\mathbf{x}',0\right)\left[\psi_0^*(\mathbf{x})\psi_0(\mathbf{x})+g^{(0)}\left(\mathbf{x},0;\mathbf{x},0\right)\right] \\ &\quad+g^{(0)}\left(\mathbf{x}',0;\mathbf{x},0\right)\left[\psi_0^*(\mathbf{x})\psi_0(\mathbf{x}')+g^{(0)}\left(\mathbf{x},0;\mathbf{x}',0\right)\right]\Bigg\}\Bigg]. \end{aligned} \tag{4.67}$$

The expression of the interaction-free partition function (3.25) and the connected non-interaction grand-canonical free energy (3.34) have already been calculated within the semiclassical approximation. If we expand the logarithm in $\Gamma\left[\Psi_{\min}^*,\Psi_{\min},g_{\min}\right]$, we get the following result for the free energy

$$\begin{aligned}\mathcal{F} &= N_0(\mu_0-\mu)+\mathcal{F}^{(0)}+\frac{1}{2}\int d^Dx\int d^Dx'\,V^{(\mathrm{int})}(\mathbf{x},\mathbf{x}') \\ &\quad\times\Big\{\psi_0(\mathbf{x})^2\psi_0(\mathbf{x}')^2+g^{(0)}\left(\mathbf{x}',0;\mathbf{x}',0\right)g^{(0)}\left(\mathbf{x},0;\mathbf{x},0\right)+g^{(0)}\left(\mathbf{x}',0;\mathbf{x},0\right)g^{(0)}\left(\mathbf{x},0;\mathbf{x}',0\right) \\ &\quad+2g^{(0)}\left(\mathbf{x}',0;\mathbf{x}',0\right)\psi_0^*(\mathbf{x},0)\psi_0(\mathbf{x},0)+2g^{(0)}\left(\mathbf{x}',0;\mathbf{x},0\right)\psi_0^*(\mathbf{x},0)\psi_0(\mathbf{x}',0)\Big\}. \end{aligned} \tag{4.68}$$

Here the wave functions and propagators are given by (4.45) and (4.46), respectively. The calculation of the terms happens pretty similar to the one of the chemical potential. We also use the Schwinger representation (4.54) for the long-range interaction. The spatial integrals are again Gaussians and the Schwinger integrals are of the type of the master integral (4.58) and we obtain

$$\begin{aligned}\mathcal{F} &= N_0(\mu_0-\mu)-\frac{1}{\beta\left(\hbar\beta\tilde{\omega}\right)^3}\zeta_4\left(e^{\beta\mu}\right)+\frac{N_0^2}{\lambda_{\mathrm{T}}^3}\left(\hbar\beta\tilde{\omega}\right)^{3/2}\left[g+\frac{4\pi\hbar^2C\beta}{M\left(\hbar\beta\tilde{\omega}\right)}f\left(\sqrt{\kappa}\right)\right] \\ &\quad+2\frac{g}{\lambda_{\mathrm{T}}^3}\left\{\frac{1}{2}\frac{\zeta_{\frac{3}{2},\frac{3}{2},\frac{3}{2}}\left(e^{\beta\mu}\right)}{\left(\hbar\beta\tilde{\omega}\right)^3}+N_0\sum_{n=1}^{\infty}\frac{e^{n\beta\mu}}{n^{3/2}}\left[\prod_{i=1}^{3}\left(1+\frac{n\beta\hbar\omega_i}{2}\right)\right]^{-1/2}\right\} \\ &\quad+\frac{1}{2}\frac{4\pi\hbar^2C\beta}{\lambda_{\mathrm{T}}^3\left(\hbar\beta\tilde{\omega}\right)^5M}\zeta_{\frac{5}{2},\frac{5}{2},\frac{1}{2}}\left(e^{\beta\mu}\right)f\left(\kappa\right)+\frac{1}{2}\frac{4\pi\hbar^2C\beta}{\lambda_{\mathrm{T}}^3\left(\hbar\beta\tilde{\omega}\right)^3M}\zeta_{\frac{1}{2},\frac{1}{2},\frac{5}{2}}\left(e^{\beta\mu}\right) \\ &\quad+\frac{4\pi\hbar^2C\beta N_0}{\lambda_{\mathrm{T}}^3\left(\hbar\beta\tilde{\omega}\right)^2M}\sum_{n=1}^{\infty}\frac{e^{n\beta\mu}}{n^{5/2}\sqrt{1+n\beta\hbar\omega_{\mathrm{r}}/2}}\left(\frac{n\beta\omega_{\mathrm{r}}\hbar+2}{n\beta\omega_{\mathrm{z}}\hbar+2}\right)^{1/6}f\left(\kappa\sqrt{\frac{n\beta\omega_{\mathrm{z}}\hbar+2}{n\beta\omega_{\mathrm{r}}\hbar+2}}\right) \\ &\quad+\frac{4\pi\hbar^2C\beta N_0}{\lambda_{\mathrm{T}}^3M}\sum_{n=1}^{\infty}\frac{e^{n\beta\mu}\left(\frac{n\beta\omega_{\mathrm{z}}\hbar+2}{n\beta\omega_{\mathrm{z}}\hbar+2}\right)^{1/6}}{n^{1/2}\left(1+n\beta\hbar\omega_{\mathrm{r}}/2\right)^{3/2}\left(1+n\beta\hbar\omega_{\mathrm{z}}/2\right)}f\left(\sqrt{\frac{n\beta\omega_{\mathrm{r}}\hbar+2}{n\beta\omega_{\mathrm{z}}\hbar+2}}\right). \end{aligned} \tag{4.69}$$

The expression for μ as $\mu = \mu_0 + \mu_1$ was calculated to first-order in the previous section but not inserted here for brevity. We notice again that the complete calculation was possible without knowledge of the first-order wave function ψ_1 but only with the orthogonality of the wave functions. In (4.69) we used the generalization of the polylogarithmic function (3.36)

$$\zeta_{a,b,c}(x) = \sum_{n',n=1}^{\infty} \frac{x^{(n+n')}}{n^a n'^b (n+n')^c} \,. \tag{4.70}$$

Eq. (4.69) is a first-order expression for the free energy that is valid for all temperatures. In fact, it can be used to describe both, the condensed and gas phase. In the BEC phase the number of condensed particle N_0 becomes large and quantum phenomena are important: $\hbar\omega\beta \gg 1$. On the other hand, the gas phase is obtained in the thermodynamic limit $\hbar\omega\beta \ll 1$ where the thermal energy is larger than the quantum energy.

We will use the results of the chemical potential and the grand-canonical free energy, that have been derived in this chapter, to calculate the shift of the critical temperature effected by the two interactions with respect to the non-interacting result (3.44). This will be done in Chapter 7.

5. Gross-Pitaevskii Theory

This chapter attends the behaviour of the condensate at temperatures close to absolute zero. In that domain the most appropriate theory is the Gross-Pitaevskii theory. We derived the Gross-Pitaevskii equation within our mean-field theory in Section 4.4.

At first, we will solve the time-independent Gross-Pitaevskii equation in Thomas-Fermi approximation and later on include the kinetic term within a variational approach. Finally, we compare the two results to check the validity of the Thomas-Fermi approximation in our special case.

Generally, we will focus on the attractive long-range interaction but we will state some results also for a repulsive one during the calculations.

5.1. Thomas-Fermi Approximation

The time-independent Gross-Pitaevskii equation (4.36) for a Bose gas in an isotropic harmonic trap interacting via both a contact interaction and a gravitation-like $1/r$-interaction is given by

$$\bar{\mu}\Psi(\mathbf{x}) = \left[-\frac{\hbar^2}{2M}\nabla^2 + g|\Psi(\mathbf{x})|^2 + \frac{M\omega^2 r^2}{2} - u\int \frac{|\Psi(\mathbf{x}')|^2}{|\mathbf{x}-\mathbf{x}'|}\,d^3x'\right]\Psi(\mathbf{x}). \tag{5.1}$$

Here g and u are constants that describe the strength of either interaction. They are expressed through the s-wave scattering length a for the contact interaction according to Eq. (1.2) and the characteristic length a_{G} for the $1/r$ interaction introduced in (2.33).

To simplify the equation we use the Thomas-Fermi-approximation and neglect the kinetic term in (5.1). That approximation is valid as long as the condensate wave function varies only sparsely. So, it is a good approximation within a certain volume of the condensate but breaks down at the borders. We will specify these conditions during the calculation. Hence, we get the integral equation

$$\bar{\mu} = g|\Psi(\mathbf{x})|^2 + \frac{M\omega^2 r^2}{2} - u\int \frac{|\Psi(\mathbf{x}')|^2}{|\mathbf{x}-\mathbf{x}'|}\,d^3x'. \tag{5.2}$$

To solve this equation, we introduce spherical coordinates and first assume the wavefunction to be radial symmetric, i.e., $\Psi(\mathbf{x}) = \Psi(r)$, which is fulfilled for the ground state,

and carry out the angular integrals. Due to rotational symmetry the φ-integration gives just a factor 2π. The remaining ϑ-integration reads

$$\int_{-1}^{+1} d\cos\vartheta \frac{1}{\sqrt{r^2+r'^2-2rr'\cos\vartheta}} = \frac{1}{rr'}\left(|r+r'|-|r-r'|\right). \tag{5.3}$$

For the following r'-integration we subdivide it into two parts from 0 to r and from r to R_0 that denotes the yet unknown Thomas-Fermi-radius. This quantity is introduced as a measure of the domain of the Thomas-Fermi approximation. It is obtained from $\Psi(R_0)=0$ and we will later on introduce a Heavyside-function which secures that the wave function is restricted to the defined volume. For brevity we skip to note it here but keep it in mind. Herewith, Eq. (5.2) becomes

$$\bar{\mu} = g|\Psi(r)|^2 + \frac{M\omega^2 r^2}{2} - 4\pi u\left[\int_0^r \frac{|\Psi(r')|^2}{r} r'^2 dr' + \int_r^{R_0} \frac{|\Psi(r')|^2}{r'} r'^2 dr'\right]. \tag{5.4}$$

The next step is to multiply by r and differentiate the equation twice to get rid of both integrals:

$$0 = g\frac{d^2}{dr^2}\left[r|\Psi(r)|^2\right] + 3M\omega^2 r - 4\pi u\frac{d^2}{dr^2}\left[\int_0^r |\Psi(r')|^2 r'^2 dr' + r\int_r^{R_0} |\Psi(r')|^2 r' dr'\right]. \tag{5.5}$$

The differentiation of the integrals works using

$$\frac{d}{dx}\int_a^x f(x,y)\,dy = \int_a^x \frac{df(x,y)}{dx}\,dy + f(x,x). \tag{5.6}$$

After the differentiation, Eq. (5.5) reads

$$0 = g\frac{d^2}{dr^2}\left[r|\Psi(r)|^2\right] + 3M\omega^2 r + 4\pi u r|\Psi(r)|^2. \tag{5.7}$$

Performing the substitution $|\Psi(r)|^2 = \varphi(r)/r$ simplifies the equation further. Herewith we end up with the differential equation

$$0 = \frac{d^2}{dr^2}\varphi(r) + \frac{4\pi u}{g}\varphi(r) + \frac{3M\omega^2}{g}r. \tag{5.8}$$

Fortunately, Eq. (5.8) is the well known equation for a harmonic oscillator with the inhomogeneous part $3M\omega^2 r/g$, whose solution can be easily found. At this point we add the already mentioned Heavyside function and get the result

$$|\Psi(r)|^2 = \left[\frac{1}{r}(A\sin kr + B\cos kr) - \frac{3M\omega^2}{4\pi u}\right]\Theta(R_0 - r) \tag{5.9}$$

with the abbreviation

$$k = \sqrt{\frac{4\pi u}{g}}\,. \tag{5.10}$$

To determine the integration constants A, B, the chemical potential $\bar{\mu}$, and the size of the Thomas-Fermi radius, we proceed just as follows:

i. The function (5.9) shall remain finite. Here, the troubling point is the origin. This fixes $B = 0$.

ii. We reinsert our solution into (5.4) and obtain $A = A(\bar{\mu}, R_0)$ because we lost the chemical potential due to the double differentiation.

iii. The normalization condition (4.37) gives $\bar{\mu} = \bar{\mu}(N)$ and therefore we yield $A(\bar{\mu}, R_0) \to A(N, R_0)$.

iv. We use the definition of the Thomas-Fermi-radius $\Psi(R_0) = 0$ in order to calculate R_0.

If one adheres to the instructions i to iv one easily yields

$$A(\bar{\mu}, R_0) = \frac{2\bar{\mu}k^2 - 3M\omega^2(k^2{R_0}^2 - 2)}{2gk^3\cos(kR_0)}, \tag{5.11}$$

$$\bar{\mu}(N, R_0) = \frac{1}{4}\left\{\frac{6M\omega^2(k^2{R_0}^2 - 2)}{k^2} + \frac{gk^3N + 4\pi k{R_0}^3M\omega^2}{\pi\left[\tan(kR_0) - kR_0\right]}\right\}, \tag{5.12}$$

$$A(N, R_0) = -\frac{gk^2N + 4\pi{R_0}^3M\omega^2}{4\pi g[kR_0\cos(kR_0) - \sin(kR_0)]}, \tag{5.13}$$

$$(kR_0)^2\cot(kR_0) = -\frac{Ngk^5}{12\pi M\omega^2} - \frac{(kR_0)^3}{3} + kR_0. \tag{5.14}$$

Here, the expression for A has already been plugged into the definition of R_0. In the general case we can not determine the Thomas-Fermi radius from (5.14) analytically but anyhow graphically. Thus, we can simply read off the value for kR_0 as the intersection of the left- and right-hand side functions of (5.14) which are sketched for some typical numerical values in Fig. 5.1. Although we have plotted the curve for different values of the particle number, these do actually not affect the general form but merely shift the right-hand side curve of (5.14). The general dependence of the condensate size R_0 on the different parameters, i.e., particle number N, trap frequency ω, and the interaction strengths a and a_{G} is shown separately in Fig. 5.2. The plots show the expected qualitative behaviour. The condensate size increases with a higher particle number and a stronger repulsion by the contact interaction, see Fig. 5.2(a) and Fig. 5.2(b). On the other hand it decreases with a higher trap frequency in Fig. 5.2(c).

The last plot, Fig. 5.2(d), concerns the long-range interaction. It has been drawn for positive and negative values of the interaction parameter a_{G}. As the interaction depends

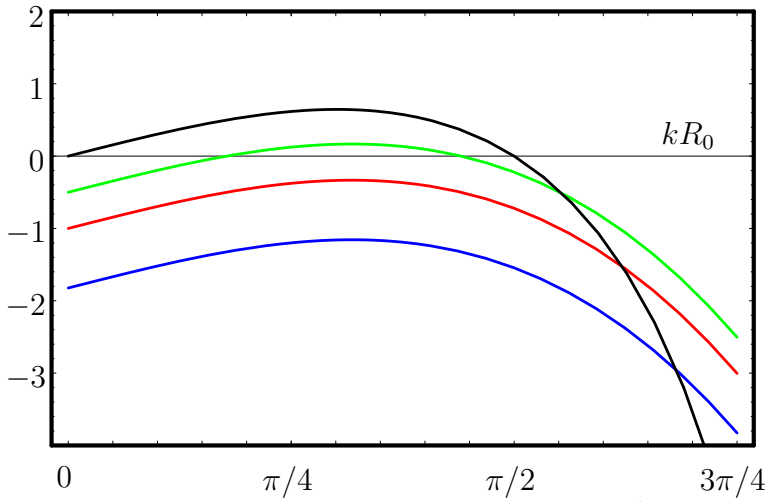

Fig. 5.1: Graphical solution for R_0. Intersection of $(kR_0)^2 \cot kR_0$ (black line) and $-Ngk^5/12\pi M\omega^2 - (kR_0)^3/3 + kR_0$ from Eq. (5.14) for different numbers of sodium atoms $(5000, 10000, 20000$, green, red, blue) and $\omega = 2\pi \cdot 100\,\mathrm{Hz}$. The other values have been taken from Tab. 2.5 on page 17.

on the reciprocal of a_G (compare to (2.33)) we read off an increasing and even diverging Thomas-Fermi-radius for negative (repulsive) values of a_G. On the other hand, for a strong attractive interaction the condensate will finally collapse, if the contact interaction can not balance the attraction any more.

After the general discussion we focus on some special cases that are analytically treatable. First we investigate the situation without a trap, where the condensate is still stable because the contact repulsion balances the $1/r$-attraction. Afterwards, we will modify the results to a repulsive long-range interaction and finally recover the known result without the $1/r$ interaction to confirm our calculation.

5.1.1. Self-Binding Case without Trap

An important case is the self-binding regime without an external trap, i.e., $\omega = 0$, that reduces the solution (5.9) to: $|\Psi(r)|^2 = A \sin(kr)/r\,\Theta(R_0 - r)$. If we follow again the above mentioned steps i to iv, we get the analytical results

$$A = \frac{N}{4{R_0}^2}\,, \tag{5.15}$$

$$R_0 = \frac{\pi}{k} = \frac{\sqrt{\pi g}}{2\sqrt{u}} = \frac{\sqrt{a a_\mathrm{G}}}{2}\,, \tag{5.16}$$

$$\bar{\mu}_\mathrm{SB} = -\frac{Nu}{R_0} = -\frac{N}{2}\sqrt{\frac{u^3}{\pi g}} = -\frac{8N\pi^2\hbar^2}{M\sqrt{a a_\mathrm{G}^3}}. \tag{5.17}$$

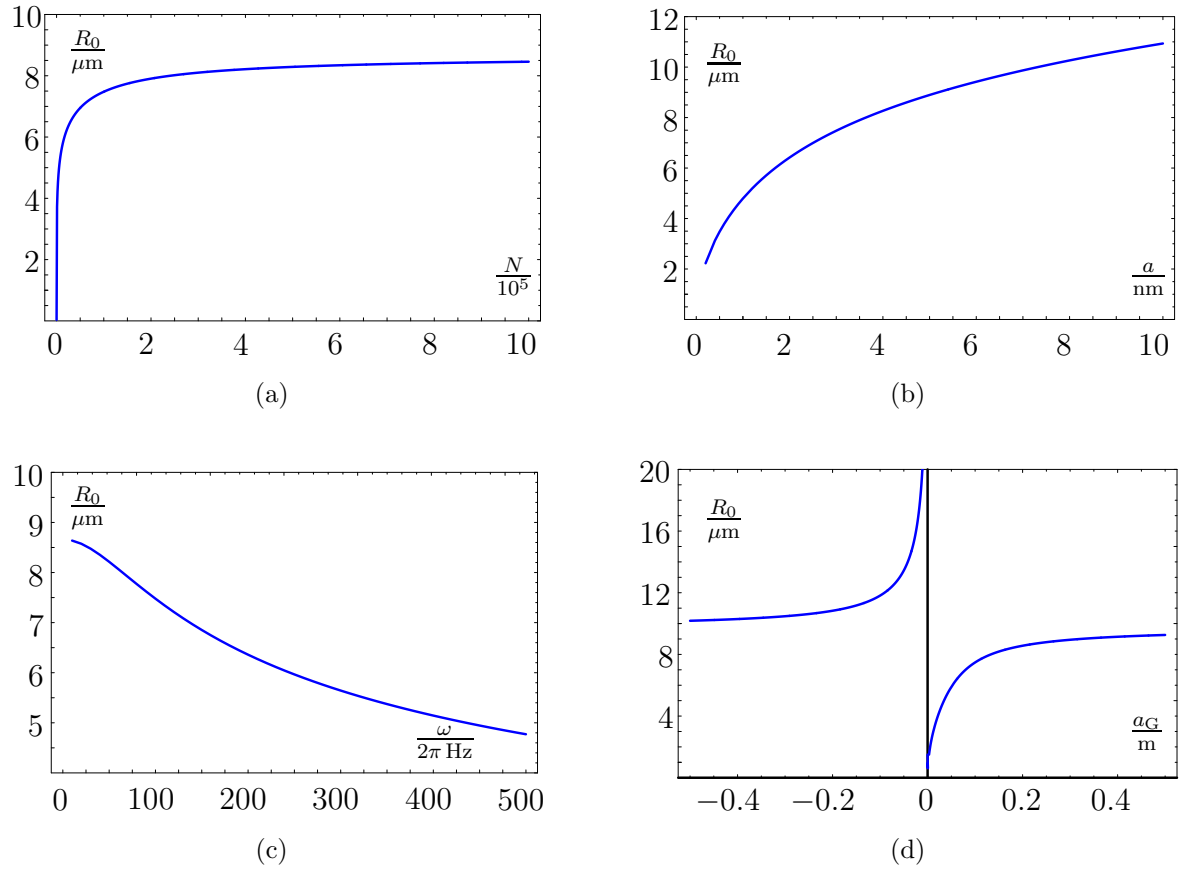

Fig. 5.2: Dependence of the Thomas-Fermi radius on several parameters. While one of them is varied, the other are fixed: $N = 10^5$, $\omega = 2\pi \cdot 100\,\mathrm{Hz}$, $a = 3\,\mathrm{nm}$, $a_\mathrm{G} = 0.1\,\mathrm{m}$. We emphasize that the long-range interaction strength u is defined by the inverse of the characteristic length a_G in subfigure (d).

It is interesting to notice that the size of the condensate R_0 does not depend on the number of particles. Instead it only depends on the ratio of the interaction strengths. The final Thomas-Fermi solution of the Gross-Pitaevskii equation reads [22]

$$\boxed{\Psi_{\mathrm{SB}}(r) = \frac{\sqrt{N}}{2R_0}\sqrt{\frac{\sin(\pi r/R_0)}{r}}\,\Theta(R_0 - r).} \tag{5.18}$$

Another interesting quantity in that region is the total energy per particle. It can be calculated by integrating Eq. (5.17) because of the thermodynamic relation $\bar{\mu} = \partial E/\partial N$:

$$\frac{E_{\mathrm{SB}}}{N} = \frac{1}{2}\bar{\mu}_{\mathrm{SB}}. \tag{5.19}$$

This result has to be considered critically. Inserting (5.17) into Eq. (5.19), the energy per particle rises with the number of particles, if the volume given by the Thomas-Fermi radius (5.16) is fixed. But the latter depends only on the two interacting strengths which are actually constants. Thus, in the thermodynamical limit, $N \to \infty$, we also have to enlarge the volume given by the Thomas-Fermi radius (5.16) to keep the density finite. This means, one has to adjust the long-range interaction strength by tuning the laser intensity according to (2.30).

5.1.2. Thomas-Fermi Result for Repulsive $1/r$ Interaction

In the second case we survey in detail a repulsive $1/r$ interaction. Then a confining trap is essential to guarantee the stability of the condensate. The only change in the upper calculations will be the substitution

$$u \to -u\,, \qquad k \to \imath k\,. \tag{5.20}$$

With that simple alteration Eqs. (5.9), (5.13), and (5.14) become

$$|\Psi(r)|^2 = \left[\frac{\imath\mathcal{A}}{r}\sinh kr + \frac{3M\omega^2}{4\pi u}\right]\Theta(R_0 - r)\,, \tag{5.21}$$

$$\imath\,\mathcal{A}(N, R_0) = -\frac{-gk^2N + 4\pi {R_0}^3 M\omega^2}{4\pi g[kR_0\cosh(kR_0) - \sinh(kR_0)]}, \tag{5.22}$$

$$(kR_0)^2\coth(kR_0) = -\frac{Ngk^5}{12\pi M\omega^2} + \frac{(kR_0)^3}{3} + kR_0. \tag{5.23}$$

The behaviour of the Thomas-Fermi radius for a repulsive $1/r$ interaction can be seen in Fig. 5.2(d). For a strong repulsive interaction the condensate is dispersed and its size diverges.

5.1.3. Vanishing Long-Range Interaction

At the end of this section we consider the calculation of the previous sections for the case of a vanishing $1/r$ interaction, i.e., for $u \to 0$ that means $k \to 0$ just as well. In that limit (5.2) simply gives

$$|\Psi(r)|^2 = \frac{\bar{\mu} - M\omega^2 r^2/2}{g}\,. \tag{5.24}$$

Now we try to gain the same result by expanding our solution (5.9) with $B = 0$ and A given by (5.11) for small k:

$$\sin(kr) \approx kr - \frac{k^3 r^3}{6}\,, \qquad A(\bar{\mu}, R_0) \approx \frac{3Mw^2}{gk^3} + \frac{\bar{\mu}}{gk}. \tag{5.25}$$

If we insert (5.25) into (5.9), we obtain

$$|\Psi(r)|^2 = \left(\frac{3Mw^2}{gk^3} + \frac{\bar{\mu}}{gk}\right)(k - k^3 r^2/6) - \frac{3M\omega^2}{gk^2} \overset{k\to 0}{=} \frac{\bar{\mu} - M\omega^2 r^2/2}{g}, \tag{5.26}$$

which is the expected result of a flipped parabola. Applying the normalization condition (4.37), we get for the chemical potential

$$\bar{\mu} = \left(\frac{225 g^2 M^3 N^2 \omega^6}{512\pi}\right)^{1/5}\,. \tag{5.27}$$

And therefore, the Thomas-Fermi radius becomes according to its definition

$$R_0 = \sqrt{\frac{2\bar{\mu}}{M\omega^2}} \tag{5.28}$$

with the chemical potential (5.27). For the values used in Fig. 5.2(d) we get $R_0 = 9.727\,\mu$m which reproduces the asymptotic behaviour of the curves.

5.2. Variational Approach

Now we treat the entire Gross-Pitaevskii-equation (5.1) not just in Thomas-Fermi approximation. As we are not able to solve this nonlinear integro-differential equation analytically, we aim at an approximative solution by using a variational method.

In Section 4.4 we have shown that we determined the Gross-Pitaevskii equation following from extremizing some effective potential. Now we will use a similar approach and plug a test function into the Lagrange density of the action (4.32), specialized to an isotropic harmonic trap and the two interactions,

$$\begin{aligned}\mathcal{L} \;=\; & \imath\hbar\Psi^*(\mathbf{x},t)\frac{\partial\Psi(\mathbf{x},t)}{\partial t} - \frac{\hbar^2}{2M}\nabla\Psi^*(\mathbf{x},t)\nabla\Psi(\mathbf{x},t) - \frac{M\omega^2 r^2}{2}|\Psi(\mathbf{x},t)|^2 - \frac{g}{2}|\Psi(\mathbf{x},t)|^4 \\ & + \frac{u}{2}|\Psi(\mathbf{x},t)|^2 \int \frac{|\Psi(\mathbf{x}',t)|^2}{|\mathbf{x}-\mathbf{x}'|}\,d^3x'\,.\end{aligned} \tag{5.29}$$

minima	TF-Grav	TF-Hard	Ideal	Grav
parameter	$\kappa = 0,\ w = 0$	$\kappa = 0,\ \tilde{u} = 0$	$\tilde{g} = 0,\ \tilde{u} = 0$	$\tilde{g} = 0,\ w = 0$
λ_0	$\sqrt{\tilde{g}/\tilde{u}}$	$\tilde{g}^{1/5}$	1	$1/\tilde{u}$
borders	TF-Hard↔TF-Grav	TF-Grav↔Grav	Grav ↔Ideal	
$\tilde{g}(\tilde{u})$	$\tilde{g} = \tilde{u}^{5/3}$	$\tilde{g} = \tilde{u}^{-1}$	$\tilde{u} = 1$	
N	$\frac{9\sqrt{3/2}\,a^{3/2}{a_\mathrm{G}}^{5/2}M^2\omega^2}{32\pi^{9/2}\hbar^2}$	$\sqrt{\frac{3a_\mathrm{G}}{8\pi a}}$	$\frac{3a_\mathrm{G}}{(2\pi)^{3/2}}\sqrt{\frac{M\omega}{\hbar}}$	

Fig. 5.3: Summary of results of (5.39). Upper part shows the minima conditions of Eq. (5.40). Lower part borders of different regions of the diagram in Fig. 5.4. The parameters κ, w, $\tilde{u}$, $\tilde{g}$ stand for kinetic energy, trap, long-range and contact interaction, respectively.

Just like in classical mechanics we differentiate the Lagrange function that is obtained as the integral of the Lagrange density

$$L = \int d^3x \mathcal{L} \tag{5.30}$$

with respect to the variational parameter λ and calculate the respective Euler-Lagrange equations

$$0 \;=\; \frac{\partial L}{\partial \lambda} - \frac{d}{dt}\frac{\partial L}{\partial \dot{\lambda}}\,. \tag{5.31}$$

Here, we assume the spatial integrals to converge that fast that we can integrate until infinity, while we restricted the condensate within the Thomas-Fermi radius before. The test function that we will use, is a Gaussian wave package with the variational parameter λ. This parameter describes the width of the Gaussian. The test function normalized to the number of particles reads

$$\Psi(r) = \frac{\sqrt{N}}{\pi^{3/4}\lambda^{3/2}l^{3/2}} \exp\left(-\frac{r^2}{2\lambda^2 l^2}\right)\,. \tag{5.32}$$

Here, $l = \sqrt{\hbar/M\omega}$ denotes the oscillator length. The results of the respective spatial

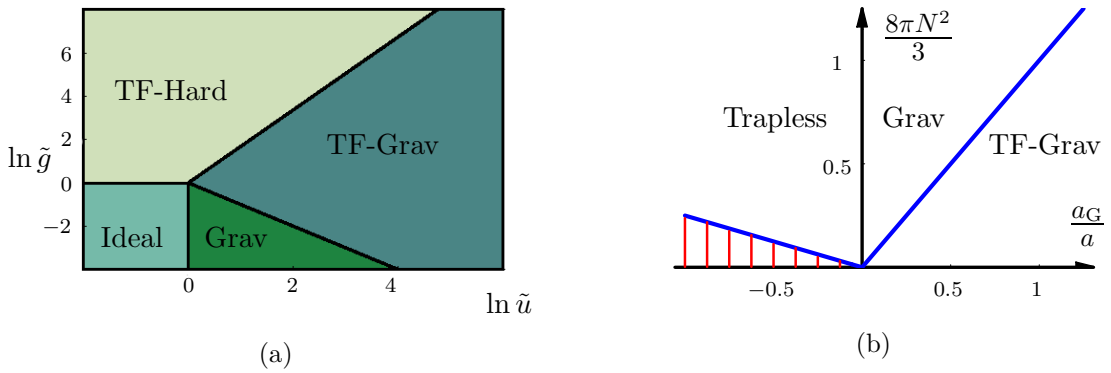

Fig. 5.4: (a): Diagram in a double logarithmic scale showing the different physical regimes listed and defined in Fig. 5.3 according to [22]. (b): Diagram of the new regimes including the long-range interaction, where particle number is plotted versus the characteristic lengths. The "Trapless" regime is valid for the entire area but especially in the regime of negative a_G/a where the other two collapse. The red hatched region is not accessible.

integrations read

$$\int d^3x \frac{\hbar^2}{2M} \nabla\Psi^*(r)\nabla\Psi(r) = \frac{3N\hbar\omega}{4}\lambda^{-2}\,, \tag{5.33}$$

$$\int d^3x \Psi^*(r) \frac{M\omega^2 r^2}{2}\Psi(r) = \frac{3N\hbar\omega}{4}\lambda^{2}\,, \tag{5.34}$$

$$\int d^3x \frac{g}{2}|\Psi(r)|^4 = \frac{3N\hbar\omega}{4}\frac{16aN}{3\sqrt{\pi 8}l}\lambda^{-3}\,, \tag{5.35}$$

$$\int d^3x \Psi^*(r)\frac{u}{2}\int d^3x' \frac{|\Psi(r')|^2}{|\mathbf{x}-\mathbf{x}'|}\Psi(r) = \frac{3N\hbar\omega}{4}\frac{4Nl\sqrt{32\pi}}{3a_G}\lambda^{-1}\,. \tag{5.36}$$

For the following discussion it is useful to introduce the dimensionless parameters

$$\tilde{u} = \frac{\pi N l\sqrt{32\pi}}{3a_G}\,, \qquad \tilde{g} = \frac{\sqrt{2/\pi}Na}{l}\,, \tag{5.37}$$

which are connected with the previously used interaction strengths via

$$\tilde{u} = \sqrt{\frac{2}{\pi}}\frac{NlM}{3\hbar^2}\,u\,, \qquad \tilde{g} = \sqrt{\frac{1}{8\pi^3}}\frac{NM}{l\hbar^2}\,g\,. \tag{5.38}$$

Instead of the Lagrangian, we will now use the Hamilton function which reads $H(\lambda) =$

$-L(\lambda)$ for time-independent variational functions. It is more convenient to use the Hamilton function because it coincides with the variational energy. We also introduce the artificial parameters w and κ to keep in mind that the terms came either from the trap or kinetic part:

$$\frac{H(\lambda)}{N\hbar\omega} = \frac{3}{4}\left(\kappa\lambda^{-2} + w\lambda^2 + \frac{2\tilde{g}}{3}\lambda^{-3} - 2\,\tilde{u}\lambda^{-1}\right). \tag{5.39}$$

The differentiation with respect to the variational parameter λ leads to the fifth-order algebraic equation

$$0 = -\kappa\lambda + w\lambda^5 - \tilde{g} + \tilde{u}\lambda^2\,. \tag{5.40}$$

According to Figs. 5.3 and 5.4 we can asymptotically distinguish different physical regions in our parameter space. The borders do not sharply bound the regions. The "TF-Hard" regime is characterized by the interplay of contact interaction and the trap and it corresponds to the solution (5.24). In the "Ideal" case both interactions are negligible and the stability is assured by the balance of kinetic energy and the trap. The more interesting regions are the remaining two as their stability does not require an external trap. After the atoms are collected, the trap can be turned off adiabatically and the system will survive nevertheless. The "TF-Grav" regimes corresponds to the solution of the Gross-Pitaevskii equation from Section 5.1.1. In the "Grav"-case the balance is ensured by the interplay of kinetic energy and attractive interaction.

Although it can not be analytically included into the diagram of Fig. 5.4(a), there is another interesting regime with the kinetic term but without an external trap, called "Trapless". With $w = 0$, the condition for an extremum reduces to a quadratic equation solved by

$$\lambda_{0_{1,2}} = \frac{1 \pm \sqrt{1 + 4\,\tilde{g}\,\tilde{u}}}{2\,\tilde{u}}, \tag{5.41}$$

where the "+" sign belongs to the bound state. This can be seen checking the sign of the second derivative of the Hamiltonian at the extremal λ:

$$H''(\lambda_0) = 0 \quad \leftrightarrow \quad \sqrt{1 + 4\tilde{g}\tilde{u}} = 0\,. \tag{5.42}$$

Hence, there exist bound states for all $\tilde{u}\tilde{g} > -1/4$. So, as long as the contact interaction is not tuned to attractiveness using Feshbach resonances, we always get stable solutions. But let us look on the product $\tilde{u}\tilde{g}$. Using the definitions (5.37) we get

$$\tilde{u}\tilde{g} = \frac{8\pi}{3}\,N^2\frac{a}{a_{\mathrm{G}}}\,. \tag{5.43}$$

Therefore the only important quantities are the particle number and the two characteristic lengths. A graphical interpretation of the regimes "Grav", "TF-Grav", and "Trapless" as a function of particle number depending on the ratio of the interacting strengths is depicted in Fig. 5.4(b).

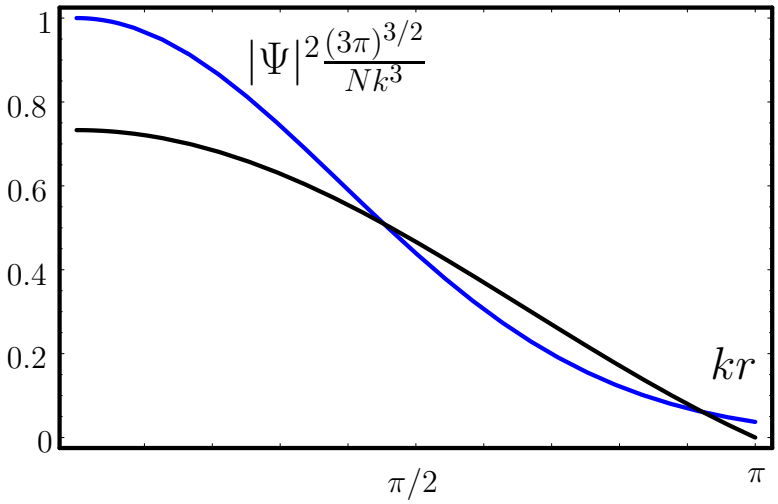

Fig. 5.5: Comparison between the densities of the exact result of the Gross-Pitaevskii-equation and the Gaussian variational approach in the TF-Grav regime. The black line belongs to the exact solution of the self-binding regime from Section 5.1.1; the blue line depicts the corresponding Gaussian result.

5.3. Comparing Exact and Variational Results

At the end of this chapter, we compare the results of the Thomas-Fermi treatment from Section 5.1 and the Gaussian variational approach from Section 5.2.

Until now, we have not quantitatively estimated the effect of the kinetic term. This can be done by inspecting the variational approach in detail. To this end we check the validity of the approximation considering the results for the minima of the variational parameter in Eq. (5.41) and in Fig. 5.3. Eq. (5.41) appears only in connection with the oscillator length and can be rewritten as

$$l\lambda_{0_{1,2}} = \frac{l}{2\,\tilde{u}} + \sqrt{l^2/(4\,\tilde{u}^2) + l^2\tilde{g}/\tilde{u}} \tag{5.44}$$

but using the definitions (5.37), $l/\tilde{u}$ is basically proportional to $1/N$ und thus rather small. Hence we might approximate (5.44) by $l\lambda_{0_{1,2}} = l\sqrt{\tilde{g}/\tilde{u}}$ which is the condition for the "TF-Grav" regime. Therefore, the Thomas-Fermi approximation is at least good in the regime of the variational approach. But a comparison of variational and Thomas-Fermi solutions shows indeed that these results match in good agreement. This can be seen from both a density comparison as in Fig. 5.5 and a comparison of the respective energies. The energy of the Thomas-Fermi case was already calculated in (5.19). The variational one simply follows from the Hamiltonian (5.39) evaluated at the minimal variational parameter λ_0 from Fig. 5.3:

$$E_{\text{var}} = \frac{2}{3}\sqrt{\frac{2\pi}{3}}\,E_{\text{SB}} \approx 0.964802\,E_{\text{SB}}\,. \tag{5.45}$$

Thus, they only differ by less than 4%. As these results are in good agreement, we can assume that the Thomas-Fermi approximation is a good choice for an exact calculation of the Gross-Pitaevskii equation.

6. Dynamics

After we have discussed the static solutions of the time-independent Gross-Pitaevskii equation in Chapter 5, we will now focus on solutions of the time-dependent Gross-Pitaevskii equation. To this end we note again the importance of the dynamical behaviour as the most suitable way to measure properties of the condensates.

In this chapter, we will tackle the dynamics within two different approaches. At first, we compare the condensate to a quantum liquid to derive equations of motion similar to those of a liquid in hydrodynamics. And later, we generalize the variational approach in Section 5.2 to a time-dependent one. In both approaches the goal is to calculate the frequencies of collective excitations because these are the experimentally accessible parameters rather than the specific eigenfunctions of the motion.

6.1. Hydrodynamic Equations

The time-dependent Gross-Pitaevskii equation can be used to derive hydrodynamic equations that describe the dynamics of the condensate as a quantum liquid at zero temperature [59,61]. This theory has originally been derived by Bogoliubov [62] for homogeneous systems and a contact interaction. Here, we generalize these hydrodynamic equations to a general two-particle interaction and treat, in particular, the consequences for an attractive long-range interaction.

6.1.1. General Formalism

We start with the time-dependent Gross-Pitaevskii equation (4.33) and its conjugate (4.34) where the external and two-body interaction potentials are time-independent but otherwise yet arbitrary and will be specified once necessary.

First, we show that a continuity equation can be derived for the Gross-Pitaevskii equation that corresponds to the one of the ordinary Schrödinger equation. To this end, we have to multiply (4.33) with Ψ^* and (4.34) with Ψ and subtract both from each other. This leads directly to the continuity equation

$$\frac{\partial}{\partial t} n(\mathbf{x}, t) + \nabla \cdot \mathbf{j}(\mathbf{x}, t) = 0 \tag{6.1}$$

with the particle density

$$n(\mathbf{x}, t) = |\Psi(\mathbf{x}, t)|^2 \tag{6.2}$$

and the current density

$$\mathbf{j}(\mathbf{x},t) = \frac{\hbar}{2M\imath}\left[\Psi^*(\mathbf{x},t)\nabla\Psi(\mathbf{x},t) - \Psi(\mathbf{x},t)\nabla\Psi^*(\mathbf{x},t)\right] . \tag{6.3}$$

They are connected by the velocity $\mathbf{v}(\mathbf{x},t)$ via

$$\mathbf{j}(\mathbf{x},t) = n(\mathbf{x},t)\mathbf{v}(\mathbf{x},t). \tag{6.4}$$

The main goal is to derive equations of motion for the particle density and velocity which are equivalent to (4.33) and (4.34). Due to (6.1) to (6.4), the continuity equation determines the particle density, once the velocity is known:

$$\frac{\partial}{\partial t}\, n(\mathbf{x},t) + \nabla\cdot\left[n(\mathbf{x},t)\mathbf{v}(\mathbf{x},t)\right] = 0\,. \tag{6.5}$$

Now we need a separate equation of motion which determines the velocity. Therefore, we rewrite the condensate wave function as

$$\Psi(\mathbf{x},t) = \sqrt{n(\mathbf{x},t)}\,\exp\left[\imath\,\varphi(\mathbf{x},t)\right] . \tag{6.6}$$

Substituting (6.6) into (6.3) and the result into (6.4), we obtain an important relation between the phase $\varphi(\mathbf{x},t)$ of the condensate and its velocity

$$\mathbf{v}(\mathbf{x},t) = \frac{\hbar}{M}\nabla\varphi(\mathbf{x},t). \tag{6.7}$$

Inserting (6.6) into (4.33), we get

$$\begin{aligned}\imath\hbar\left(\frac{\partial n}{\partial t}\frac{1}{2\sqrt{n}} + \imath\sqrt{n}\,\frac{\partial\varphi}{\partial t}\right) &= -\frac{\hbar^2}{2M}\Big[\nabla^2\sqrt{n} + \imath(2\nabla\sqrt{n}\nabla\varphi + \sqrt{n}\nabla^2\varphi) - \sqrt{n}(\nabla\varphi)^2\Big] \\ &\quad + V^{(\mathrm{ext})}\sqrt{n} + \sqrt{n}\int V^{(\mathrm{int})} n\, d^3x'.\end{aligned} \tag{6.8}$$

The imaginary part of (6.8) is exactly the continuity equation (6.5). The real part of (6.8) leads to

$$-\hbar\frac{\partial\varphi}{\partial t} = -\frac{\hbar^2}{2M}\left[\frac{\nabla^2\sqrt{n}}{\sqrt{n}} - (\nabla\varphi)^2\right] + V^{(\mathrm{ext})} + \int V^{(\mathrm{int})} n\, d^3x'. \tag{6.9}$$

As we rather need equations for $\mathbf{v}$ and n but not for the phase φ, we convert the equation into an equation of motion by taking the gradient of (6.9) and keeping in mind (6.7):

$$M\frac{\partial\mathbf{v}}{\partial t} = -\nabla\left(\frac{M\mathbf{v}^2}{2} + V^{(\mathrm{ext})} + \int V^{(\mathrm{int})} n\, d^3x' - \frac{\hbar^2}{2M}\frac{\nabla^2\sqrt{n}}{\sqrt{n}}\right). \tag{6.10}$$

Equation (6.10) is just an Euler-equation [63,64] for the velocity field $\mathbf{v}$ of an ideal, inviscid liquid that is governed by forces given by the gradients of the kinetic energy,

trap, interaction potential, and the latter term, the quantum pressure. This term impacts on the spatial behaviour and is important when the condensate varies spatially but thus can be neglected within the Thomas-Fermi approximation. Finally, we get the second equation of motion

$$\frac{\partial \mathbf{v}(\mathbf{x},t)}{\partial t} = -\frac{\nabla \mathbf{v}(\mathbf{x},t)^2}{2} - \frac{\nabla}{M}\left[V^{(\mathrm{ext})}(\mathbf{x}) + \int V^{(\mathrm{int})}(\mathbf{x},\mathbf{x}')n(\mathbf{x}',t)d^3x'\right], \quad (6.11)$$

yielding together with (6.5) a system of two coupled equations.

6.1.2. Linearization

Now we are going to investigate just small deviations from the equilibrium configuration. Therefore, we split the density and velocity into equilibrium solutions plus weak deviations

$$n(\mathbf{x},t) = n_{\mathrm{eq}}(\mathbf{x},t) + \delta n(\mathbf{x},t)\,, \quad (6.12)$$
$$\mathbf{v}(\mathbf{x},t) = \mathbf{v}_{\mathrm{eq}}(\mathbf{x},t) + \delta \mathbf{v}(\mathbf{x},t). \quad (6.13)$$

The equilibrium solutions belong to the time-independent Gross-Pitaevskii equation in Thomas-Fermi approximation which have already been calculated in Section 5.1 for a contact and an additional $1/r$-interaction. Because we assumed both interaction potentials to be time-independent in the beginning of this section, the equilibrium solutions do not depend on time as well and, of course, the velocity equilibrium mode $\mathbf{v}_{\mathrm{eq}}$ simply vanishes.

Because we expect the deviations to be reasonably small, it is sufficient to neglect higher than first orders in $\delta n(\mathbf{x},t)$, $\delta \mathbf{v}(\mathbf{x},t)$. Hence, we insert (6.12) and (6.13) into (6.5), (6.11) and drop higher order terms:

$$\frac{\partial}{\partial t}\,\delta n(\mathbf{x},t) = -\nabla_{\mathbf{x}}\left[n_{\mathrm{eq}}(\mathbf{x})\,\delta \mathbf{v}(\mathbf{x},t)\right], \quad (6.14)$$
$$\frac{\partial}{\partial t}\,\delta \mathbf{v}(\mathbf{x},t) = -\frac{1}{M}\,\nabla_{\mathbf{x}}\left\{V^{(\mathrm{ext})}(\mathbf{x}) + \int V^{(\mathrm{int})}(\mathbf{x},\mathbf{x}')\,\left[n_{\mathrm{eq}}(\mathbf{x}') + \delta n(\mathbf{x}',t)\right]\,d^3x'\right\}. \quad (6.15)$$

If we differentiate (6.14) once with respect to t, we can replace the velocity term by (6.15). Consequently, we get one differential equation just for the density deviations alone

$$\frac{\partial^2}{\partial t^2}\,\delta n(\mathbf{x},t) = \nabla_{\mathbf{x}}\left[n_{\mathrm{eq}}(\mathbf{x})\;\frac{1}{M}\,\nabla_{\mathbf{x}}\left\{V^{(\mathrm{ext})}(\mathbf{x}) + \int V^{(\mathrm{int})}(\mathbf{x},\mathbf{x}')\;\left[n_{\mathrm{eq}}(\mathbf{x}') + \delta n(\mathbf{x}')\right]\,d^3x'\right\}\right]. \quad (6.16)$$

Now we use the time-independent Gross-Pitaevskii equation (4.36) in Thomas-Fermi approximation to replace the external potential, according to

$$V^{(\mathrm{ext})}(\mathbf{x}) = \bar{\mu} - \int V^{(\mathrm{int})}(\mathbf{x},\mathbf{x}')\,n_{\mathrm{eq}}(\mathbf{x}')\,d^3x'. \quad (6.17)$$

This means that the external potential merely appears through the equilibrium solution. Instead, we have to take into account the chemical potential which does not depend on the spatial variable and drops out by reason of the ∇-differentiation. So, we obtain

$$\begin{aligned} M\frac{\partial^2}{\partial t^2}\,\delta n(\mathbf{x},t) &= [\nabla_{\mathbf{x}}\, n_{\mathrm{eq}}(\mathbf{x})]\cdot\left[\nabla_{\mathbf{x}}\int V^{(\mathrm{int})}(\mathbf{x},\mathbf{x}')\,\delta n(\mathbf{x}',t)\,d^3x'\right] \\ &\quad +n_{\mathrm{eq}}(\mathbf{x})\,\Delta_{\mathbf{x}}\int V^{(\mathrm{int})}(\mathbf{x},\mathbf{x}')\,\delta n(\mathbf{x}',t)\,d^3x'. \end{aligned} \tag{6.18}$$

6.1.3. Specifying the Interaction

As neither the equilibrium solution nor the interaction potentials depend explicitly on time, we can separate the time variable off. Furthermore, we introduce spherical coordinates for the spatial function:

$$\delta n(\mathbf{x},t) = \cos(\Omega t+\phi)F(r,\vartheta,\varphi) \tag{6.19}$$

The differential equation for the spatial function $F(r,\vartheta,\varphi)$ then follows from (6.18) as

$$\begin{aligned} -M\Omega^2 F(r,\vartheta,\varphi) &= [\nabla_{\mathbf{x}}\, n_{\mathrm{eq}}(\mathbf{x})]\cdot\left[\nabla_{\mathbf{x}}\int V^{(\mathrm{int})}(\mathbf{x},\mathbf{x}')\,F(r',\vartheta',\varphi')\,d^3x'\right] \\ &\quad +n_{\mathrm{eq}}(\mathbf{x})\,\Delta_{\mathbf{x}}\int V^{(\mathrm{int})}(\mathbf{x},\mathbf{x}')\,F(r',\vartheta',\varphi')\,d^3x'. \end{aligned} \tag{6.20}$$

Now we specialize to the two interaction potentials (1.2), (1.5), while the integrals containing the contact interaction can immediately be evaluated:

$$\begin{aligned} -M\Omega^2 F(r,\vartheta,\varphi) &= [\nabla_{\mathbf{x}}\, n_{\mathrm{eq}}(\mathbf{x})]\cdot\nabla_{\mathbf{x}}\left[gF(r,\vartheta,\varphi)-\int\frac{u}{|\mathbf{x}-\mathbf{x}'|}\,F(r',\vartheta',\varphi')\,d^3x'\right] \\ &\quad +n_{\mathrm{eq}}(\mathbf{x})\left[g\,\Delta_{\mathbf{x}}F(r,\vartheta,\varphi)-u\,\Delta_{\mathbf{x}}\int\frac{1}{|\mathbf{x}-\mathbf{x}'|}\,F(r',\vartheta',\varphi')\,d^3x'\right]. \end{aligned} \tag{6.21}$$

The last term in (6.21) can easily be evaluated as the Laplacian acts on $\mathbf{x}$ only, while the integration runs over $\mathbf{x}'$. Thus, we can use the distributional identity

$$\Delta\frac{1}{|\mathbf{x}-\mathbf{x}'|} = -4\pi\delta(\mathbf{x}-\mathbf{x}')\,, \tag{6.22}$$

which is well known from electrostatics, and carry out the spatial integration. The other spatial integral in (6.21) is treated by splitting the spatial arguments into radial and angular parts: $F(r,\vartheta,\varphi) = f(r)\,Y_{lm}(\vartheta,\varphi)$, where the angular part consists of the spherical

harmonics. Furthermore, we use the expansion of $1/|\mathbf{x}-\mathbf{x}'|$ in spherical harmonics [65]

$$\begin{aligned}\frac{1}{|\mathbf{x}-\mathbf{x}'|} &= \sum_{l=0}^{\infty}\sum_{m=-l}^{l}\frac{4\pi}{2l+1}\frac{r'^l}{r^{l+1}}\,Y_{lm}^*(\vartheta',\varphi')\,Y_{lm}(\vartheta,\varphi)\,\Theta(r-r') \\ &\quad+\sum_{l=0}^{\infty}\sum_{m=-l}^{l}\frac{4\pi}{2l+1}\frac{r^l}{r'^{l+1}}\,Y_{lm}^*(\vartheta',\varphi')\,Y_{lm}(\vartheta,\varphi)\,\Theta(r'-r).\end{aligned} \tag{6.23}$$

Herewith, we obtain

$$\begin{aligned}\nabla_{\mathbf{x}}\int\frac{1}{|\mathbf{x}-\mathbf{x}'|}\,F(r',\vartheta',\varphi')\,d^3x' &= \nabla_{\mathbf{x}}\sum_{l'=0}^{\infty}\sum_{m'=-l'}^{l'}\frac{4\pi}{2l'+1}\,Y_{l'm'}(\vartheta,\varphi) \\ &\quad\times\left[\int\frac{r'^{l'}}{r^{l'+1}}\,Y_{l'm'}^*(\vartheta',\varphi')\,Y_{lm}(\vartheta',\varphi')\Theta(r-r')f(r')\,d^3x'\right. \\ &\quad+\left.\int\frac{r^{l'}}{r'^{l'+1}}\,Y_{l'm'}^*(\vartheta',\varphi')\,Y_{lm}(\vartheta',\varphi')\Theta(r'-r)f(r')\,d^3x'\right].\end{aligned} \tag{6.24}$$

The angular integrals are solved using the orthonormality relation of the spherical harmonics

$$\int d\Omega\,Y_{l'm'}^*(\vartheta,\varphi)\,Y_{lm}(\vartheta,\varphi)=\delta_{ll'}\delta_{mm'}. \tag{6.25}$$

The Kronecker symbols make it possible to calculate the sums in (6.24) which leads to the final expression:

$$\begin{aligned}\nabla_{\mathbf{x}}\int\frac{1}{|\mathbf{x}-\mathbf{x}'|}\,F(r',\vartheta',\varphi')\,d^3r' &= \frac{4\pi}{2l+1}\nabla_{\mathbf{x}}\left\{Y_{lm}(\vartheta,\varphi)\left[\int_0^{\infty}\frac{r'^{l+2}}{r^{l+1}}\,\Theta(r-r')f(r')\,dr'+\right.\right. \\ &\quad\left.\left.+\int_0^{\infty}\frac{r^l}{r'^{l-1}}\,\Theta(r'-r)f(r')\,dr'\right]\right\}.\end{aligned} \tag{6.26}$$

If we look back at Section 5.1, we notice that the equilibrium solution $n_{\mathrm{eq}}(r)$ in (5.18) depends only on the radial coordinate which means that the scalar product in (6.20) is only non-zero in the r-component. Hence, we have to consider just the differentiation with respect to r in (6.26), whereby we are able to separate radial and angular coordinates in (6.20). We split the Laplacian into radial and angular part according to

$$\Delta_{\mathbf{x}}=\Delta_r+\frac{1}{r^2}\Delta_{\vartheta,\varphi} \tag{6.27}$$

with the two parts

$$\Delta_r \frac{1}{r^2}\frac{\partial}{\partial r} r^2 \frac{\partial}{\partial r}, \qquad \Delta_{\vartheta,\varphi} = \frac{1}{\sin\vartheta}\frac{\partial}{\partial\vartheta}\sin\vartheta\frac{\partial}{\partial\vartheta} + \frac{1}{\sin^2\vartheta}\frac{\partial^2}{\partial\varphi^2}\,. \tag{6.28}$$

For the angular part we get the equation

$$\Delta_{\vartheta,\varphi}\, Y_{lm}(\vartheta,\varphi) = -l(l+1)\, Y_{lm}(\vartheta,\varphi)\,, \tag{6.29}$$

which is the defining equation of the spherical harmonics with the separation constant $-l(l+1)$. Up to now we have found the solution

$$\delta n(\mathbf{r},t) = f(r)\, Y_{lm}(\vartheta,\varphi)\, \cos(\Omega t + \phi)\,, \tag{6.30}$$

from where we get a rather difficult integro-differential equation for $f(r)$ after collecting all the previous results (6.21), (6.22), (6.26), and (6.29)

$$\begin{aligned} 0 \;=\; & \Delta_r f(r) + f(r)\left[\frac{4\pi u}{g} + \frac{M\Omega^2}{g n_{\mathrm{eq}}(r)} - \frac{l(l+1)}{r^2}\right] + \left[\frac{1}{n_{\mathrm{eq}}(r)}\frac{\partial n_{\mathrm{eq}}(r)}{\partial r}\right] \\ & \times\left\{\frac{\partial f(r)}{\partial r} + \frac{4\pi u}{g(2l+1)}\left[\frac{l+1}{r^{l+2}}\int_0^r r'^{l+2} f(r')dr' - l r^{l-1}\int_r^\infty \frac{1}{r'^{l-1}} f(r')dr'\right]\right\}\,. \end{aligned} \tag{6.31}$$

Some numerical results of (6.31), in the case of the self-trapping solution (5.18), can be found in Ref. [66]. As we are rather interested in analytical calculations, we investigate Eq. (6.31) for a special case in the following section.

6.1.4. Solutions for Small Radii

To simplify the equation (6.31), we remind on the fact, that we consider only small deviations from equilibrium here. As a first approach we investigate the limit of small r in Eq. (6.31). According to (5.18) the equilibrium solution is given by

$$n_{\mathrm{eq}}(r) = \frac{A}{r}\sin(kr)\,\Theta(R_0 - r)\,. \tag{6.32}$$

In the limit of small r we get the following expansions

$$\frac{1}{n_{\rm eq}(r)} \approx \frac{1}{Ak}\left[1+\frac{(kr)^2}{6}\right], \tag{6.33}$$

$$\frac{1}{n_{\rm eq}(r)}\frac{\partial n_{\rm eq}(r)}{\partial r} \approx -kr/3\,, \tag{6.34}$$

$$\frac{1}{r^{l+2}}\int_0^r r'^{l+2} f(r')dr' \approx f(0)r+\frac{1}{2}f'(0)r^2\,, \tag{6.35}$$

$$r^{l-1}\int_r^\infty \frac{1}{r'^{l-1}} f(r')dr' \approx \int_0^\infty dr' f(r') - f(0)r - \frac{1}{2}f'(0)r^2\,. \tag{6.36}$$

For the expansions of the integrals, we used the relation (5.6). Inserting these results into (6.31) leads to a rough estimation to lowest order in r

$$0 = \frac{\partial^2 f(r)}{\partial r^2} + \frac{2}{r}\frac{\partial f(r)}{\partial r} + f(r)\left[\frac{4\pi u}{g} + \frac{M\Omega^2}{gkA} - \frac{l(l+1)}{r^2}\right]. \tag{6.37}$$

This is a Bessel differential equation with the general solution [60, 8.401–8.403]

$$f(r) = c_1\frac{J_{\frac{1}{2}(2l+1)}\left(r\sqrt{\frac{Agk^3+M\Omega^2}{Akg}}\right)}{\sqrt{r}} + c_2\frac{Y_{\frac{1}{2}(2l+1)}\left(r\sqrt{\frac{Agk^3+M\Omega^2}{Akg}}\right)}{\sqrt{r}}\,, \tag{6.38}$$

where $J_\nu(x)$ and $Y_\nu(x)$ are Bessel functions of first and second kind. For the *monopole mode: l=0*, we obtain

$$f(r) = \frac{\sqrt{\frac{2}{\pi}}\left[c_1\sin\left(r\sqrt{k^2+\frac{M\Omega^2}{Agk}}\right) - c_2\cos\left(r\sqrt{k^2+\frac{M\Omega^2}{Agk}}\right)\right]}{r\sqrt{k^2+\frac{M\Omega^2}{Agk}}}\,. \tag{6.39}$$

However, we additionally need boundary conditions. To keep the function finite in the limit $r \to 0$, we have to set $c_2 = 0$. Furthermore, we assume the condition that the excitations vanish at the Thomas-Fermi radius, $f(R_0) = 0$, respectively as the equilibrium solution does at $R_0 = \pi/k$:

$$R_0\sqrt{k^2+\frac{M\Omega^2}{Agk}} = n\pi\,. \tag{6.40}$$

Using the definitions of A of (5.15) and k of (5.10), we get

$$\Omega^2 = (n^2-1)\frac{N8\sqrt{\pi}}{M}\frac{u^{5/2}}{g^{3/2}}\,. \tag{6.41}$$

For $n = 0$ the whole equation (6.40) vanishes and so does the function $f(r)$ in (6.39). And for $n = 1$ the frequency vanishes and the result goes back to the static solution. So, the first excitation occurs for $n = 2$.

6.2. Time-Dependent Variational Approach

In this section we follow Ref. [67] and use a variational test function to calculate the dynamics of the condensate at $T = 0$. The test function that we use is almost the same as the one we had previously used in Section 5.2. But now we take into account time-dependent parameters $\lambda(t)$ and $B(t)$. With the oscillator length l, we introduce

$$\Psi(r,t) = \frac{\sqrt{N}}{\pi^{3/4}\lambda(t)^{3/2}l^{3/2}} \exp\left\{-r^2\left[\frac{1}{2\lambda(t)^2l^2} + \imath B(t)\right]\right\}. \tag{6.42}$$

Here, $\lambda(t)$ describes the time-dependent spatial width of the Gaussian and $B(t)$ is the curvature and corresponds to the width in momentum space, which is necessary as shown in Ref. [68]. The function has to be plugged into the Lagrange-density (5.29) and integrated over d^3r to receive the Lagrange-function. We use an isotropic harmonic trap only. Anisotropy would just give rise to frequencies that are affected by different trap modes, but trap features are not a main goal of this thesis. The result for the Lagrangian depending on $\lambda(t)$ and $B(t)$, compare to (5.33) to (5.36), reads with dots for partial time derivatives

$$L = \frac{3N\hbar^2}{2M\omega}\dot{B}\lambda^2 - \frac{3N\hbar^2}{4M}\left[\frac{M\omega}{\hbar\lambda^2} + \frac{(2B\lambda)^2\hbar}{M\omega}\right] - \frac{3N\hbar\omega}{4}(\lambda^2 + \frac{2}{3}\tilde{g}\lambda^{-3} - 2\tilde{u}\lambda^{-1}) \tag{6.43}$$

with the dimensionless parameters $\tilde{u}$ and $\tilde{g}$ that were already introduced in (5.37). To derive equations of motion for λ and B, we have to calculate the corresponding Euler-Lagrange-equations

$$\frac{\partial L}{\partial \lambda} - \frac{d}{dt}\frac{\partial L}{\partial \dot{\lambda}} = 0\,, \qquad \frac{\partial L}{\partial B} - \frac{d}{dt}\frac{\partial L}{\partial \dot{B}} = 0 \tag{6.44}$$

that lead to the following system of coupled differential equations

$$\frac{\hbar}{M\omega}\dot{B}\lambda - \frac{\hbar}{4M}\left(-\frac{2M\omega}{\hbar\lambda^3} + \frac{8B^2\lambda\hbar}{M\omega}\right) - \frac{\omega}{2}\left(\lambda - \tilde{g}\lambda^{-4} - \tilde{u}\lambda^{-2}\right) = 0\,, \tag{6.45}$$

$$B = -\frac{M\dot{\lambda}}{2\hbar\lambda}\,. \tag{6.46}$$

After inserting $B(t)$ and $\dot{B}(t)$ from (6.46) into (6.45), we obtain a resulting differential equation for $\lambda(t)$

$$\boxed{\ddot{\lambda} - \omega^2/\lambda^3 = -\omega^2\left(\lambda - \tilde{g}\lambda^{-4} + \tilde{u}\lambda^{-2}\right).} \tag{6.47}$$

The result (6.47) can be understood as a particle moving in a time-dependent potential

$$\ddot{\lambda}(t) = -\frac{\partial V(t)}{\partial \lambda} \tag{6.48}$$

with the potential

$$V(\lambda) = \frac{\omega^2}{2}\left(w\lambda^2 + \kappa\lambda^{-2} + \frac{2}{3}\tilde{g}\lambda^{-3} - 2\tilde{u}\lambda^{-1}\right). \tag{6.49}$$

Here we introduced again the parameters w and κ to keep in mind that the terms originated from the trap and kinetic energy, respectively.

Our goal was to investigate the dynamics of the condensate. Therefore we assume the condensate to be slightly elongated out of rest: $\lambda(t) = \lambda_0 + \delta\lambda(t)$ where λ_0 is the rest position and $\delta\lambda(t)$ the small excitation. First, it is necessary to calculate the rest positions, i.e., the minima of the potential, but the attentive reader immediately notices that (6.49) corresponds to $H(\lambda)$ in (5.39) and we may just copy the values of λ_0 from Section 5.2, see Fig. 5.3 and Eq. (5.41). Now we can plug the expansion into (6.48), (6.49) and collect all terms of the same order in $\delta\lambda$:

$$V(\lambda_0, \delta\lambda) = V(\lambda_0) + \frac{\delta\lambda^2\omega^2}{2}\left(w + \frac{3\kappa}{{\lambda_0}^4} + \frac{4\,\tilde{g}}{{\lambda_0}^5} - \frac{2\,\tilde{u}}{{\lambda_0}^3}\right) + \dots . \tag{6.50}$$

Here, we can simply read off the oscillation frequency

$$\Omega/\omega = \sqrt{w + \frac{3\kappa}{{\lambda_0}^4} + \frac{4\,\tilde{g}}{{\lambda_0}^5} - \frac{2\,\tilde{u}}{{\lambda_0}^3}}\,. \tag{6.51}$$

The mode corresponding to our frequency is the breathing mode as illustrated in Fig. 6.1 as the test function depends only on the radial coordinate. This simple mode just grows and shrinks along the radial coordinate. Finally, we can compare the modes of the different regions listed in the table in Fig. 6.1 (compare to Section 5.2) which lead to the three rather simple results of Fig. 6.1. The frequencies of "TF-Hard" and "Ideal" are proportional to the trap frequency and so just modulated by the applied potential. The third, "Grav", is proportional to the square of the magnitude of the long-range interaction and so implicitly to the square of the oscillator length wherefore the trap frequency is cancelled in Ω/ω.

TF-Grav and Trapless Modes

The important regimes of "TF-Grav", $\kappa = 0$, $w = 0$, and "Trapless", $w = 0$, will be discussed in more detail. To avoid ambiguities, as there is still the trap frequency included in $\tilde{u}$, $\tilde{g}$, we return to a description using the interaction strengths according to (5.37).

These two regimes differ only in the kinetic term which is included in the Trapless case. For the "TF-Grav" regime, we obtain the result

$$\Omega_{\mathrm{TF-Grav}} = \sqrt{2}\,\frac{\tilde{u}^{5/4}}{\tilde{g}^{3/4}}\,\omega = \frac{8\pi^2\hbar\sqrt{N}}{3M}\left(\frac{2\pi}{3}\frac{1}{a^3 a_{\mathrm{G}}^5}\right)^{1/4}. \tag{6.52}$$

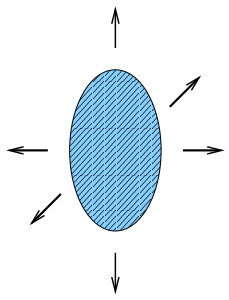

	TF-Hard $\kappa = 0,\ \tilde{u} = 0$	**Ideal** $\tilde{g} = 0,\ \tilde{u} = 0$	**Grav** $\tilde{g} = 0,\ w = 0$
Ω/ω	$\sqrt{5}$	2	$\tilde{u}^2$

Fig. 6.1: Illustration of the breathing mode and summary of three simple excitation frequencies. In the Grav-regime, $\tilde{u}^2$ is proportional to $1/\omega$ by its definition (5.37).

This regime describes the self-stability of the condensate enabled by the balance of the two interactions. In the "Trapless" region the kinetic term adds to the repulsive contact interaction. The comparison of the two gives again rise to the strength of the kinetic term and the validity of the Thomas-Fermi approximation. In the second case, we get with

$$\Omega_{\text{Trapless}} = 4\tilde{u}^2 \, \frac{(1+4\tilde{u}\tilde{g})^{1/4}}{(1+\sqrt{1+4\tilde{u}\tilde{g}})^2} \, \omega = \frac{128N^2\pi^3\hbar}{9Ma_{\text{G}}^2} \, \frac{\left(1+\frac{32aN^2\pi}{3a_{\text{G}}}\right)^{1/4}}{\left(1+\sqrt{1+\frac{32aN^2\pi}{3a_{\text{G}}}}\right)^2} \, . \tag{6.53}$$

For reasonable particle numbers, we can approximate $32aN^2\pi/3a_{\text{G}} \gg 1$ and neglect all "+1" summands in (6.53). In that limit (6.53) passes over to (6.52). Therefore, it is sufficient to discuss only the "TF-Grav" regime. Graphical results are depicted in Fig. 6.2. The set of curves shows the oscillation frequency particularly as a function of the characteristic lengths of the interactions, a, a_{G}, for several values of the other parameter. In the "Trapless" case the curves look almost the same except for slight shifts.

The differential equation (6.48) has also been solved numerically for the Trapless regime, depicted in Fig. 6.2(b). The chosen initial conditions are

$$\lambda(0) = \lambda_0 \, , \qquad \dot{\lambda}(0) = 0 \, , \tag{6.54}$$

while λ_0 was given in (5.41). Here, we used the dimensionless quantities as given in (6.48). So, we still had the trap frequency involved but it drops out in all results. To compare the frequency, we can estimate the periodic time from the plot Fig. 6.2(b). For instance, for the black curve we get $\Omega = 2.37$, while the value from (6.53) yields $\Omega = 2.18$. So, we can assume that the linearization of (6.50) is a good approximation. We also see that for larger relation $\tilde{u}/\tilde{g}$ the oscillation frequency rises.

Comparison with Hydrodynamic Result

The result of the "TF-Grav" regime (6.52) can be compared with the approximative result of the hydrodynamic theory for small radii Eq. (6.41). The quantities $\tilde{g}$ and $\tilde{u}$ were defined

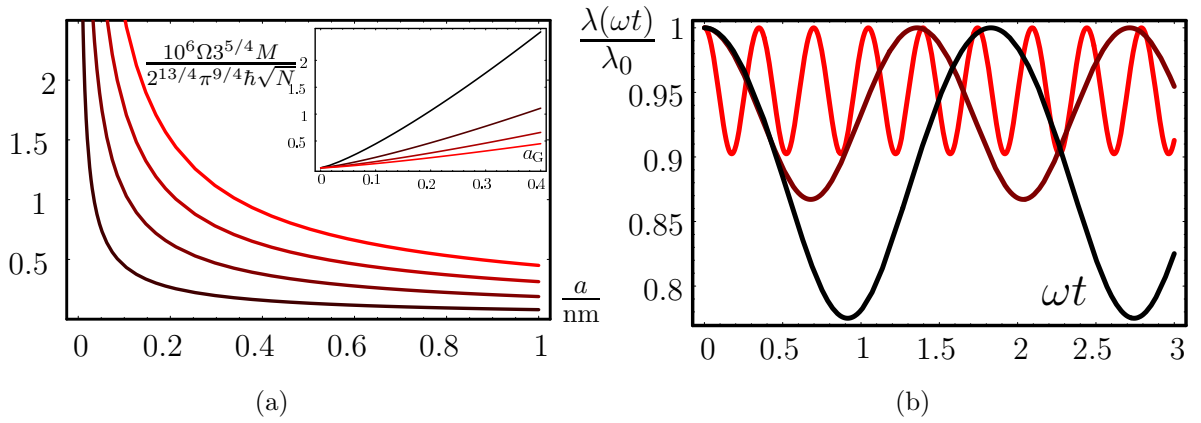

(a) (b)

Fig. 6.2: Excitation frequency of the TF-Grav regime. (a): as a function of the s-wave scattering length a for different values of the long-range length a_G for (dark red to light red): 0.1, 0.2, 0.3, 0.4 m. Inlet: vice versa, excitation frequency as a function a_G for different a: 1, 3, 6, 10 nm. The ordinate has the same label in both cases. (b): Numerical solutions of (6.48) in the Trapless regime with the initial conditions (6.54). Here, for $\tilde{u} = 20$ and different $\tilde{g}$: $5, 40, 80$ (light to dark red).

proportional to the interaction strengths g and u in (5.38). Thus, both results (6.41) and (6.52) show already the same dependence on u and g. So, it remains to compare the coefficients of the excitation frequency. Expressing $\tilde{u}$, $\tilde{g}$ by u, g in (6.52), we obtain

$$2\frac{\tilde{u}^{5/2}}{\tilde{g}^{3/2}}\omega^2 = \frac{512\pi N}{9\sqrt{3}M}\frac{u^{5/2}}{g^{3/2}}\,. \tag{6.55}$$

Hence, we get for the two frequencies, with the lowest order $n = 2$ for (6.41),

$$\Omega^2_{\text{Hy}} = 3\,\frac{N8\sqrt{\pi}}{M}\frac{u^{5/2}}{g^{3/2}}\,, \qquad \Omega^2_{\text{TF-Grav}} = \frac{64\sqrt{\pi}}{9\sqrt{3}}\,\frac{N8\sqrt{\pi}}{M}\,\frac{u^{5/2}}{g^{3/2}}\,. \tag{6.56}$$

The coefficient of the right-hand side is $\frac{64\sqrt{\pi}}{9\sqrt{3}} = 7.28$ which makes the result for $\Omega_{\text{TF-Grav}}$ about 2.4 times than Ω_{Hy}. As the approximation for small radii in Section 6.1.4 was pretty rough, we rather trust the result of the variational approach but the dependence on the interaction strengths $\tilde{u}^{5/4}/\tilde{g}^{3/2}$ was confirmed.

7. Shift of Critical Temperature

In this part of the thesis we focus our attention on the critical region around the phase transition. In detail, we will calculate the temperature shift that is caused by both interactions, the contact interaction (1.2) and the long-range $1/r$ interaction (1.5). In the first section we will derive the tools to get the shift using Feynman's diagrammatic technique of many-body physics for an arbitrary two-particle interaction [14,38,69–72]. Because the gas is dilute, it is sufficient to calculate only the first-order diagrams of the grand-canonical free energy and the corresponding self-energy. The latter describes the effect of the interaction to the correlation function and is of big importance as it is an indicator of the phase transition as we have already seen discussing the non-interacting case in Section 3.5. As we will not take into account the order parameter, this method is valid when we approach the critical point from above. In Section 7.4.2 we will show that we get the same result starting from the Hartree-Fock mean-field theory derived in Section 4. In contrast to the first method, this method includes a fraction of condensed particles and reaches the critical point from below T_c. The results will be discussed in Section 7.5.

7.1. First-Order Perturbation Theory

In this section we investigate the influence of a weak interaction to the thermodynamics of Bose gases. Therefore, we determine the grand-canonical free energy within first-order perturbation theory in the case of an arbitrary two-particle interaction potential $V^{(\mathrm{int})}(\mathbf{x}-\mathbf{x}')$. At first, we need the partition function of the full problem (4.6) with the action (4.7). The associated correlation function is defined just like the non-interacting one according to (3.27) as

$$G(\mathbf{x},\tau;\mathbf{x}',\tau') = \frac{1}{\mathcal{Z}} \oint \mathcal{D}\psi^* \, \mathcal{D}\psi \;\, \psi(\mathbf{x},\tau)\psi^*(\mathbf{x}',\tau') \, e^{-\left(\mathcal{A}^{(0)}[\psi^*,\psi]+\mathcal{A}^{(\mathrm{int})}[\psi^*,\psi]\right)/\hbar} \,. \tag{7.1}$$

As we assumed the interaction to be reasonably small, we expand the functional integrals in (4.6) in powers of $V^{(\mathrm{int})}(\mathbf{x}-\mathbf{x}')$ up to first order:

$$\begin{aligned} \mathcal{Z} = \oint \mathcal{D}\psi^* \, \mathcal{D}\psi \; e^{-\mathcal{A}^{(0)}[\psi^*,\psi]} \Big[1 - \frac{1}{2\hbar} \int_0^{\hbar\beta} d\tau \int d^3x \int d^3x' \psi^*(\mathbf{x},\tau)\psi^*(\mathbf{x}',\tau) \\ \times \psi(\mathbf{x},\tau)\psi(\mathbf{x}',\tau) V^{(\mathrm{int})}(\mathbf{x}-\mathbf{x}') \; + \ldots \Big]. \end{aligned} \tag{7.2}$$

The first term is just the interaction free partition function, while the second contains the interaction-free expectation values of the fields. The expectation of the four fields can be evaluated with the help of Wick's rule, i.e., a pairwise contraction of the fields. With (3.27) and the constraint that we regard only normal averages, we get

$$\begin{aligned}\langle\psi^*(\mathbf{x},\tau)\psi^*(\mathbf{x}',\tau)\psi(\mathbf{x},\tau)\psi(\mathbf{x}',\tau)\rangle^{(0)} &= G^{(0)}(\mathbf{x},\tau;\mathbf{x},\tau)\,G^{(0)}(\mathbf{x}',\tau;\mathbf{x}',\tau)\\ &\quad + G^{(0)}(\mathbf{x},\tau;\mathbf{x}',\tau)\,G^{(0)}(\mathbf{x}',\tau;\mathbf{x},\tau)\,.\end{aligned} \tag{7.3}$$

The notation can be simplified, if we use Feynman diagrams, which are constructed out of lines and vertices. The construction of the diagram follows from a few *Feynman rules*. A straight line with an arrow represents the interaction-free correlation function (3.27), also known as the propagator from space-time point $(\mathbf{x}',\tau')$ to $(\mathbf{x},\tau)$:

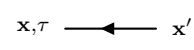

$$\equiv \quad G^{(0)}(\mathbf{x},\tau;\mathbf{x}',\tau')\,. \tag{7.4}$$

Furthermore, spatio-temporal integrals over the two-particle interaction potential are pictured by two vertices connected by a dashed line

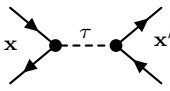

$$\equiv \quad -\frac{1}{\hbar}\int_0^{\hbar\beta} d\tau \int d^3x \int d^3x'\, V^{(\mathrm{int})}(\mathbf{x}-\mathbf{x}') \quad . \tag{7.5}$$

Up to the first order in the two-particle interaction, the grand-canonical free energy (3.3) reads with the upper diagrammatic rules

$$\mathcal{F} \;=\; \mathcal{F}^{(0)} - \frac{1}{\beta}\Bigg\{ \;\frac{1}{2}$$

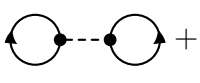

$$+\,\frac{1}{2}$$

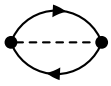

$$+\,\ldots\Bigg\}\,. \tag{7.6}$$

The first term in (7.6) is the interaction-free contribution to the grand-canonical free energy (3.34). The second term in (7.6) is called direct or Hartree-like vacuum diagram because the vertex connects only propagators with equal spatio-temporal arguments. Finally, in the third term, propagators with different spatial arguments are connected; that is the reason why it is called exchange or Fock-like vacuum diagram. Besides, it is worth while to mention, that all these and higher-order connected vacuum diagrams together with their proper weights follow from solving a graphical recursion relation [73]. The

diagrammatic contributions have the following analytic expressions:

$$\mathcal{F}^{(\mathrm{D})} = \frac{1}{2\hbar\beta}\int_0^{\hbar\beta} d\tau \int d^3x \int d^3x'\, V^{(\mathrm{int})}(\mathbf{x}-\mathbf{x}')\, G^{(0)}(\mathbf{x},\tau;\mathbf{x},\tau) G^{(0)}(\mathbf{x}',\tau;\mathbf{x}',\tau)\,, \quad (7.7)$$

$$\mathcal{F}^{(\mathrm{E})} = \frac{1}{2\hbar\beta}\int_0^{\hbar\beta} d\tau \int d^3x \int d^3x'\, V^{(\mathrm{int})}(\mathbf{x}-\mathbf{x}')\, G^{(0)}(\mathbf{x},\tau;\mathbf{x}',\tau) G^{(0)}(\mathbf{x}',\tau;\mathbf{x},\tau)\,. \quad (7.8)$$

Both expressions contain the interaction-free correlation function (3.27) with equal imaginary times, which is given in semiclassical approximation in Eq. (3.31). The calculation of Eq. (7.7) and (7.8) is pretty straight-forward. We only add for this purpose, that we replace the interaction potential by its Fourier transform

$$V(\mathbf{x}-\mathbf{x}') = \int \frac{d^3q}{(2\pi\hbar)^3} V(\mathbf{q}) e^{\imath\mathbf{q}(\mathbf{x}-\mathbf{x}')/\hbar}. \quad (7.9)$$

For the special case of the harmonic trap potential (3.33), we obtain

$$\mathcal{F}^{(\mathrm{D})} = \frac{1}{2(\hbar\beta\tilde{\omega})^6}\sum_{n=1}^{\infty}\sum_{n'=1}^{\infty}\frac{e^{(n+n')\beta\mu}}{n^3 n'^3}\int \frac{d^3q}{(2\pi\hbar)^3} V^{(\mathrm{int})}(\mathbf{q}) \exp\left\{-\sum_{j=1}^{3}\frac{(n+n')\,q_j^2}{2\hbar^2\beta M n n'\omega_j^2}\right\}, \quad (7.10)$$

$$\mathcal{F}^{(\mathrm{E})} = \frac{1}{2(\hbar\beta\tilde{\omega})^3}\sum_{n=1}^{\infty}\sum_{n'=1}^{\infty}\frac{e^{(n+n')\beta\mu}}{(n+n')^3}\int \frac{d^3q}{(2\pi\hbar)^3} V^{(\mathrm{int})}(\mathbf{q}) \exp\left\{-\frac{\beta n n'\mathbf{q}^2}{2M(n+n')}\right\}. \quad (7.11)$$

In the calculation from (7.7) and (7.8) to (7.10) and (7.11) the spatial integrals with respect to $\mathbf{x}$ and $\mathbf{x}'$ had to be evaluated. These two only converge if a trapping potential is present. The geometric mean trap frequency $\tilde{\omega}$ was already defined in (3.35).

7.2. Corrections to Chemical Potential

In Section 3.5, we found for the non-interacting Bose gas the criterion for the phase transition from a Bose gas to BEC to be a divergence of the correlation function $G^{(0)}(\mathbf{x},\tau;\mathbf{x}',\tau')$, i.e., its functional inverse $G^{(0)-1}(\mathbf{x},\tau;\mathbf{x}',\tau')$ had to vanish. The same argument will be used to find the critical point also in the interacting case. But due to the two-particle interaction, we have to take into account the correlation function (7.1) of the full partition function (4.6). This is not any more given by the integral kernel (3.19), but gets additional terms because of the interaction. All interaction effects are incorporated by the so-called self-energy $\Sigma(\mathbf{x},\tau;\mathbf{x}',\tau')$:

$$G^{-1}(\mathbf{x},\tau;\mathbf{x}',\tau') = G^{(0)\,-1}(\mathbf{x},\tau;\mathbf{x}',\tau') - \Sigma(\mathbf{x},\tau;\mathbf{x}',\tau')\,. \quad (7.12)$$

Writing the interaction action (4.8) with an integral kernel $\Sigma(\mathbf{x},\tau;\mathbf{x}',\tau')$ according to (3.19), we obtain in first order perturbation theory the two contributions [18]:

$$\Sigma^{(\mathrm{D})}(\mathbf{x},\tau;\mathbf{x}',\tau') = \frac{-1}{\hbar}\,\delta(\tau-\tau')\delta(\mathbf{x}-\mathbf{x}')\int d^3x''\,V^{(\mathrm{int})}(\mathbf{x}-\mathbf{x}'')G^{(0)}(\mathbf{x}'',\tau;\mathbf{x}'',\tau)\,, \quad (7.13)$$

$$\Sigma^{(\mathrm{E})}(\mathbf{x},\tau;\mathbf{x}',\tau') = \frac{-1}{\hbar}\,\delta(\tau-\tau')V^{(\mathrm{int})}(\mathbf{x}-\mathbf{x}')G^{(0)}(\mathbf{x},\tau;\mathbf{x}',\tau)\,. \quad (7.14)$$

Eq. (7.13) is the direct of Hartree term of the self energy and (7.14) the exchange or Fock term. These results could have also been obtained by the functional differentiation (4.29)

$$\Sigma(\mathbf{x},\tau;\mathbf{x}',\tau') = -\beta\frac{\delta\mathcal{F}}{\delta G^{(0)}(\mathbf{x}'',\tau';\mathbf{x}''',\tau'')}\,. \quad (7.15)$$

Graphically, this functional differentiation corresponds to the amputation of a line in every connected vacuum diagram of the grand-canonical free energy [53,54]. Thus, we obtain from (7.6)

$\Sigma(\mathbf{x},\tau;\mathbf{x}',\tau') =$ 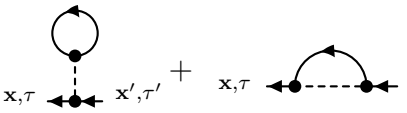 (7.16)

For the critical point, we have to find the zero of (7.12). Therefore, we consider its Fourier-Matsubara transform

$$G^{-1}(\mathbf{x},\tau;\mathbf{x}',\tau') = \frac{1}{\hbar\beta}\sum_{m=-\infty}^{\infty} e^{-\imath\omega_m(\tau-\tau')}\int\frac{d^3p}{(2\pi\hbar)^3}\,e^{\imath\,\mathbf{p}(\mathbf{x}-\mathbf{x}')/\hbar}\,G^{-1}(\mathbf{p},\omega_m;\mathbf{x})\,, \quad (7.17)$$

where the Matsubara frequencies are defined in (3.15). This leads with (3.40) to the equation

$$G^{-1}(\mathbf{p},\omega_m;\mathbf{x}) = \frac{1}{\hbar}\left\{-\imath\hbar\omega_m + \frac{\mathbf{p}^2}{2M} + V^{(\mathrm{ext})}(\mathbf{x}) - \mu\right\} - \Sigma(\mathbf{p},\omega_m;\mathbf{x}) = 0\,, \quad (7.18)$$

where the Fourier-Matsubara transform of the self-energy follows in analogy to Eq. (3.37) from

$$\Sigma(\mathbf{p},\omega_m;\mathbf{x}) = \int_0^{\hbar\beta} d\tau\,e^{\imath\omega_m\tau}\int d^Dx'\,e^{-\imath\mathbf{p}\mathbf{x}'/\hbar}\,\Sigma\left(\mathbf{x}+\frac{\mathbf{x}'}{2},\tau;\mathbf{x}-\frac{\mathbf{x}'}{2},0\right)\,. \quad (7.19)$$

The critical point is reached as the lowest possibility to fulfill Eq. (7.18). This happens up to lowest perturbative order at vanishing momentum $\mathbf{p}=\mathbf{0}$ and Matsubara frequency

$\omega_m = 0$ like in the Section 3.5. Furthermore, we conclude that the additional contributions (7.13), (7.14) of the self-energy do not change the location of the potential minimum $\mathbf{x}_{\min} = \mathbf{0}$. So, we get from Eq. (7.18) the equation for the new critical potential as

$$\mu_c = -\hbar\,\Sigma(\mathbf{0}, 0; \mathbf{0})\,. \tag{7.20}$$

Here, we also have two contributions to the chemical potential, namely the direct term $\mu_c^{(\mathrm{D})} = -\hbar\,\Sigma^{(\mathrm{D})}(\mathbf{0}, 0; \mathbf{0})$ and the exchange term $\mu_c^{(\mathrm{E})} = -\hbar\,\Sigma^{(\mathrm{E})}(\mathbf{0}, 0; \mathbf{0})$. So, we obtain up to first order the complete critical potential $\mu_c = 0 + \mu_c^{(\mathrm{D})} + \mu_c^{(\mathrm{E})} + \ldots$, where the respective terms read, according to (3.30), (7.13), and (7.14):

$$\mu_c^{(\mathrm{D})} = \frac{1}{(\hbar\beta\tilde{\omega})^3} \sum_{n=1}^{\infty} \frac{1}{n^3} \int \frac{d^3q}{(2\pi\hbar)^3}\, V^{(\mathrm{int})}(\mathbf{q})\, \exp\left\{ -\sum_{j=1}^{3} \frac{q_j^2}{2\hbar^2 \beta M n \omega_j^2} \right\}, \tag{7.21}$$

$$\mu_c^{(\mathrm{E})} = \sum_{n=1}^{\infty} \int \frac{d^3q}{(2\pi\hbar)^3}\, V^{(\mathrm{int})}(\mathbf{q})\, \exp\left\{ -\sum_{j=1}^{3} \frac{\beta n\, q_j^2}{2M} \right\}. \tag{7.22}$$

During the calculation of (7.21) and (7.22), we had to insert the correlation function (3.30) into (7.13) and (7.14). That Eq. (3.30) contains the factor $e^{n\beta\mu}$, which was set to "1" in first order in (7.21) and (7.22), according to $\mu_c^{(0)} = 0$ from (3.41).

7.3. Model Interaction

In the following section, we calculate the grand-canonical free energy and self-energy terms for a contact plus long-range interaction. At first, we need their Fourier-transforms to further evaluate the expressions (7.10), (7.11), (7.21), and (7.22).

7.3.1. Fourier Transform of Interaction

The expressions for the self-energy and grand-canonical free energy contain the Fourier transform (7.9) of the interaction, which has to be further specified. In the case of a contact interaction, we immediately get

$$V_\delta^{(\mathrm{int})}(\mathbf{q}) = \frac{4\pi\hbar^2 a}{M}\,. \tag{7.23}$$

In more detail we will show how to get the Fourier transform of $V^{(\mathrm{int})}(\mathbf{x}) = C/|\mathbf{x}|$:

$$V^{(\mathrm{int})}(\mathbf{q}) = \int d^3x\, \frac{C}{|\mathbf{x}|}\, e^{-\imath\mathbf{q}\mathbf{x}/\hbar}\,. \tag{7.24}$$

In total we will work out three different methods. *First*, the direct calculation, yields with spherical coordinates:

$$V^{(\mathrm{int})}(\mathbf{q}) = 2\pi \int_0^\infty dr\, r \int_{-1}^{+1} d\cos\vartheta\, C\, e^{-\imath q r \cos\vartheta/\hbar}. \tag{7.25}$$

The ϑ-integration can easily be evaluated but we have to introduce a convergence factor "$\lim_{\eta\to 0} e^{-\eta r}$" for the remaining r-integration:

$$V^{(\mathrm{int})}(\mathbf{q}) = \frac{4\pi\hbar C}{\mathbf{q}} \lim_{\eta\to 0} \int_0^\infty dr \sin\left(\frac{qr}{\hbar}\right) e^{-\eta r}. \tag{7.26}$$

After integrating and taking the limit, we end up with the result

$$V^{(\mathrm{int})}(\mathbf{q}) = \frac{4\pi C\hbar^2}{\mathbf{q}^2}. \tag{7.27}$$

In the *second* version we integrate Eq. (7.24) twice by parts. Here we have to mention, that the boundary terms vanish:

$$V^{(\mathrm{int})}(\mathbf{q}) = -C \int d^3x \left(\Delta \frac{1}{|\mathbf{x}|}\right) \frac{\hbar^2}{\mathbf{q}^2} e^{-\imath \mathbf{q}\mathbf{x}/\hbar}. \tag{7.28}$$

Now we use the distributional relation (6.22) and get the same result, Eq. (7.27).

Last, in the *third* version, we will use the Schwinger proper-time representation (4.54). After plugging Eq. (4.54) into Eq. (7.24), we complete the exponent to a quadratic form in $\mathbf{x}$ and substitute $\mathbf{x} \to \mathbf{x} + \imath\mathbf{q}/(2\hbar y)$:

$$V^{(\mathrm{int})}(\mathbf{q}) = \int_0^\infty dy\, e^{-\frac{\mathbf{q}^2}{4\hbar^2 y}} y^{-1/2} \int d^3x\, e^{-y\mathbf{x}^2}. \tag{7.29}$$

The latter integral is simply Gaussian, thus we get, with $\Gamma(1/2) = \sqrt{\pi}$,

$$V^{(\mathrm{int})}(\mathbf{q}) = \pi C \int_0^\infty dy\, \frac{1}{y^2}\, e^{-\frac{\mathbf{q}^2}{4\hbar^2 y}}\,. \tag{7.30}$$

The integral in Eq. (7.30) is of the form $\int dx f(x) f'(x)$, thus we again obtain the result Eq. (7.27).

7.3.2. Semiclassical Results

Combining both interactions (7.23) and (7.27), we can write the total two-particle model interaction using $g = 4\pi\hbar^2 a/M$ as

$$V^{(\mathrm{int})}(\mathbf{q}) = \frac{4\pi\hbar^2 C}{\mathbf{q}^2} + g\,. \tag{7.31}$$

In the following, we again restrict ourselves to a cylinder-symmetric trap, $\omega_1 = \omega_2 = \omega_\mathrm{r}$, $\omega_3 = \omega_\mathrm{z}$, as illustrated in Fig. 4.1. Now we calculate the influence of the interaction (7.31) on the thermodynamical quantities. To this end, we mention that the remaining integrals in (7.10), (7.11) and (7.21), (7.22) are either Gaussian or of the form

$$I(a_1, a_3) = \int d^3q\, \frac{1}{\mathbf{q}^2}\, \exp\left[-a_1(q_1^2 + q_2^2) - a_3 q_3^2\right]\,. \tag{7.32}$$

The latter integral can be solved by applying the Schwinger proper-time representation (4.54) and we get a simplified form of the master integral (4.58):

$$I(a_1, a_3) = \int_0^\infty dy \left[(a_1 + y)\sqrt{a_3 y + y^2}\,\right]^{-1} \tag{7.33}$$

With the definition of the anisotropy function $f(\kappa)$ of (4.64) with $\kappa = \omega_\mathrm{r}/\omega_\mathrm{z}$, we get:

$$I(a_1, a_3) = \frac{2\pi^{3/2}}{\sqrt{a_1}}\,\kappa^{-1/3} f(\kappa)\,. \tag{7.34}$$

Therefore, we find for our perturbative results (7.10), (7.11) and (7.21), (7.22):

$$\mathcal{F}^{(\mathrm{D})} = \frac{1}{2(\hbar\beta\tilde{\omega})^3}\,\frac{1}{\lambda_\mathrm{T}^3}\left[g\,\zeta_{\frac{3}{2},\frac{3}{2},\frac{3}{2}}(e^{\beta\mu}) + \frac{4\pi\hbar^2 C\beta}{M\,(\hbar\beta\tilde{\omega})^2}\,\zeta_{\frac{5}{2},\frac{5}{2},\frac{1}{2}}(e^{\beta\mu})\,f(\kappa)\right]\,, \tag{7.35}$$

$$\mathcal{F}^{(\mathrm{E})} = \frac{1}{2(\hbar\beta\tilde{\omega})^3}\,\frac{1}{\lambda_\mathrm{T}^3}\left[g\,\zeta_{\frac{3}{2},\frac{3}{2},\frac{3}{2}}(e^{\beta\mu}) + \frac{4\pi\hbar^2 C\beta}{M}\,\zeta_{\frac{1}{2},\frac{1}{2},\frac{5}{2}}(e^{\beta\mu})\right]\,, \tag{7.36}$$

$$\mu_c^{(\mathrm{D})} = \frac{1}{\lambda_\mathrm{T}^3}\left[g\,\zeta\left(\frac{3}{2}\right) + \frac{4\pi\hbar^2 C\beta}{M\,(\hbar\beta\tilde{\omega})^2}\,\zeta\left(\frac{5}{2}\right)\,f(\kappa)\right]\,, \tag{7.37}$$

$$\mu_c^{(\mathrm{E})} = \frac{1}{\lambda_\mathrm{T}^3}\left[g\,\zeta\left(\frac{3}{2}\right) + \frac{4\pi\hbar^2 C\beta}{M}\,\zeta\left(\frac{1}{2}\right)\right]\,, \tag{7.38}$$

where λ_T is the thermal de Broglie wavelength (1.1) and $\zeta_{a,b,c}(z)$ the generalization of the polylogarithmic function (4.70). One can see, that the terms in (7.35) to (7.38) depend only on the ratio and the geometric mean of the trap frequencies (3.35).

7.3.3. Divergence of Chemical Potential

In Eq. (7.38), we obtained the diverging term $\zeta(1/2)$ which is shorthanded for the summation

$$\zeta\left(\frac{1}{2}\right) = \sum_{n=1}^{\infty} \frac{1}{\sqrt{n}}\,. \tag{7.39}$$

Actually, it is not correct to write (7.39) in this representation. The left-hand side is a zeta function which has a fixed value $\zeta(1/2) = -1.4604$ as its analytic continuation and on the right-hand side we have a diverging sum. As using the analytic continuation of $\zeta(1/2)$ is not justified physically, we investigate its origin.

It appeared through the integration in (7.22). If one performs the summation over n first, which is a geometric series, one gets for the long-range interaction

$$\mu_c^{(\mathrm{E})}(g=0) = \int \frac{d^3q}{(2\pi\hbar)^3}\,\frac{4\pi\hbar^2 C}{\mathbf{q}^2}\,\frac{1}{1-\exp\left\{-\frac{\beta\,\mathbf{q}^2}{2M}\right\}}\,. \tag{7.40}$$

The integral diverges for $\mathbf{q}=0$, which is the infrared divergence of a $1/r$-interaction. Here, the reason of its occurrence is the semiclassical approximation of the correlation function (3.31) in (7.14). Therefore, we evaluate the expressions of grand-canonical free energy and self-energy again, this time, however, by using the quantum-mechanical propagator of a harmonic oscillator instead of the semiclassical one.

7.3.4. Quantum-Mechanical Calculation

The many-body propagator follows from the imaginary-time amplitude according to (A.21) and Ref. [36] for equal imaginary times as

$$\begin{aligned} G^{(0)}(\mathbf{x},\tau;\mathbf{x}',\tau) \;=\; & \sum_{n=1}^{\infty} e^{n\beta\mu}\left[\prod_{j=1}^{3}\sqrt{\frac{M\omega_j}{2\pi\hbar\sinh\hbar\beta\omega_j n}}\right. \\ & \left.\times\exp\left\{-\frac{M\omega_j}{2\hbar\sinh\hbar\beta\omega_j n}\left[\left(x_j^2+x_j'^2\right)\cosh\hbar\beta\omega_j n - 2x_jx_j'\right]\right\}\right]. \end{aligned} \tag{7.41}$$

We have seen in Fig. 4.2 in Section 4.5 that the anisotropy function $f(\kappa)$ has its maximum for an isotropic trap and the same holds for the critical temperature according to the semiclassical results of Section 7.3.2. As the results for a cylinder-symmetric trap show a rather difficult shape, we restrict ourselves here to the isotropic case but state the more general results for a cylinder-symmetric trap in Appendix B.

For the free energy (7.7), (7.8) and the critical chemical potential (7.20) we solve the integrals similar to the semiclassical way and get the following results

$$\mathcal{F}^{(D)}_{\rm QM} = \frac{1}{2\lambda_{\rm T}^3(\hbar\beta\tilde{\omega})^3}\left[g\zeta^{(D)}_{\mathcal{F}g}\left(e^{\beta\mu}\right)+\frac{4\pi\hbar^2 C\beta}{M(\hbar\beta\tilde{\omega})^2}\,\zeta^{(D)}_{\mathcal{F}C}\left(e^{\beta\mu}\right)\right], \tag{7.42}$$

$$\mathcal{F}^{(E)}_{\rm QM} = \frac{1}{2\lambda_{\rm T}^3(\hbar\beta\tilde{\omega})^3}\left[g\,\zeta^{(E)}_{\mathcal{F}g}\left(e^{\beta\mu}\right)+\frac{4\pi\hbar^2 C\beta}{M}\,\zeta^{(E)}_{\mathcal{F}C}\left(e^{\beta\mu}\right)\right], \tag{7.43}$$

$$\mu^{(D)}_{\rm QM} = \frac{1}{\lambda_{\rm T}^3}\left[g\,\zeta^{(E)}_{\mu g}+\frac{4\pi\hbar^2 C\beta}{M(\hbar\beta\tilde{\omega})^3}\zeta^{(D)}_{\mu C}\right], \tag{7.44}$$

$$\mu^{(\rm E)}_{\rm QM} = \frac{1}{\lambda_{\rm T}^3}\left[g\,\zeta^{(E)}_{\mu g}+\frac{4\pi C\hbar^2}{M}\,\zeta^{(E)}_{\mu C}\right]. \tag{7.45}$$

Here, we introduced the modified zeta-functions of the free energy which depend on $\hbar\beta\omega$

$$\zeta^{(D)}_{\mathcal{F}g}\left(e^{\beta\mu}\right) = \sum_{n,m=1}^{\infty} e^{\beta\mu(m+n)}\left[\frac{(\hbar\beta\omega)^2}{\sinh(\hbar\beta\omega n)\sinh(\hbar\beta\omega m)}\,\frac{\hbar\beta\omega/2}{\left(\tanh\frac{\hbar\beta\omega n}{2}+\tanh\frac{\hbar\beta\omega m}{2}\right)}\right]^{3/2}, \tag{7.46}$$

$$\zeta^{(E)}_{\mathcal{F}g}\left(e^{\beta\mu}\right) = \zeta^{(D)}_{\mathcal{F}g}\left(e^{\beta\mu}\right), \tag{7.47}$$

$$\zeta^{(D)}_{\mathcal{F}C}\left(e^{\beta\mu}\right) = \sum_{n,m=1}^{\infty} e^{\beta\mu(m+n)}\frac{\sinh[\hbar\beta\omega(n+m)/2]\,\hbar\beta\omega/2}{\sinh(\hbar\beta\omega n/2)\sinh(\hbar\beta\omega m/2)} \times\left[\frac{(\hbar\beta\omega)^2}{\sinh(\hbar\beta\omega n)\sinh(\hbar\beta\omega m)}\,\frac{\hbar\beta\omega/2}{\tanh\hbar\beta\omega n/2+\tanh\hbar\beta\omega m/2}\right]^{3/2}, \tag{7.48}$$

$$\zeta^{(E)}_{\mathcal{F}C}\left(e^{\beta\mu}\right) = \sum_{n,m=1}^{\infty} e^{\beta\mu(n+m)}\left[\frac{(\hbar\beta\omega)^2}{\sinh(\hbar\beta\omega n)\sinh(\hbar\beta\omega m)}\right]^{3/2} \times\frac{\sqrt{\hbar\beta\omega/2}}{\left(\tanh\frac{\hbar\beta\omega n}{2}+\tanh\frac{\hbar\beta\omega m}{2}\right)^{3/2}}\,\frac{1}{\left(\coth\frac{\hbar\beta\omega n}{2}+\coth\frac{\hbar\beta\omega m}{2}\right)}. \tag{7.49}$$

The corresponding expressions for the functions appearing in the chemical potential read

$$\zeta^{(D)}_{\mu g} = \sum_{n=1}^{\infty}\left[\frac{\hbar\beta\omega}{\sinh\hbar\beta\omega n}\right]^{3/2}, \tag{7.50}$$

$$\zeta^{(E)}_{\mu g} = \zeta^{(D)}_{\mu g}, \tag{7.51}$$

$$\zeta^{(D)}_{\mu C} = \sum_{n=1}^{\infty}\left[\frac{\hbar\beta\omega}{\sinh\hbar\beta\omega n}\right]^{3/2}\frac{\hbar\beta\omega/2}{\tanh(\hbar\beta\omega n/2)}, \tag{7.52}$$

$$\zeta^{(E)}_{\mu C} = \sum_{n=1}^{\infty}\left[\frac{\hbar\beta\omega}{\sinh\hbar\beta\omega n}\right]^{3/2}\frac{\tanh(\hbar\beta\omega n/2)}{\hbar\beta\omega/2}. \tag{7.53}$$

The results (7.42)– (7.44) reduce to (7.35)– (7.37) in the limit $\hbar\beta\omega \ll 1$ that corresponds to the semiclassical approximation. The comparison between the Riemann zeta functions and new corresponding zeta functions is illustrated in Fig. 7.1. We see, that for larger particle numbers the results approach the semiclassical values. But now the previous divergence of the second sum in (7.45) is suppressed by the exponentially growing factor $\sinh \hbar\beta\omega n$ in the denominator and we get finite values. This also means that the analytic continuation of $\zeta(1/2)$ fails in this case.

7.4. Critical Temperature

In this section we calculate the specific shift of the critical temperature for a fixed particle number in an isotropic trap. At first, we use the method that we worked out in this chapter and in the subsequent section, starting from the Hartree-Fock mean-field theory. As we said in the introduction of this chapter, the Feynman perturbation theory approaches the critical point from above and the Hartree-Fock theory from below.

7.4.1. Feynman Perturbation Expansion

The total grand-canonical free energy follows from Eq. (7.6) as the sum of (3.34), (7.35), and (7.36). We will see shortly that the expression for the critical temperature shift only depends on differences of the respective zeta functions. As the zeta functions of the direct term of the long-range interaction for adequate particle numbers are close to the semiclassical generalized zeta-functions and both below the semiclassical values, taking their difference will even diminish errors caused by this approximation. For the contributions of the other terms, we use the quantum results derived in Section 7.3.4.

The complete first-order free energy becomes

$$(\hbar\beta\omega)^3\mathcal{F} = -\frac{1}{\beta}\zeta_4\left(e^{\beta\mu}\right) + \frac{g\,\zeta_{\mathcal{F}g}^{(D,E)}\left(e^{\beta\mu}\right)}{\lambda_{\mathrm{T}}^3} + \frac{4\pi\hbar^2 C\beta}{2M\lambda_{\mathrm{T}}^3}\left[\zeta_{\mathcal{F}C}^{(E)}\left(e^{\beta\mu}\right) + \frac{\zeta_{\frac{5}{2},\frac{5}{2},\frac{1}{2}}\left(e^{\beta\mu}\right)}{(\hbar\beta\omega)^2}\right] \ldots . \tag{7.54}$$

The full problem has to be studied at a fixed particle number $N = -\partial\mathcal{F}/\partial\mu$ which is valid above the critical temperature:

$$(\hbar\beta\omega)^3 N = \zeta_3\left(e^{\beta\mu}\right) - \frac{g\,\beta}{\lambda_{\mathrm{T}}^3}\frac{\partial\zeta_{\mathcal{F}g}^{(D,E)}\left(e^{\beta\mu}\right)}{\partial(\beta\mu)} - \frac{4\pi\hbar^2 C\beta^2}{2M\lambda_{\mathrm{T}}^3}\left[\frac{\partial\zeta_{\mathcal{F}C}^{(E)}\left(e^{\beta\mu}\right)}{\partial(\beta\mu)} + \frac{\zeta_{\frac{5}{2},\frac{5}{2},-\frac{1}{2}}\left(e^{\beta\mu}\right)}{(\hbar\beta\omega)^2}\right] \ldots . \tag{7.55}$$

The first term in Eq. (7.55) contains the interaction-free part. The second term embodies the exchange as well as direct contribution of the contact interaction, while the latter two arise due to the long-range interaction. The term holding the frequency dependence originates in the direct diagram and the remaining one stems from the exchange part. The

N	10	100	10^3	10^4	10^5	10^6
$\hbar\beta_c^{(0)}\omega$	0.4935	0.2291	0.1063	0.0494	0.0229	0.01063
$\zeta_{\mu g}^{(D,E)}$	1.4347	1.8041	2.0604	2.2361	2.3561	2.4388
$\zeta_{\mu g}^{(D,E)}/\zeta\left(\frac{3}{2}\right)$	0.5492	0.6906	0.7887	0.8560	0.9019	0.9336
$\zeta_{\mu g\mathrm{HF}}^{(D,E)}$	1.1431	1.5045	1.8055	2.0379	2.2093	2.3324
$\zeta_{\mu g\mathrm{HF}}^{(D,E)}/\zeta(\frac{3}{2})$	0.4376	0.5759	0.6911	0.7801	0.8457	0.8928
$\partial\zeta_{\mathcal{F}g}^{(D,E)}/\partial(\beta\mu)$	1.3656	1.8443	2.1246	2.2728	2.3470	2.3697
$\partial\zeta_{\mathcal{F}g}^{(D,E)}/\partial(\beta\mu)/\zeta(\frac{3}{2},\frac{3}{2},\frac{1}{2})$	0.5650	0.7631	0.8790	0.9404	0.9711	0.9805
$\zeta_{\mu C}^{(E)}$	2.0607	3.7052	6.1210	9.9161	15.2095	24.2802
$\zeta_{\mu C\mathrm{HF}}^{(E)}$	1.3445	2.5374	4.3497	7.0403	11.0041	16.8290
$\partial\zeta_{\mathcal{F}C}^{(E)}/\partial(\beta\mu)$	0.8661	1.4057	1.8703	2.2335	2.4882	2.6146
$\partial\zeta_{\mathcal{F}C}^{(E)}/\partial(\beta\mu)/\zeta(\frac{1}{2},\frac{1}{2},\frac{3}{2})$	0.2760	0.4480	0.5960	0.7118	0.7929	0.8332
$\zeta_{\mu C}^{(D)}$	1.1865	1.2865	1.32281	1.3353	1.3395	1.3408
$\zeta_{\mu C}^{(D)}/\zeta(5/2)$	0.8844	0.9590	0.9861	0.9954	0.9985	0.9995
$\partial\zeta_{\mathcal{F}C}^{(D)}/\partial(\beta\mu)$	2.3047	2.7912	3.0213	3.1255	3.1719	3.2617
$\partial\zeta_{\mathcal{F}C}^{(D)}/\partial(\beta\mu)/\zeta(\frac{5}{2},\frac{5}{2},-\frac{1}{2})$	0.7178	0.8693	0.9410	0.9734	0.9879	1.0158

Fig. 7.1: Comparing the difference between the Riemann zeta functions and the modified zeta functions for an isotropic trap. At the critical point we get from Eq. (3.44): $\hbar\beta_c^{(0)}\omega = [\zeta(3)/N]^{1/3}$. Blue terms: troubling $\zeta_{\mu C}^{(E)}$ and the corresponding values of the Hartree-Fock result $\zeta_{\mu C\mathrm{HF}}^{(E)}$. We see, that the analytic continuation $\zeta(1/2) = -1.4604$ disagrees in this case. The zeta functions of the free energy are defined in this way because the functions appear this way in the results (7.60), (7.69). Furthermore, after the differentiation the chemical potential has to be set to 0.

critical temperature T_c is obtained from Eq. (7.55) in the limit $\mu \uparrow \mu_c = 0 + \mu_c^{(\mathrm{D})} + \mu_c^{(\mathrm{E})} + \ldots$ Of course, the differentiation with respect to $(\beta\mu)$ has to be done before we go to the limit $\mu \to 0$, which is indicated at the particular terms:

$$\begin{aligned} N &= \frac{1}{(\hbar\beta_c\omega)^3}\zeta(3) + \frac{\beta_\mathrm{c}}{(\hbar\beta_c\omega)^3}\left[\mu_c^{(\mathrm{D})} + \mu_c^{(\mathrm{E})}\right]\zeta(2) - \frac{g\beta_\mathrm{c}}{\lambda_{\mathrm{T_c}}^3(\hbar\beta_c\omega)^3}\left.\frac{\partial\zeta_{\mathcal{F}g}^{(D,E)}\left(e^{\beta\mu}\right)}{\partial(\beta\mu)}\right|_{\mu\to 0} \\ &\quad -\frac{4\pi\hbar^2 C{\beta_\mathrm{c}}^2}{2M\lambda_{\mathrm{T_c}}^3(\hbar\beta_c\omega)^3}\left[\left.\frac{\partial\zeta_{\mathcal{F}C}^{(E)}\left(e^{\beta\mu}\right)}{\partial(\beta\mu)}\right|_{\mu\to 0} + \frac{1}{(\hbar\beta_\mathrm{c}\omega)^2}\,\zeta\left(\frac{5}{2},\frac{5}{2},-\frac{1}{2}\right)\right] + \ldots \end{aligned} \tag{7.56}$$

Recalling (7.37), (7.38), we obtain within first-order perturbation theory

$$\begin{aligned} N &= \frac{\zeta(3)}{(\hbar\beta_c\omega)^3} + \frac{2g\beta_\mathrm{c}}{\lambda_{\mathrm{T_c}}^3(\hbar\beta_c\omega)^3}\left[\zeta(2)\,\zeta_{\mu g}^{(D,E)} - \frac{1}{2}\left.\frac{\partial\zeta_{\mathcal{F}g}^{(D,E)}\left(e^{\beta\mu}\right)}{\partial(\beta\mu)}\right|_{\mu\to 0}\right] \\ &\quad + \frac{4\pi\hbar^2 C{\beta_\mathrm{c}}^2}{M\lambda_{\mathrm{T_c}}^3(\hbar\beta_c\omega)^3}\left[\zeta(2)\,\zeta_{\mu C}^{(E)} - \frac{1}{2}\left.\frac{\partial\zeta_{\mathcal{F}C}^{(E)}\left(e^{\beta\mu}\right)}{\partial(\beta\mu)}\right|_{\mu\to 0}\right] \\ &\quad + \frac{4\pi\hbar^2 C{\beta_\mathrm{c}}^2}{M\lambda_{\mathrm{T_c}}^3}\frac{1}{(\hbar\beta_\mathrm{c}\omega)^5}\left[\zeta(2)\,\zeta\left(\frac{5}{2}\right) - \zeta\left(\frac{3}{2},\frac{5}{2},\frac{1}{2}\right)\right] + \ldots \end{aligned} \tag{7.57}$$

Here, we used for the last term the fact that the generalized zeta-functions obey the identity $\zeta(a,a,c) = 2\,\zeta(a-1,a,c+1)$. The first term in Eq. (7.57) stems from $\mathcal{F}^{(0)}$ and thus contains the interaction-free critical temperature Eq. (3.44) and its first-order correction. In order to get the shift of the critical temperature, we expand

$$\frac{1}{\beta_\mathrm{c}} \approx \frac{1}{\beta_\mathrm{c}^{(0)}}\left(1 + \frac{\Delta T_\mathrm{c}}{T_\mathrm{c}^{(0)}} + \ldots\right) \tag{7.58}$$

and restrict ourselves again to the first order. Within that first order, the shift of the critical temperature, caused by the interactions, reads

$$\begin{aligned} \frac{\Delta T_\mathrm{c}}{T_\mathrm{c}^{(0)}} = -\frac{1}{3\zeta(3)\lambda_{\mathrm{T_c}^{(0)}}^3}\Bigg\{ & 2g\beta_\mathrm{c}^{(0)}\left[\zeta(2)\,\zeta_{\mu g}^{(D,E)} - \frac{1}{2}\left.\frac{\partial\zeta_{\mathcal{F}g}^{(D,E)}\left(e^{\beta\mu}\right)}{\partial(\beta\mu)}\right|_{\mu\to 0}\right] \\ & + \frac{4\pi\hbar^2 C\left[\beta_\mathrm{c}^{(0)}\right]^2}{M}\left[\zeta(2)\,\zeta_{\mu C}^{(E)} - \frac{1}{2}\left.\frac{\partial\zeta_{\mathcal{F}C}^{(E)}\left(e^{\beta\mu}\right)}{\partial(\beta\mu)}\right|_{\mu\to 0}\right] \\ & + \frac{4\pi\hbar^2 C}{M}\frac{\left[\beta_\mathrm{c}^{(0)}\right]^2}{(\hbar\beta_\mathrm{c}^{(0)}\omega)^2}\left[\zeta(2)\zeta\left(\frac{5}{2}\right) - \zeta\left(\frac{3}{2},\frac{5}{2},\frac{1}{2}\right)\right]\Bigg\}. \end{aligned} \tag{7.59}$$

Here we have three contributing terms. The first one comes from the contact interaction and contains direct as well as exchange contributions. The other two are due to the long-range interaction. The second one represents the exchange diagram, while the third has again the frequency dependence and belongs to the direct term. If we specialize to the gravitation-like interaction $C_{\mathrm{G}} = -4\pi^2\hbar^2/(Ma_{\mathrm{G}})$, we express the result in a dimensionless form

$$\boxed{\left(\frac{\Delta T_{\mathrm{c}}}{T_{\mathrm{c}}^{(0)}}\right)^{(\mathrm{QM})} = -c_\delta \frac{a}{\lambda_{T_{\mathrm{c}}^{(0)}}} + \frac{\lambda_{T_{\mathrm{c}}^{(0)}}}{a_{\mathrm{G}}}\left[c_{\mathrm{E}} + c_{\mathrm{D}}\frac{1}{\left(\hbar\beta_{\mathrm{c}}^{(0)}\omega\right)^2}\right], \qquad (7.60)}$$

where a_{G} is defined in (2.33) and numerical values are given in Fig. 2.5. Furthermore, we defined the coefficients

$$c_\delta = \frac{4}{3\zeta(3)}\left[\zeta(2)\,\zeta_{\mu g}^{(D,E)} - \frac{1}{2}\left.\frac{\partial\zeta_{\mathcal{F}g}^{(D,E)}\left(e^{\beta\mu}\right)}{\partial(\beta\mu)}\right|_{\mu\to 0}\right], \qquad (7.61)$$

$$c_{\mathrm{E}} = \frac{4\pi}{3\zeta(3)}\left[\zeta(2)\,\zeta_{\mu C}^{(E)} - \frac{1}{2}\left.\frac{\partial\zeta_{\mathcal{F}C}^{(E)}\left(e^{\beta\mu}\right)}{\partial(\beta\mu)}\right|_{\mu\to 0}\right], \qquad (7.62)$$

$$c_{\mathrm{D}} = \frac{4\pi}{3\zeta(3)}\left[\zeta(2)\,\zeta\left(\frac{5}{2}\right) - \zeta\left(\frac{3}{2},\frac{5}{2},\frac{1}{2}\right)\right] \approx 2.0951\,, \qquad (7.63)$$

which still depend on $\hbar\beta_c^{(0)}\omega$ that can be expressed by the particle number using (3.44). The result is graphically shown in Fig. 7.2. We will derive the results starting from the Hartree-Fock theory in the following section and thereafter discuss both results jointly.

7.4.2. Hartree-Fock Mean-Field Theory

In addition to the previous result, we can show how to get the equation for the shift starting from the Hartree-Fock mean-field theory derived in Section 4. This approach takes into account a non-vanishing number N_0 of condensed particles. So, in contrast to the previous calculation we approach here the critical point from the condensate phase.

The first-order free energy in semiclassical approximation has been calculated in Eq. (4.69) in the case of a cylinder-symmetrical trap. To get comparable results with the previous calculation of the shift, we again restrict ourselves to an isotropic trap. At first, we

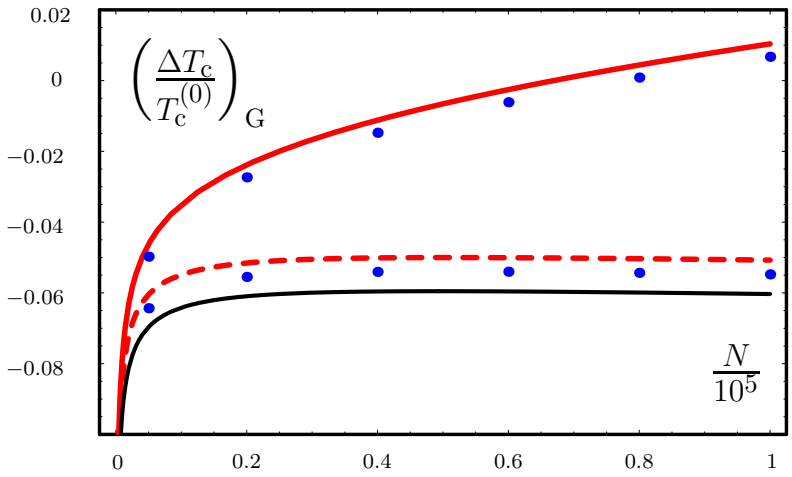

Fig. 7.2: Shift of the critical temperature including contact and gravitation-like interaction. Additionally, we took into account the finite-size correction (3.46). The blue dots show the quantum result (7.60), while the red curve shows the shift obtained by the Hartree-Fock mean-field theory (7.69). In the upper curves both interactions are included, while the lower three are only due to the contact interaction. The black line depicts the corresponding behaviour of the shift Eq. (7.73). All plotted for ^{87}Rb, an isotropic trap with $\omega = 2\pi \cdot 100\,\mathrm{Hz}$, $a = 5.31\,\mathrm{nm}$, and $a_G = 0.027\,\mathrm{m}$.

calculate the particle number using (3.6):

$$\begin{aligned} N &= N_0\Bigg\{1 - \frac{2g\beta}{\lambda_T^3}\sum_{n=1}^{\infty}\frac{e^{n\beta\mu}}{n^{1/2}}\left[\left(1+\frac{n\beta\hbar\omega}{2}\right)\right]^{-3/2} - \frac{4\pi\hbar^2C\beta^2}{\lambda_T^3\left(\hbar\beta\omega\right)^2 M}\sum_{n=1}^{\infty}\frac{e^{n\beta\mu}}{n^{3/2}\sqrt{1+n\beta\hbar\omega/2}} \\ &\quad -\frac{4\pi\hbar^2C\beta^2}{\lambda_T^3 M}\sum_{n=1}^{\infty}\frac{e^{n\beta\mu}n^{1/2}}{\left(1+n\beta\hbar\omega/2\right)^{3/2}\left(1+n\beta\hbar\omega/2\right)}\Bigg\} + \frac{\zeta_3\left(e^{\beta\mu}\right)}{\left(\hbar\beta\omega\right)^3} - \frac{g\beta}{\lambda_T^3}\frac{\zeta_{\frac{3}{2},\frac{3}{2},\frac{1}{2}}\left(e^{\beta\mu}\right)}{\left(\hbar\beta\omega\right)^3} \\ &\quad -\frac{1}{2}\frac{4\pi\hbar^2C\beta^2}{\lambda_T^3\left(\hbar\beta\omega\right)^5 M}\zeta_{\frac{5}{2},\frac{5}{2},-\frac{1}{2}}\left(e^{\beta\mu}\right) - \frac{1}{2}\frac{4\pi\hbar^2C\beta^2}{\lambda_T^3\left(\hbar\beta\omega\right)^3 M}\zeta_{\frac{1}{2},\frac{1}{2},\frac{3}{2}}\left(e^{\beta\mu}\right)\,. \end{aligned} \tag{7.64}$$

As we approach the critical point from below, we have some terms proportional to the number of condensed particles N_0. But the remaining three terms of (7.64) without this dependence are equal to the results of the semiclassical evaluation Eqs. (7.35) and (7.36).

Now we plug in the first-order chemical potential, μ_0 and μ_1 from (4.63). At the critical point, there are almost no particles in the ground state and we can assume $N_0 \to 0$.

Herewith, we obtain

$$\begin{aligned} N &= \frac{\zeta(3)}{(\hbar\beta\omega)^3} + \frac{C4\pi\hbar^2\beta^2\zeta(2)}{\lambda_{\mathrm{T}}^3 M\,(\hbar\beta\omega)^5}\sum_{n=1}^{\infty}\frac{e^{n\beta\mu_0}}{n^{5/2}} - \frac{g\beta}{\lambda_{\mathrm{T}}^3}\frac{\zeta_{\frac{3}{2},\frac{3}{2},\frac{1}{2}}\left(e^{\beta\mu_0}\right)}{(\hbar\beta\omega)^3} \\ &+2\,\frac{g\beta\zeta(2)}{\lambda_{\mathrm{T}}^3\,(\hbar\beta\omega)^3}\sum_{n=1}^{\infty}\frac{e^{n\beta\mu_0}}{n^{3/2}}\left[\left(1+\frac{n\beta\hbar\omega}{2}\right)\right]^{-3/2} - \frac{1}{2}\frac{4\pi\hbar^2C\beta^2}{\lambda_{\mathrm{T}}^3\,(\hbar\beta\omega)^5\,M}\zeta_{\frac{5}{2},\frac{5}{2},-\frac{1}{2}}\left(e^{\beta\mu_0}\right) \\ &-\frac{1}{2}\frac{4\pi\hbar^2C\beta^2}{\lambda_{\mathrm{T}}^3\,(\hbar\beta\omega)^3\,M}\zeta_{\frac{1}{2},\frac{1}{2},\frac{3}{2}}\left(e^{\beta\mu_0}\right) + \frac{C4\pi\hbar^2\beta^2\zeta(2)}{\lambda_{\mathrm{T}}^3 M\,(\hbar\beta\omega)^3}\sum_{n=1}^{\infty}\frac{e^{n\beta\mu_0}}{n^{1/2}}\,\frac{1}{(1+n\beta\omega\hbar/2)^{5/2}}\,. \end{aligned} \tag{7.65}$$

Furthermore, we set $\mu_0 \to 0$ at the critical point as in the previous calculation. The first term in Eq. (7.65) has contains again the interaction-free critical temperature Eq. (3.44) and its first correction. In order to get the shift of the critical temperature, we again expand β_{c} as in (7.58) and proceed as in the previous section. Within that first order, the shift of the critical temperature reads

$$\begin{aligned} \frac{\Delta T_{\mathrm{c}}}{T_{\mathrm{c}}^{(0)}} = -\frac{1}{3\zeta(3)\lambda_{\mathrm{T}_{\mathrm{c}}^{(0)}}^3}\Bigg\{ & 2g\beta_{\mathrm{c}}^{(0)}\left[\zeta(2)\zeta_{\mu g\mathrm{HF}}^{(D,E)}(N) - \zeta\left(\frac{1}{2},\frac{3}{2},\frac{3}{2}\right)\right] \\ & + \frac{4\pi\hbar^2C\left[\beta_{\mathrm{c}}^{(0)}\right]^2}{M}\left[\zeta(2)\zeta_{\mu C\mathrm{HF}}^{(E)}(N) - \zeta\left(-\frac{1}{2},\frac{1}{2},\frac{5}{2}\right)\right] \\ & + \frac{4\pi\hbar^2C}{M}\,\frac{\beta_{\mathrm{c}}^{(0)}}{(\hbar\beta_{\mathrm{c}}^{(0)}\omega)^2}\left[\zeta(2)\zeta\left(\frac{5}{2}\right) - \zeta\left(\frac{3}{2},\frac{5}{2},\frac{1}{2}\right)\right]\Bigg\}\,. \end{aligned} \tag{7.66}$$

Here, we introduced modified zeta-functions of the Hartree-Fock theory. Their numerical values are given for certain particle numbers in Fig. 7.1 to compare them to the quantum-mechanical results. At the critical point, we use (3.44) to replace $\beta_{\mathrm{c}}^{(0)}$ by N and obtain

$$\zeta_{\mu g\mathrm{HF}}^{(D,E)} = \sum_{n=1}^{\infty}\frac{1}{n^{3/2}\{1+[\zeta(3)/N]^{1/3}\,n/2\}^{3/2}}\,, \tag{7.67}$$

$$\zeta_{\mu C\mathrm{HF}}^{(E)} = \sum_{n=1}^{\infty}\frac{1}{n^{1/2}\{1+[\zeta(3)/N]^{1/3}\,n/2\}^{5/2}}\,. \tag{7.68}$$

Eq. (7.66) can be brought to an analogous form to (7.60) but with slightly different constants:

$$\boxed{\left(\frac{\Delta T_{\mathrm{c}}}{T_{\mathrm{c}}^{(0)}}\right)^{(\mathrm{HF})} = -\bar{c}_\delta\frac{a}{\lambda_{\mathrm{T}_{\mathrm{c}}^{(0)}}} + \frac{\lambda_{\mathrm{T}_{\mathrm{c}}^{(0)}}}{a_{\mathrm{G}}}\left[\bar{c}_{\mathrm{E}} + c_{\mathrm{D}}\frac{1}{\left(\hbar\beta_c^{(0)}\omega\right)^2}\right]\,.} \tag{7.69}$$

Here, the combinations of the zeta-functions are defined as

$$\bar{c}_\delta = \frac{4}{3\zeta(3)}\left[\zeta(2)\,\zeta^{(D,E)}_{\mu g\mathrm{HF}} - \zeta\left(\frac{1}{2},\frac{3}{2},\frac{3}{2}\right)\right], \tag{7.70}$$

$$\bar{c}_\mathrm{E} = \frac{4\pi}{3\zeta(3)}\left[\zeta(2)\,\zeta^{(E)}_{\mu C\mathrm{HF}} - \zeta\left(-\frac{1}{2},\frac{1}{2},\frac{5}{2}\right)\right], \tag{7.71}$$

$$c_\mathrm{D} = \frac{4\pi}{3\zeta(3)}\left[\zeta(2)\,\zeta\left(\frac{5}{2}\right) - \zeta\left(\frac{3}{2},\frac{5}{2},\frac{1}{2}\right)\right] \approx 2.0951\,. \tag{7.72}$$

Comparing the results (7.60) and (7.69), we register that the term caused by the direct term is equal in both expressions.

7.5. Discussion of Results

In this final section, we discuss the physical implications of our first-order perturbative results (7.60) and (7.69). In the beginning, we discuss the results for a long-range interaction plus contact interaction and later on compare the different results for the contact interaction only.

In the case of the gravitationally bound gas, the results of the quantum and Hartree-Fock calculation are analyzed graphically in Fig. 7.2. We see that the shift of the contact interaction is negative, as repulsive interactions always lower the critical temperature. It is of the size of about $5-6\%$ for 10^4-10^5 numbers. The additional long-range interaction shifts the critical temperature above as expected for an attractive interaction. For about $6{\cdot}10^4$ particles the shift of the long-range interaction clears the one of the contact interaction. At this place, both interactions equalize each other and the system can get into the self-trapping situation without an external trap. A positive shift can serve as an experimental possibility to prove the long-range interaction within a Bose gas. Actually, the combined curves of long-range plus contact interaction diverge for higher particle numbers because the direct term of the $1/r$ interaction in both results is proportional to $\sqrt{N}$. We have already seen in Section 5.1.1 concerning the self-binding solution of the Gross-Pitaevskii equation in Thomas-Fermi approximation, that the energy per particle rises with the particle number (5.19). Here, we get the same thermodynamical instability.

Comparing the results of quantum and Hartree-Fock calculation, we see that the curve of the Hartree-Fock theory is shifted slightly upwards. This can be understood from the results (7.60) and (7.69). Both of them have the same direct term which is proportional to $\sqrt{N}$. Thus, for the 10^4-10^5 particles as in Fig. 7.2 it is about a factor 100 higher than the exchange term. Hence, the difference is determined by the contact interaction.

Therefore, we discuss the contact interaction separately. By setting $C=0$, i.e., $a_\mathrm{G}\to\infty$, we obtain the result of the temperature shift for the contact interaction in an isotropic trap. In the semiclassical limit of $\hbar\beta\omega\to 0$, which is equivalent to the thermodynamical

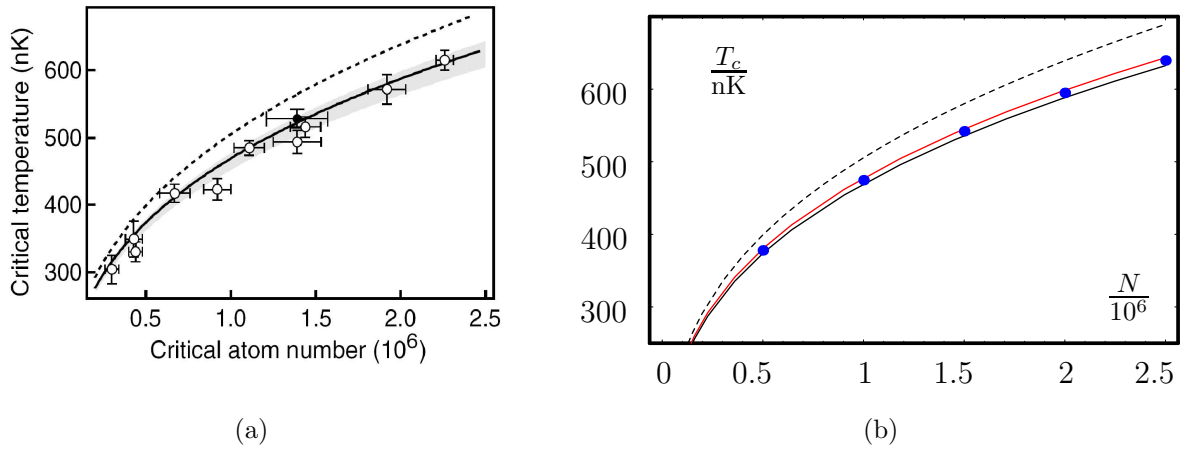

(a) (b)

Fig. 7.3: (a): Experiment measuring the shift of the critical temperature as a function of the particle number [39]. The dashed line belongs to the ideal gas including the finite-size correction (3.46). The solid black line corresponds to (7.73) and the grey shaded area indicates possible results taking statistical and systematic errors into account. (b): Same representation with all three possible theoretical results: black line=semiclassical result (7.73); blue dots=quantum result; blue line=Hartree-Fock result. The curves are plotted for a cylinder-symmetric trap. To derive expressions equivalent to (7.60) and (7.69), we used (B.1) and (B.7) for the quantum result and started with the anisotropic results for chemical potential (4.44) and free energy (4.69) in the Hartree-Fock case.

limit $N \to \infty$ at the critical point, we obtain the semiclassical result for the shift of the critical temperature:

$$\frac{\Delta T_\mathrm{c}}{T_\mathrm{c}^{(0)}} = -\frac{4}{3\zeta(3)}\left[\zeta(2)\,\zeta\left(\frac{3}{2}\right) - \zeta\left(\frac{1}{2},\frac{3}{2},\frac{3}{2}\right)\right]\frac{a}{\lambda_{T_\mathrm{c}^{(0)}}} = -3.42603\,\frac{a}{\lambda_{T_\mathrm{c}^{(0)}}}\,, \tag{7.73}$$

which depends only on the geometric mean trap frequency via $\lambda_{T_\mathrm{c}^{(0)}}$. This result has originally been derived within a mean-field approach using the Popov-approximation in Ref. [74].

The difference between our results and (7.73) is determined by the values of c_δ and $\bar{c}_\delta$. We see from Fig. 7.1 that both approach the semiclassical value rather slow. For instance, the Hartree-Fock result is for 10^6 particles still 10% below the semiclassical value. To compare the results to experimental data, we again use the experiment of Ref. [39] presented in Section 3.5. We shortly repeat that the shift of the critical temperature was measured as a function of the particle number in a full-polarized ^{87}Rb gas confined in a cylinder-symmetric trap with $\omega_\mathrm{r} = 2\pi \cdot 413\,\mathrm{Hz}$ and $\omega_\mathrm{z} = 2\pi \cdot 8.69\,\mathrm{Hz}$. The measurements coincide quite well with the prediction of (7.73), see Fig. 7.3(a). In fact, the majority of

the data points lies rather slightly below the theoretical prediction by (7.73). To compare it to our results, we repeated the calculation of the shift of the critical temperature for the contact interaction using the anisotropic (4.44) and (4.69) for a cylinder-symmetric trap. In the quantum case, we replaced the modified zeta-functions in (7.60) by (B.1) and (B.7). Actually, the quantum result (7.60) should reproduce the shift best as there are fewer approximations made but this produces an even smaller shift, see Fig.7.3(b). However, our results are still in agreement with the experimental data taking the statistical and systematic errors of the experiment into account.

8. Summary and Outlook

In conclusion, we have studied thermal and dynamical properties of a Bose-Einstein condensate underlying a short-range contact as well as a long-range $1/r$ interaction. At first, we have elucidated in Chapter 2 how an attractive long-range interaction can artificially be created. It follows from treating the interaction of neutral atoms with a radiation field within a fourth order perturbative quantum-electrodynamical calculation [26–28]. Altogether, 24 Feynman diagrams have been taken into account to derive the potential Eq. (2.24) which reduces to purely $1/r$ in the near-zone, a well fulfilled approximation for a dilute Bose gas. Furthermore, we have shown how the experiment could be set up either with a combination of static [22] or rotating lasers. Here, our latter approach has the advantage of requiring less lasers and thus might be favourable to realize.

To describe interacting bosons, we have used the functional integral formalism of many-body physics. After recalling some features of the non-interacting Bose gas in Chapter 3, we have derived a self-consistent Hartree-Fock mean-field theory using the background method in Chapter 4. The result is a set of two coupled equations, one integro-differential equation (4.30) for the background field, which is the order parameter of BEC, and a second equation (4.16) for the correlation function that describes the thermal bosons. A first-order perturbative solution of this set represents the starting point of investigating two special cases.

In the limit of zero temperature, we have analyzed the Gross-Pitaevskii equation in Chapter 5. On the one hand, we have shown how the equation is solved in Thomas-Fermi approximation. The self-binding case without an external trap (5.18) corresponds to the physical situation of a Bose star. We have also applied a Gaussian variational test function to include the kinetic term. A comparison of both approximations has shown that the Thomas-Fermi approximation is well fulfilled. Furthermore, we have treated dynamical properties of a BEC by using two approaches in Chapter 6. At first, we have compared the BEC to a quantum liquid applying the hydrodynamic theory. After we had obtained a differential equation for the density corrections, we have separated the angular part and have derived with (6.31) a second-order integro-differential equation for the radial part. From there, the excitation frequencies are obtainable as eigenvalues. Although we could not solve the equation exactly, we have shown, that it becomes a Bessel differential equation in the limit of small radii for the self-binding case without an external trap. Applying proper boundary conditions, we have obtained the excitation frequency Eq. (6.41) which depends on the total number of particles and the two interaction strengths. In a second approach, we have used a time-dependent Gaussian variational test function.

There, we could investigate the breathing mode for different physical regimes in the case of an isotropic harmonic trap, shown in Figs. 6.1 and 6.2. In the self-binding case, the two approaches have shown the same dependence on the interaction strengths.

The second special case of interest has been the regime of the critical temperature. In fact, in Chapter 7 we have calculated the first-order shift of the critical temperature caused by the interactions adopting two methods. In both of them, we have used a harmonic trapping potential and the constraint of conserving the total number of particles. On the one hand, we have applied Feynman's diagrammatic perturbation theory. Two Feynman diagrams have been calculated both for the free energy and self-energy. First, we tried to use the semiclassical approximation but this method has shown an infrared divergence in the exchange diagram of the self-energy. The problem was solved using the quantum-mechanical propagator rather than the semiclassical one, yielding the T_C-shift Eq. (7.60). On the other hand, we have used the Hartree-Fock mean-field theory of Chapter 4. Here, we obtained the result (7.69) which is in good agreement with the former calculation. Furthermore, we have improved the results adding the quantum-mechanical finite-size correction to the semiclassical expression of the interaction-free shift and interpreted the result graphically in Fig. 7.2. For the attractive long-range interaction we got an upward shift as expected, while the repulsive contact interaction has lowered the critical temperature. In the limit of a vanishing long-range interaction, the known result for the shift of a contact interaction could be confirmed in the semiclassical limit with recent data and theory [39,74], depicted in Fig. 7.3. The combined shift of both interactions can take positive or negative values depending on the particle number and can thus serve as an experimental possibility to prove that a long-range interaction is, indeed, present.

Of course, not all points of interest could be treated within this thesis. Our suggestion in Chapter 2 to use a rotating scheme in the realization of the experiment is only valid within a quasi-static regime. To extend it to higher rotation speeds a time-dependent perturbative treatment of the quantum-electrodynamical derivation of the potential would be necessary. Furthermore, the mean-field theory derived in Chapter 4 can be improved by considering also anomalous averages within a Hartree-Fock-Bogoliubov theory. We also had the ambition to handle the system analytically, although there are some interesting areas which are only numerically accessible. As an interpolation between the analytically treatable case of zero and the critical temperature, the temperature-dependence of the specific heat could be calculated. In the zero-temperature limit possible goals are a solution of the Gross-Pitaevskii equation including the kinetic term or a numerical result for the excitation frequency following from (6.31).

Summarizing, we basically restricted ourselves to describe the main properties of a BEC underlying the additional long-range interaction. With this, we set the framework for an analysis what is expected to happen to a Bose gas which is exposed to the new interaction in the laboratory. But if cosmology is simulated this way, specific calculations

for cosmological quantities must be the purpose of future work as well as opening the possibility to measure their characteristics. So, there are lots of open questions and it is passed to theorists as well as experimentalists to further push research in this field.

A. Auxiliary Calculations

In this first part of the appendix, we calculate in detail some quantities of the grand-canonical ensemble that appeared in the thesis.

A.1. Free Energy

The grand-canonical free energy follows from Eq. (3.3) with the non-interacting partition function (3.25) as

$$\mathcal{F}^{(0)} = \frac{1}{\beta} \sum_{\mathbf{k}} \sum_{m=-\infty}^{\infty} \ln \left[\beta \left(-\imath \hbar \omega_m + E_{\mathbf{k}} - \mu \right) \right]. \tag{A.1}$$

The first step is to evaluate the sum over the Matsubara frequencies defined in (3.15). Therefore, we use the Poisson sum rule [72, Chap. 2] and introduce a convergence factor $\lim_{\eta \to 0} e^{2\pi \imath \omega_m \eta}$ to guarantee the normal ordering:

$$\sum_{m=-\infty}^{\infty} f(\omega_m) = \frac{\hbar \beta}{2\pi} \sum_{n=-\infty}^{\infty} \int_{-\infty}^{\infty} d\omega_m f(\omega_m) e^{-\imath n \hbar \beta \omega_m}. \tag{A.2}$$

The choice of the introduced factor refers to the definition of the Heavyside-function in Eq. (3.30), where one has to take the limit $\tau' \downarrow \tau$ (compare to Eq. (7.7) to (7.11)). We rewrite (A.1)

$$\mathcal{F}^{(0)} = \lim_{\eta \to 0} \frac{\hbar}{2\pi} \sum_{\mathbf{k}} \sum_{n=-\infty}^{\infty} \int_{-\infty}^{\infty} d\omega_m \ln \left[\beta \left(-\imath \hbar \omega_m + E_{\mathbf{k}} - \mu \right) \right] e^{-\imath \hbar \beta \omega_m (n-\eta)}. \tag{A.3}$$

We express the logarithm as

$$\ln x = -\frac{\partial}{\partial a} \frac{1}{x^a} \Big|_{a=0} \tag{A.4}$$

and use the Schwinger formula [50]

$$-\frac{\partial}{\partial a} \frac{1}{x^a} \Big|_{a=0} = -\frac{\partial}{\partial a} \frac{1}{\Gamma(a)} \int_0^{\infty} dy \, y^{a-1} e^{-yx} \Big|_{a=0}. \tag{A.5}$$

Inserting Eq. (A.5) into Eq. (A.3) and interchanging the integrals, we get

$$\mathcal{F}^{(0)} = -\lim_{\eta\to 0}\frac{\hbar}{2\pi}\sum_{\mathbf{k}}\sum_{n=-\infty}^{\infty}\frac{\partial}{\partial a}\frac{1}{\Gamma(a)}\int_0^\infty dy\, y^{a-1}e^{-y\beta(E_{\mathbf{k}}-\mu)}\int_{-\infty}^{\infty}d\omega_m e^{\imath\hbar\beta\omega_m(y+\eta-n)}\Big|_{a=0}. \quad (A.6)$$

The latter integral is known as

$$\int_{-\infty}^{\infty}d\omega_m e^{\imath\hbar\beta\omega_m(y+\eta-n)} = \frac{2\pi}{\hbar\beta}\delta\left(y+\eta-n\right). \quad (A.7)$$

The y-integration in Eq. (A.6) runs over all positive y. That means, as η is arbitrary small, that we have to take into account only positive values of n. Consequently, the sum reduces to positive n as well:

$$\mathcal{F}^{(0)} = -\frac{1}{\beta}\lim_{\eta\to 0}\sum_{\mathbf{k}}\sum_{n=1}^{\infty}\frac{\partial}{\partial a}\frac{1}{\Gamma(a)}(n-\eta)^{a-1}e^{-(n-\eta)\beta(E_{\mathbf{k}}-\mu)}\Big|_{a=0}. \quad (A.8)$$

At this point, we can perform the limit $\eta \to 0$. Subsequently, we calculate the differentiation with respect to a at the point $a \to 0$. To this end, we use the relation $\Gamma(a) = \Gamma(a+1)/a$ and expand $n^{a-1}/\Gamma(a)$ to lowest order in a

$$\frac{1}{\Gamma(a)}n^{a-1} \approx \frac{a}{n}. \quad (A.9)$$

So the final expression for the free energy reads with the Taylor expansion of the logarithm $-\ln(1-x) = \sum_{n=1}^{\infty}x^n/n$:

$$\mathcal{F}^{(0)} = \frac{1}{\beta}\sum_{\mathbf{k}}\ln\left[1-e^{\beta(\mu-E_{\mathbf{k}})}\right]. \quad (A.10)$$

At the end of this section, we show how the free energy is connected to the free propagator (3.27) in a formal language. If we look at (3.13), (3.18) and (3.19), we see that the functional integration in the partition function is of Gaussian type and it can be solved formally as

$$\mathcal{Z}^{(0)} = \frac{1}{\det G^{(0)-1}}, \quad (A.11)$$

where "det" denotes the functional determinant. Using (3.3) and the matrix identity $\ln\det A = \mathrm{Tr}\ln A$, we get the relation between grand-canonical free energy and the propagator

$$\mathcal{F} = \frac{1}{\beta}\mathrm{Tr}\ln G^{(0)}. \quad (A.12)$$

The calculation of the free propagator will be the topic of the next section.

A.2. Free Propagator

In the following, we calculate the free propagator in the functional integral formalism, starting from its definition (3.27) by using the grand-canonical partition function Eq. (3.13) and the free action Eq. (3.18). Again, we decompose the bosonical Schrödinger fields according to Eqs. (3.16) and (3.17) and apply Eq. (3.20):

$$\begin{aligned} G^{(0)}(\mathbf{x},\tau;\mathbf{x}',\tau') &= \frac{1}{\mathcal{Z}^{(0)}}\left[\prod_{\mathbf{k}}\prod_{m=-\infty}^{\infty}\frac{1}{2\pi}\int dc^*_{\mathbf{k}m}dc_{\mathbf{k}m}\right]\sum_{\mathbf{k}'}\sum_{m'=-\infty}^{\infty}c_{\mathbf{k}'m'}\psi_{\mathbf{k}'}(\mathbf{x})e^{-\imath\omega_{m'}\tau} \\ &\times\sum_{\mathbf{k}''}\sum_{m''=-\infty}^{\infty}c^*_{\mathbf{k}''m''}\psi^*_{\mathbf{k}''}(\mathbf{x}')e^{\imath\omega_{m''}\tau'}\prod_{\mathbf{k}}\prod_{m=-\infty}^{\infty}e^{-\beta|c_{\mathbf{k}m}|^2(-\imath\hbar\omega_m+E_{\mathbf{k}}-\mu)}. \end{aligned} \tag{A.13}$$

At this point, we can simplify the problem with help of the symmetry. If $\mathbf{k}', m' \neq \mathbf{k}'', m''$, there will be one integral in the product of the form $\int_{-\infty}^{\infty} dx x e^{-x^2}$, that vanishes and so will the entire product. Thus, we can set $\mathbf{k}', m' = \mathbf{k}'', m''$:

$$\begin{aligned} G^{(0)}(\mathbf{x},\tau;\mathbf{x}',\tau') &= \frac{1}{\mathcal{Z}^{(0)}}\sum_{\mathbf{k}'}\sum_{m'=-\infty}^{\infty}\psi_{\mathbf{k}'}(\mathbf{x})\psi^*_{\mathbf{k}'}(\mathbf{x}')e^{\imath\omega_{m'}(\tau'-\tau)} \\ &\times\prod_{\mathbf{k}}\prod_{m=-\infty}^{\infty}\frac{1}{2\pi}\int dc^*_{\mathbf{k}m}dc_{\mathbf{k}m}\left|c_{\mathbf{k}'m'}\right|^2 e^{-\beta|c_{\mathbf{k}m}|^2(-\imath\hbar\omega_m+E_{\mathbf{k}}-\mu)}. \end{aligned} \tag{A.14}$$

Now we adopt Eq. (3.22) and (3.23) and extract the integral with $\mathbf{k}, m = \mathbf{k}', m'$:

$$\begin{aligned} G^{(0)}(\mathbf{x},\tau;\mathbf{x}',\tau') &= \frac{1}{\mathcal{Z}^{(0)}}\sum_{\mathbf{k}'}\sum_{m'=-\infty}^{\infty}\psi_{\mathbf{k}'}(\mathbf{x})\psi^*_{\mathbf{k}'}(\mathbf{x}')e^{\imath\omega_{m'}(\tau'-\tau)} \\ &\times\frac{1}{\pi}\int da_{\mathbf{k}'m'}db_{\mathbf{k}'m'}\left(a^2_{\mathbf{k}'m'}+b^2_{\mathbf{k}'m'}\right)e^{-\beta\left(a^2_{\mathbf{k}'m'}+b^2_{\mathbf{k}'m'}\right)(-\imath\hbar\omega_{m'}+E_{\mathbf{k}'}-\mu)} \\ &\times\prod_{\mathbf{k}\neq\mathbf{k}'}\prod_{\substack{m=-\infty\\ m\neq m'}}^{\infty}\frac{1}{\pi}\int da_{\mathbf{k}m}db_{\mathbf{k}m}e^{-\beta\left(a^2_{\mathbf{k}m}+b^2_{\mathbf{k}m}\right)(-\imath\hbar\omega_m+E_{\mathbf{k}}-\mu)}. \end{aligned} \tag{A.15}$$

After the integration, we use Eq. (3.25) and rename $\mathbf{k}', m' = \mathbf{k}, m$:

$$G^{(0)}(\mathbf{x},\tau;\mathbf{x}',\tau') = \sum_{\mathbf{k}}\sum_{m=-\infty}^{\infty}\psi_{\mathbf{k}}(\mathbf{x})\psi^*_{\mathbf{k}}(\mathbf{x}')\frac{e^{\imath\omega_m(\tau'-\tau)}}{\beta\left(-\imath\hbar\omega_m+E_{\mathbf{k}}-\mu\right)}. \tag{A.16}$$

Just as in Section A.1, we solve the sum over the Matsubara frequencies with help of the Poisson sum rule (A.2):

$$\sum_{\mathbf{k}}\sum_{m=-\infty}^{\infty}\frac{\psi_{\mathbf{k}}(\mathbf{x})\psi^*_{\mathbf{k}}(\mathbf{x}')e^{\imath\omega_m(\tau'-\tau)}}{\beta\left(-\imath\hbar\omega_m+E_{\mathbf{k}}-\mu\right)} = \lim_{\eta\downarrow 0}\sum_{\mathbf{k}}\psi_{\mathbf{k}}(\mathbf{x})\psi^*_{\mathbf{k}}(\mathbf{x}')\sum_{n=-\infty}^{\infty}\int_{-\infty}^{\infty}dz\frac{e^{\frac{2\pi\imath z}{\hbar\beta}[\tau'-\tau+(n+\eta)\hbar\beta]}}{-2\pi\imath z+\beta\left(E_{\mathbf{k}}-\mu\right)}. \tag{A.17}$$

Thus, the many-body propagator can be written for later convenience as

$$G^{(0)}(\mathbf{x},\tau;\mathbf{x}',\tau') = \lim_{\eta\downarrow 0}\sum_{n=-\infty}^{\infty} g^{(0)}(\mathbf{x},\mathbf{x}';\tau-\tau'+(n+\eta)\hbar\beta) \tag{A.18}$$

where the new function is given by

$$g^{(0)}(\mathbf{x},\mathbf{x}';\tau) = \sum_{\mathbf{k}}\psi_{\mathbf{k}}(\mathbf{x})\psi^*_{\mathbf{k}}(\mathbf{x}')\frac{\imath}{2\pi}\int_{-\infty}^{\infty} dz \frac{e^{-\frac{2\pi\imath z}{\hbar\beta}\tau}}{z+\imath\frac{\beta}{2\pi}\left(E_{\mathbf{k}}-\mu\right)}\,. \tag{A.19}$$

The integral on the right-hand side can be solved using the residue theorem. The pole of the function lies on the negative imaginary axis at $z=-\imath\beta/(2\pi)\left(E_{\mathbf{k}}-\mu\right)$, whereas we have to obey the constraint $E_{\mathbf{k}}-\mu\geq 0$. Thus the closed curve in the positive z-plane, where $\tau<0$, does not contribute. However, the way in the negative z-plane, i.e., $\tau>0$, contains the pole. Here we get the contribution given by the residue. Besides we have to regard that the integration in the negative plane is performed in the mathematically wrong direction which leads to an additional minus sign. Thus the joined result reads

$$g^{(0)}(\mathbf{x};\mathbf{x}',\tau) = \Theta\left(\tau\right)\sum_{\mathbf{k}}\psi_{\mathbf{k}}(\mathbf{x})\psi^*_{\mathbf{k}}(\mathbf{x}')e^{-(E_{\mathbf{k}}-\mu)\tau/\hbar}\,. \tag{A.20}$$

Now, we can justify the introduction of the function $g^{(0)}(\mathbf{x},;\mathbf{x}',\tau)$. Except for the Heavyside-function it is the one-particle imaginary time evolution amplitude in spectral decomposition [36,37]. Thus, the many-body propagator (A.18) can be interpreted as a periodic repetition of all one-particle amplitudes with the energy shifted by the chemical potential:

$$G^{(0)}(\mathbf{x},\tau;\mathbf{x}',\tau') = \lim_{\eta\downarrow 0}\sum_{n=-\infty}^{\infty}\Theta\left(\tau-\tau'+(n+\eta)\hbar\beta\right)\left(\mathbf{x},\tau-\tau'+(n+\eta)\hbar\beta;\mathbf{x}',0\right)|_{E_{\mathbf{k}}\to E_{\mathbf{k}}-\mu}\,. \tag{A.21}$$

To get a proper expression for $G^{(0)}$, we still have to evaluate the summation in (A.18). The domain of τ and τ' is limited by $\tau-\tau'\in[0;\hbar\beta]$. Hence, that constricts the Heavyside-function in Eq. (A.20) to the following cases: it is only non-zero, if $\tau>\tau'$and $n\leq 0$ or if $\tau<\tau'$ and $n<0$. To get a nicer expression, we rename $-n\to n$ and yield

$$\begin{aligned} G^{(0)}(\mathbf{x},\tau;\mathbf{x}',\tau') &= \lim_{\eta\downarrow 0}\sum_{\mathbf{k}}\psi_{\mathbf{k}}(\mathbf{x})\psi^*_{\mathbf{k}}(\mathbf{x}')\Bigg\{\sum_{n=0}^{\infty}\Theta\left(\tau-\tau'-\eta\right)e^{-(E_{\mathbf{k}}-\mu)[\tau-\tau'+(n+\eta)\hbar\beta]/\hbar} \\ &\quad +\sum_{n=1}^{\infty}\Theta\left(\tau'-\tau+\eta\right)e^{-(E_{\mathbf{k}}-\mu)[\tau-\tau'+(n+\eta)\hbar\beta]/\hbar}\Bigg\}\,. \end{aligned} \tag{A.22}$$

Here, we can go to the limit of $\eta\downarrow 0$. We see that the introduction of η was crucial because it determines in the case of equal imaginary times that only the second Heavyside-function in (A.22) contributes. If we can forget about the η we must keep in mind that for equal time arguments the limit becomes $\tau'\downarrow\tau$.

B. Modified Zeta-Functions

For two reasons we restricted us in Chapter 7 to the isotropic case. On the one hand, the shift of the critical temperature is the largest for an isotropic trap. And on the other hand, we could simplify the calculation enormously. In this Appendix, we state the result for the critical chemical potential and the grand-canonical free energy for a cylinder-symmetric trap. These results have to be inserted into (7.61) and (7.62) to obtain the shift of the critical temperature for a cylinder-symmetric trap. For the direct terms of the free energy we get the two expressions

$$\zeta_{\mathcal{F}g}^{(D)}\left(e^{\beta\mu}\right)= \sum_{n,m=1}^{\infty} e^{\beta\mu(m+n)}\left[\prod_{j=\mathrm{r,r,z}}\sqrt{\frac{(\hbar\beta\omega_j)^2}{\sinh(\hbar\beta\omega_j n)\sinh(\hbar\beta\omega_j m)}}\right. \tag{B.1}$$
$$\left.\times\ \sqrt{\frac{\hbar\beta\omega_j/2}{\left(\tanh\frac{\hbar\beta\omega_j n}{2}+\tanh\frac{\hbar\beta\omega_j m}{2}\right)}}\right]$$

$$\zeta_{\mathcal{F}C}^{(D)}\left(e^{\beta\mu},f_C^{(D)}\right)=\sum_{n,m=1}^{\infty} e^{\beta\mu(m+n)}\left[\prod_{j=\mathrm{r,z}}\sqrt{\frac{\sinh(\hbar\beta\omega_j(n+m)/2)\,\hbar\beta\omega_j/2}{\sinh(\hbar\beta\omega_j n/2)\sinh(\hbar\beta\omega_j m/2)}}\right] f_{C(n,m)}^{(D)}\left(\omega_\mathrm{r},\omega_\mathrm{z}\right)$$
$$\times\left[\prod_{j=\mathrm{r,r,z}}\sqrt{\frac{\hbar\beta\omega_j\hbar\beta\omega_j}{\sinh(\hbar\beta\omega_j n)\sinh(\hbar\beta\omega_j m)}\frac{\hbar\beta\omega_j/2}{\tanh\hbar\beta\omega_j n/2+\tanh\hbar\beta\omega_j m/2}}\right] \tag{B.2}$$

with the modified anisotropy function

$$f_{C(n,m)}^{(D)}\left(\omega_\mathrm{r},\omega_\mathrm{z}\right)=\left(\frac{\omega_\mathrm{r}}{\omega_\mathrm{z}}\right)^{1/3}\frac{\arccos\frac{\omega_\mathrm{r}}{\omega_\mathrm{z}}\sqrt{\frac{\tanh(\hbar\beta\omega_\mathrm{r}n/2)\tanh(\hbar\beta\omega_\mathrm{r}m/2)}{\tanh(\hbar\beta\omega_\mathrm{z}n/2)\tanh(\hbar\beta\omega_\mathrm{z}m/2)}\frac{\tanh(\hbar\beta\omega_\mathrm{z}n/2)+\tanh(\hbar\beta\omega_\mathrm{z}m/2)}{\tanh(\hbar\beta\omega_\mathrm{r}m/2)+\tanh(\hbar\beta\omega_\mathrm{z}m/2)}}}{\sqrt{1-\left(\frac{\omega_\mathrm{r}}{\omega_\mathrm{z}}\right)^2\frac{\tanh(\hbar\beta\omega_\mathrm{r}n/2)\tanh(\hbar\beta\omega_\mathrm{r}m/2)}{\tanh(\hbar\beta\omega_\mathrm{z}n/2)\tanh(\hbar\beta\omega_\mathrm{z}m/2)}\frac{\tanh(\hbar\beta\omega_\mathrm{z}n/2)+\tanh(\hbar\beta\omega_\mathrm{z}m/2)}{\tanh(\hbar\beta\omega_\mathrm{r}m/2)+\tanh(\hbar\beta\omega_\mathrm{z}m/2)}}}\,. \tag{B.3}$$

The exchange diagrams give the following contributions. The terms for the contact interaction are equal in both cases

$$\zeta_{\mathcal{F}g}^{(E)}\left(e^{\beta\mu}\right)=\zeta_{\mathcal{F}g}^{(D)}\left(e^{\beta\mu}\right)\,, \tag{B.4}$$

but the free energy differs

$$\begin{aligned}\zeta_{\mathcal{F}C}^{(E)}\left(e^{\beta\mu}\right) &= \sum_{n,m=1}^{\infty}\frac{e^{(n+m)\beta\mu}\,(\hbar\beta\omega_{\rm r})^2}{\sinh(\hbar\beta\omega_{\rm r}n)\sinh(\hbar\beta\omega_{\rm r}m)}\sqrt{\frac{(\hbar\beta\omega_{\rm z})^2}{\sinh(\hbar\beta\omega_{\rm z}n)\sinh(\hbar\beta\omega_{\rm z}m)}}\\ &\times\sqrt{\frac{\hbar\beta\omega_{\rm r}/2}{\left(\tanh\frac{\hbar\beta\omega_{\rm r}n}{2}+\tanh\frac{\hbar\beta\omega_{\rm r}m}{2}\right)}}\,\frac{\arccos\kappa_{(n,m)}}{\sqrt{1-\kappa_{(n,m)}^2}}\\ &\times\left[\prod_{j=\mathrm{r,z}}\sqrt{\frac{1}{\left(\tanh\frac{\hbar\beta\omega_j n}{2}+\tanh\frac{\hbar\beta\omega_j m}{2}\right)}\frac{1}{\left(\coth\frac{\hbar\beta\omega_j n}{2}+\coth\frac{\hbar\beta\omega_j m}{2}\right)}}\right],\end{aligned}\tag{B.5}$$

where the anisotropy factor reads for this case

$$\kappa_{(n,m)}=\sqrt{\frac{\omega_{\rm r}}{\omega_{\rm z}}\frac{\coth\frac{\hbar\beta\omega_{\rm r}n}{2}+\coth\frac{\hbar\beta\omega_{\rm r}m}{2}}{\coth\frac{\hbar\beta\omega_{\rm z}n}{2}+\coth\frac{\hbar\beta\omega_{\rm z}m}{2}}}\,.\tag{B.6}$$

For the chemical potential we obtain for the direct terms

$$\zeta_{\mu g}^{(D)} = \sum_{n=1}^{\infty}\prod_{j=\mathrm{r,r,z}}\sqrt{\frac{\hbar\beta\omega_j}{\sinh\hbar\beta\omega_j n}}\,,\tag{B.7}$$

$$\begin{aligned}\zeta_{\mu C}^{(D)} &= \sum_{n=1}^{\infty}\frac{\hbar\beta\omega_{\rm r}}{\sinh\hbar\beta\omega_{\rm r}n}\sqrt{\frac{\hbar\beta\omega_{\rm z}}{\sinh\hbar\beta\omega_{\rm z}n}}\sqrt{\frac{\hbar\beta\omega_{\rm r}/2\quad\hbar\beta\omega_{\rm z}/2}{\tanh(\hbar\beta\omega_{\rm r}n/2)\tanh(\hbar\beta\omega_{\rm z}n/2)}}\\ &\times\left(\frac{\omega_{\rm r}}{\omega_{\rm z}}\right)^{1/3}\frac{\arccos\sqrt{\frac{\omega_{\rm r}}{\omega_{\rm z}}\frac{\tanh\hbar\beta\omega_{\rm r}n/2}{\tanh\hbar\beta\omega_{\rm z}n/2}}}{\sqrt{1-\frac{\omega_{\rm r}}{\omega_{\rm z}}\frac{\tanh\hbar\beta\omega_{\rm r}n/2}{\tanh\hbar\beta\omega_{\rm z}n/2}}}\,,\end{aligned}\tag{B.8}$$

where the latter term again determines the anisotropy. The exchange terms read

$$\zeta_{\mu g}^{(E)} = \zeta_{\mu g}^{(D)}\,,\tag{B.9}$$

$$\zeta_{\mu C}^{(E)} = \sum_{n=1}^{\infty}\frac{\hbar\beta\omega_{\rm r}}{\sinh\hbar\beta\omega_{\rm r}n}\sqrt{\frac{\hbar\beta\omega_{\rm z}}{\sinh\hbar\beta\omega_{\rm z}n}}\sqrt{\frac{\tanh\left(\hbar\beta\omega_{\rm r}n/2\right)\tanh\left(\hbar\beta\omega_{\rm z}n/2\right)}{\frac{\hbar\beta\omega_{\rm r}}{2}\frac{\hbar\beta\omega_{\rm z}}{2}}}\,\frac{\arccos\kappa_{(n)}}{\sqrt{1-\kappa_{(n)}^2}}\,,\tag{B.10}$$

where the anisotropy is defined this time as

$$\kappa_{(n)}=\sqrt{\frac{\omega_{\rm r}}{\omega_{\rm z}}\,\coth\left(\frac{\hbar\beta\omega_{\rm r}n}{2}\right)\tanh\left(\frac{\hbar\beta\omega_{\rm z}n}{2}\right)}\,.\tag{B.11}$$

Danksagung

Abschließend möchte ich mich bei einigen Personen bedanken, ohne die ich diese Arbeit nicht vollendet hätte.

Erst einmal vielen Dank an Prof. Dr. Hagen Kleinert, der es erst ermöglicht hat, diese Arbeit in seiner Arbeitsgruppe anzufertigen. Mit seinem humorvollen, lebendigen und neugierigen Geist sowie seinem Ideenreichtum hat er jederzeit motiviert und bei auftretenden Problemen weitergeholfen. Zudem war es eine Freude seine illustren Gäste aus aller Welt kennenzulernen.

Weiterhin gebührt größter Dank PD Dr. Axel Pelster, der mit hohem Engagement seine wenige Zeit nutzt, um auch in Berlin Diplomanden zu betreuen. Bei allen Problemen und Fragen hat er sich geduldig Zeit genommen und mir mit seinem enormen Fundus an physikalischem Fach-und Literaturwissen sowie großem didaktischen Geschick geholfen.

Nicht unerwähnt bleiben darf Konstantin Glaum. Wann immer ich Fragen hatte, konnte ich mich getrost an ihn wenden, der er dabei mit großer Hilfsbereitschaft und Geduld seine eigenen Präferenzen in den Hintergrund stellte, um mir und anderen zu weiterzuhelfen.

Desweiteren vielen Dank für die schöne Zeit an meine Zimmerkameraden Sonja Overesch, Walja Korolevski und Parvis-Soltan-Panahi sowie die anderen Gruppenmitglieder Steffen Röthel, Alexander Hoffmann, Börsenguru Jürgen Dietel, Victor Hugo Bezerra, Xiaojiang Chen, Flavio Nogueira und Aristeu Lima.

Abschließend ein großes Dankeschön an Familie und Freunde für den wertvollen Ausgleich zum Unialltag.

List of Figures

Bibliography

[1] M.H. Anderson, J.R. Ensher, M.R. Matthews, C.E. Wieman, and E.A. Cornell, *Observation of Bose-Einstein Condensation in a Dilute Atomic Vapor*, Science **269**, 198 (1995)

[2] K.B. Davis, M.O. Mewes, M.R. Andrews, N.J. van Druten, D.S. Durfee, D.M. Kurn, and W. Ketterle, *Bose-Einstein Condensation in a Gas of Sodium Atoms*, Phys. Rev. Lett. **75**, 3969 (1995)

[3] A. Einstein, *Quantentheorie des einatomigen idealen Gases. Zweite Abhandlung*, Sitzungsber. Preuss. Akad. Wiss **1925**, 3 (1925)

[4] S.N. Bose, *Plancks Gesetz und Lichtquantenhypothese*, Zeitschrift für Physik **26**, 178 (1924)

[5] H. Feshbach, *Unified Theory of Nuclear Reactions*, Ann. Phys. (N.Y.) **5**, 357 (1958)

[6] U. Fano, *Effects of Configuration Interaction on Intensities and Phase Shifts*, Phys. Rev. **124**, 1866 (1961)

[7] S. Inouye, M.R. Andrews, J. Stenger, H.-J. Miesner, D.M. Stamper-Kurn, and W. Ketterle, *Observation of Feshbach Resonances in a Bose-Einstein Condensate*, Nature **392**, 151 (1998)

[8] M.W. Zwierlein, J.R. Abo-Shaeer, A. Schirotzek, C.H. Schunck, and W. Ketterle, *Vortices and Superfluidity in a Strongly Interacting Fermi Gas*, Nature **435**, 1047 (2005)

[9] I. Bloch, *Quantum Gases in Optical Lattices*, Physics World **17**, 25 (2004)

[10] M. Greiner, O. Mandel, T. Esslinger, T.W. Hänsch, and I. Bloch, *Quantum Phase Transition from a Superfluid to a Mott Insulator in a Gas of Ultracold Atoms*, Nature **415**, 39 (2002)

[11] I. Bloch, T.W. Hänsch, and T. Esslinger, *Atom Laser with a cw Output Coupler*, Phys. Rev. Lett. **82**, 3008 (1999)

[12] S. Chu, C. Cohen-Tannoudji, and W.D. Phillips, *Nobel Lectures in Physics 1996-2000* (World Scientific Publishing Company, Singapore, 2003)

[13] C.J. Myatt, E.A. Burt, R.W. Ghrist, E.A. Cornell, and C.E. Wieman, *Production of Two Overlapping Bose-Einstein Condensates by Sympathetic Cooling*, Phys. Rev. Lett. **78**, 586 (1997)

[14] K. Huang, *Statistical Mechanics* (John Wiley & Sons, New York, 1963)

[15] A. Griesmaier, J. Werner, S. Hensler, J. Stuhler, and T. Pfau, *Bose-Einstein Condensation of Chromium*, Phys. Rev. Lett. **94**, 160401 (2005)

[16] J. Stuhler, A. Griesmaier, T. Koch, M. Fattori, T. Pfau, S. Giovanazzi, P. Pedri, and L. Santos, *Observation of Dipole-Dipole Interaction in a Degenerate Quantum Gas*, Phys. Rev. Lett. **95**, 150406 (2005)

[17] K. Glaum, A. Pelster, H. Kleinert, and T. Pfau, *Critical Temperature of a Chromium Condensate*, Phys. Rev. Lett. (in Press), eprint: `cond-mat/0606569`

[18] K. Glaum and A. Pelster, *Bose-Einstein Condensation Temperature of Dipolar Gas in Anisotropic Harmonic Trap*, eprint: `cond-mat/0609374`

[19] S.K. Ma and C.W. Woo, *Theory of a Charged Bose Gas. I*, Phys. Rev. **159**, 165 (1967)

[20] C.W. Woo and S.K. Ma, *Theory of a Charged Bose Gas. II*, Phys. Rev. **159**, 176 (1967)

[21] E. Wigner, *Effects of the Electron Interaction on the Energy Levels of Electrons in Metals*, Trans. Faraday Soc. **34**, 678 (1938)

[22] D. O'Dell, S. Giovanazzi, G. Kuritzki, and V.M. Akulin, *Bose-Einstein Condensates with $1/r$ Interatomic Attraction: Electromagnetically Induced Gravity*, Phys. Rev. Lett. **84**, 5687 (2000); See also the comment:
J. Anglin, *Why Trapped Bosons are Attractive*, Nature **406**, 29 (2000)

[23] R. Ruffini and S. Bonazzola, *Systems of Self-Gravitating Particles in General Relativity and the Concept of an Equation of State*, Phys. Rev. **187**, 1767 (1969)

[24] G. Ingrosso and R. Ruffini, *On Systems of Self-Gravitating Bosons and Fermions Undergoing Quantum Condensation. Newtonian Approach*, Il Nuovo Cimento **101 B**, 369 (1988)

[25] J.L. Feng, *Dark Matter at the Fermi Scale*, J. Phys. G **32**, R1 (2006)

[26] D.P. Craig and T. Thirunamachandran, *Molecular Quantum Electrodynamics* (Academic Press, London, 1984)

[27] T. Thirunamachandran, *Intermolecular Interactions in the Presence of an Intense Radiation Field*, Mol. Phys. **40**, 393 (1980)

[28] D.L. Andrews and T. Thirunamachandran, *A Quantum Electrodynamical Theory of Differential Scattering Based on a Model with Two Chromophores*, Proc. R. Soc. A **358**, 297 (1978)

[29] H. Günther, *NMR-Spektroskopie*, Third Edition (Georg Thieme Verlag, Stuttgart; New York, 1992)

[30] S. Giovanazzi, A. Görlitz and T. Pfau, *Tuning the Dipolar Interaction in Quantum Gases*, Phys. Rev. Lett. **89**, 130401 (2002)

[31] B. Roth, U. Fröhlich, and S. Schiller, *Sympathetic Cooling of $^4He^+$ Ions in a Radio-Frequency Trap*, Phys. Rev. Lett. **94**, 053001 (2005)

[32] A. Drakoudis, M. Söllner, and G. Werth, *Instabilities of Ion Motion in a Linear Paul Trap*, International Journal of Mass Spectrometry **252**, 61 (2006)

[33] L.D. Landau and E.M. Lifschitz, *Mechanik*, Tenth Edition (Akademie-Verlag Berlin, 1981)

[34] W. Nolting, *Grundkurs Theoretische Physik 6: Statistische Physik*, Fourth Edition (Springer-Verlag, Berlin Heidelberg, 2002)

[35] R.P. Feynman, *Space-Time Approach to Non-Relativistic Quantum Mechanics*, Rev. Mod. Phys **20**, 367 (1948)

[36] H. Kleinert, *Path Integrals in Quantum Mechanics, Statistics, Polymer Physics, and Financial Markets*, Fourth Edition (World Scientific, Singapore, 2006)

[37] A. Pelster, *Lecture Notes on Bose-Einstein Condensation (in German)*, University Duisburg-Essen, Germany (2004),
`http://www.theo-phys.uni-essen.de/tp/ags/pelster_dir/SS04/skript.pdf`

[38] J.W. Negele and H. Orland, *Quantum Many-Particle Systems* (Addison-Wesley, New York, 1988)

[39] F. Gerbier, J.H. Thywissen, S. Richard, M. Hugbart, P. Bouyer, and A. Aspect, *Critical Temperature of a Trapped, Weakly Interacting Bose Gas*, Phys. Rev. Lett. **92**, 030405 (2004)

[40] S. Grossmann and M. Holthaus, *On Bose-Einstein Condensation in Harmonic Traps*, Phys. Lett. A **208**, 188 (1995)

[41] T. Haugset, H. Haugerud, and J.O. Andersen, *Bose-Einstein Condensation in Anisotropic Harmonic Traps*, Phys. Rev. A **55**, 2922 (1997)

[42] F. Dalfovo, S. Giorgini, L.P. Pitaevskii, and S. Stringari, *Theory of Bose-Einstein Condensation in Trapped Gases*, Rev. Mod. Phys. **71**, 463 (1999)

[43] Ph.W. Courteille, V.S. Bagnato, and V.I. Yukalov, *Bose-Einstein Condensation of Trapped Atomic Gases*, Laser Phys. **11**, 659 (2001)

[44] J. O. Andersen, *Theory of the Weakly Interacting Bose Gas*, Rev. Mod. Phys. **76**, 599 (2004)

[45] A. Griffin, *Conserving and Gapless Approximations for an Inhomogeneous Bose gas at Finite Temperatures*, Phys. Rev. B **53**, 9341 (1996)

[46] M. Timmer, *Ultrakalte Atomgase in Zufallspotentialen*, Diplomarbeit, Universität Duisburg-Essen (2006),
`http://www.theo-phys.uni-essen.de/tp/u/sp0088/index.html`

[47] J. Hubbard, *Calculation of Partition Function*, Phys. Rev. Lett. **3**, 77 (1959)

[48] R.L. Stratonovich, *On a Method of Calculating Quantum Distribution Functions*, Soviet Phys. Doklady **2**, 416 (1958)

[49] L. Pitaevskii and S. Stringari, *Bose-Einstein Condensation* (Oxford University Press, Oxford, 2003)

[50] H. Kleinert and V. Schulte-Frohlinde, *Critical Properties of ϕ^4-Theories* (World Scientific, Singapore, 2001)

[51] R. Jackiw, *Functional Evaluation of the Effective Potential*, Phys. Rev. **9**, 1686 (1974)

[52] J.P. Blaizot and G. Ripka, *Quantum Theory of Finite Systems* (MIT Press, Cambridge, MA 1986)

[53] A. Pelster, H. Kleinert, and M. Bachmann, *Functional Closure of Schwinger-Dyson Equations in Quantum Electrodynamics: 1. Generation of Connected and One-Particle Irreducible Feynman Diagrams*, Ann. Phys. (N.Y.) **297**, 363 (2002)

[54] A. Pelster and K. Glaum, *Recursive Graphical Solution of Closed Schwinger-Dyson Equations in ϕ^4-Theory – Part1: Generation of Connected and One-Particle Irreducible Feynman Diagrams*, Physica A **335**, 455 (2004)

[55] G. Baym, *Self-Consistent Approximations in Many-Body Systems*, Phys. Rev. **127**, 1391 (1962)

[56] E.P. Gross, *Classical Theory of Boson Wave Fields*, Ann. Phys. (N.Y.) **4**, 57 (1958)

[57] E.P. Gross, *Structure of a Quantized Vortex in Boson Systems*, Il Nuovo Cimento **20**, 454 (1961)

[58] L. Pitaevskii, *Vortex Lines in an Imperfect Bose Gas*, Sov. Phys. JETP **13**, 451 (1961), Zh. Eksp. Teor. Fiz. **40**, 646 (1961)

[59] C.J. Pethick and H. Smith, *Bose-Einstein Condensation in Dilute Gases* (Cambridge University Press, Cambridge, 2002)

[60] I.S. Gradshteyn and I.M. Ryzhik, *Table of Integrals, Series, and Products*, Fourth Edition, (Academic Press, London, 1965)

[61] S. Stringari, *Collective Excitations of a Trapped Bose-Condensed Gas*, Phys. Rev. Lett. **77**, 2360 (1996)

[62] N.N. Bogoliubov, *Theory of Superfluidity*, J. Phys. (Moscow) **11**, 23 (1947)

[63] L.D. Landau and E.M. Lifschitz, *Hydrodynamik* (Akademie-Verlag, Berlin, 1966)

[64] W. Greiner and H. Stock, *Theoretische Physik Band 2 A: Hydrodynamik* (Verlag Harri Deutsch, Thun, 1978)

[65] W. Greiner, *Theoretische Physik 3: Klassische ELektrodynamik* (Verlag Harri Deutsch, Frankfurt am Main, Thun, 1991)

[66] S. Giovanazzi, G. Kuritzki, I.E. Mazets, and S. Stringari, *Collective Excitations of a "Gravitationally" Self-bound Bose Gas*, Europhys. Lett. **56**, 1 (2001)

[67] V.M. Pérez-García, H. Michinel, J.I. Cirac, M. Lewenstein, and P. Zoller, *Low Energy Excitations of a Bose-Einstein Condensate: A Time-Dependent Variational Analysis*, Phys. Rev. Lett. **77**, 5320 (1996)

[68] M. Desaix, D. Anderson, and M. Lisak, *Variational Approach to Collapse of Optical Pulses*, J. Opt. Soc. Am. B **8**, 2082 (1991)

[69] A.A. Abrikosov, L.P. Gorkov, and I.E. Dzyaloshinski, *Methods of Quantum Field Theory in Statistical Physics* (Pergamon Press, New York, 1965)

[70] A.L. Fetter and J.D. Walecka, *Quantum Theory of Many-Particle Systems* (McGraw-Hill, New York, 1971)

[71] E.K.U. Gross, E. Runge, and O. Heinonen, *Many Particle Theory* (Adam Hilger, Bristol, 1991)

[72] G.D. Mahan, *Many-Particle Physics*, Third Edition (Kluwer Academic/Plenum Publisher, New York, 2000)

[73] A. Pelster and K. Glaum, *Many-Body Vacuum Diagrams and Their Recursive Graphical Construction*, Phys. Stat. Sol. B **237**, 72 (2003)

[74] S. Giorgini, L.P. Pitaevskii, and S. Stringari, *Condensate Fraction and Critical Temperature of a Trapped Interacting Bose Gas*, Phys. Rev. A **54**, R4633 (1996)